


July 2018

Interrogation of Protein Function with Peptidomimetics

Olapeju Bolarinwa

University of South Florida, ooyesiku@mail.usf.edu

Follow this and additional works at: <https://scholarcommons.usf.edu/etd>

 Part of the [Biochemistry Commons](#), and the [Organic Chemistry Commons](#)

Scholar Commons Citation

Bolarinwa, Olapeju, "Interrogation of Protein Function with Peptidomimetics" (2018). *Graduate Theses and Dissertations*.
<https://scholarcommons.usf.edu/etd/7667>

This Dissertation is brought to you for free and open access by the Graduate School at Scholar Commons. It has been accepted for inclusion in Graduate Theses and Dissertations by an authorized administrator of Scholar Commons. For more information, please contact scholarcommons@usf.edu.

Interrogation of Protein Function with Peptidomimetics

by

Olapeju Bolarinwa

A dissertation submitted in partial fulfillment
of the requirements for the degree of
Doctor of Philosophy
Department of Chemistry
College of Arts and Sciences
University of South Florida

Major Professor: Jianfeng Cai, Ph.D.
James Leahy, Ph.D.
Wayne Guida, Ph.D.
Cheng, Feng, Ph.D.

Date of Approval:
June 27, 2018

Keywords: γ -AApeptide, amylin, hIAPP, diabetes, MPP8, peptidomimetics, protein-protein interaction

Copyright © 2018, Olapeju Bolarinwa

DEDICATION

I dedicate this work to the Almighty God who sustained me through it all.

ACKNOWLEDGEMENTS

I would like to express my profound gratitude to my Lord Jesus Christ for His undeniable faithfulness that kept me through this program. I am sincerely grateful, Lord.

To my husband, Olufemi Daniel Bolarinwa, I appreciate your firm support through it all. I could not have asked for a better man in my life. I will always love you. Thank you for your understanding. Thank you for staying by me through the thicks and thin.

To God's heritage, Oluwalani and Oluwatoni, I am grateful to have you both. You are the sunshine in my world. You made this journey easier for me. I cherish those warm hugs that we shared. Thank you both for the "welcome home" song that cheered me up every evening, after a tiring day. I love you and cherish you both in my life.

To my Advisor, Dr. Cai, thank you for always believing in me. Thank you for those kind words of encouragement. I admire the level of understanding that you showed with every student in the lab. I appreciate your leadership and mentorship. Thank you for giving me a chance to prove myself.

To my committee members: Dr. Wayne Guida, Dr. James Leahy, Dr. Feng Cheng and Dr. Cao, I am grateful for your advisement. Thank you for sharing part of your valued time with me at USF. Thank you for believing in me.

To members of the Cai Lab, thank you for making this journey worthwhile. Thank you for always being there for me. Thank you for your help.

To my Parents and Parents-in-law, your words of encouragement were always timely. Thank you for your support all the way. You have always given me the feeling that we were into this together. You have always got my back. Oluwalani and Oluwatoni will never forget you. Thank you for always making yourself available anytime we call on you. I can boldly say that you are the best.

To my siblings - Olamide (Sister mi), Fisayo, Oluwaseyi (King), Oluwatosin (Queen) and Olufunmilayo (Princess), I am very grateful to have you. You all are the best. Thanks for those sincere concerns you expressed. I love you all.

To the Ogunade, Oloke and Owotoki families, thanks for your all time support. Thank you for your prayers, words of assurance and encouragement. I am grateful for the privilege to have you.

To my church family, I am sincerely grateful for all your prayers and words of encouragement. I love you all.

TABLE OF CONTENTS

List of Tables	iv
List of Figures	v
List of Abbreviations	ix
Abstract	xii
Chapter 1 : Introduction	1
1.1 Peptidomimetics.....	1
1.2 Protein-Protein Interactions (PPIs)	1
1.3 γ -AApeptides	3
1.4 Outline of the Dissertation	4
1.5 References.....	5
Chapter 2 : Sulfonyl- γ -AA Modified Peptides That Inhibit HIV-1 Fusion	7
2.1 Introduction.....	7
2.2 Results and Discussion	11
2.3 Conclusion	16
2.4 General Information.....	16
Peptide synthesis	16
Synthesis of sulfonyl- γ -AApeptides	16
Synthesis of Cbz-aminoethanesulfonyl chloride	16
Synthesis of Fmoc-sulfonyl- γ -AA1	17
Solid phase synthesis	18
Olefin metathesis and purification.....	19

Circular dichroism analysis.....	20
HIV-1 neutralization assay.	20
Protease stability assay.	21
2.5 References.....	24
Chapter 3 : γ -AApeptides –Based Small Molecule Ligands That Disaggregate Human	
Islet Amyloid Polypeptide	27
3.1 Introduction.....	27
3.2 Results and Discussion	29
3.3 Conclusion	42
3.4 Materials and Methods.....	43
Peptides synthesis	43
General information	43
Solid phase peptide synthesis.....	43
hIAPP sample preparation	45
Thioflavin T fluorescence assay	45
Transmission electron microscopy (TEM)	46
Atomic force microscopy (AFM)	46
Percentage inhibition	47
Cell viability/proliferation assay.....	47
3.5 References.....	50
Chapter 4 : Evaluation of the Sequence-Dependent Aggregation And Inhibitory	
Potential Of Islet Amyloid Polypeptide-Derived Retro-Peptides.....	53
4.1 Introduction.....	53
4.2 Results and Discussion	56
4.3 Conclusion	69
4.4 General information	70
Peptide synthesis.....	70
Congo red binding assay.....	70
Circular dichroism studies.	71
Thioflavin T fluorescence assay	71
Transmission electron microscopy (TEM)	72

Kinetic aggregation assay	72
4.5 References	73
Chapter 5 : Development of Potent Chemical Probes Targeting MPP8-H3K9me	
Interaction	75
5.1 Introduction.....	75
5.2 Results and Discussion	80
5.3 Conclusion	83
5.4 General information	83
Peptide synthesis.....	83
Synthesis of building blocks	85
Cell fractionation assay.....	87
5.5 References.....	87
Chapter 6 : Conclusion and Future Outlook	89
Appendix A: Publishing Rights	91

LIST OF TABLES

Table 2.1	Antiviral activity from Viral infection assay	14
Table 2.2	Enzymatic hydrolysis assay with chymotrypsin	15
Table 2.3	HPLC purities and retention time of peptides 1-4	23
Table 3.1	Percent Inhibition (Based on ThT Fluorescence assay) of HW-155,C1 and 1-8	30
Table 3.2	HPLC purities and retention time of peptides 1-8 and HW-155	48
Table 4.1	Peptide sequences of designed retro-peptides	56
Table 4.2	Molecular weight of peptides and their percent yield.....	73

LIST OF FIGURES

Figure 1.1	General structure of α -peptide and γ -AApeptide.....	4
Figure 2.1	Schematic illustration of the different regions of HIV-1 gp41.....	9
Figure 2.2	General structures of α -peptide, γ -AApeptides, and Sulfonyl- γ -AApeptides.....	10
Figure 2.3	C-HR derived peptides.....	12
Figure 2.4	CD spectra of peptides 1 – 4.....	13
Figure 2.5	Melting curve of peptides 1-4.....	13
Figure 2.6	The degradation curves of 1-4	15
Figure 2.7	Synthesis of Cbz-aminoethanesulfonylchloride	17
Figure 2.8	Synthesis of Fmoc-sulfonyl- γ -AA1.....	18
Figure 2.9	Solid phase synthesis of stapled peptides.....	19
Figure 2.10	^1H NMR (400 MHz, CDCl_3) and MS of Fmoc-sulfonyl- γ -AA1	22
Figure 2.11	^{13}C NMR (400 MHz, $\text{DMSO}-d_6$) of Fmoc-sulfonyl- γ -AA1.....	22
Figure 2.12	HPLC spectra of peptides 1-4.....	23
Figure 3.1	Peptide Sequences HW-155, control C1 and 1-8.....	29
Figure 3.2	Time-dependent ThT assay of hIAPP ₁₋₃₇ (10 μM) and various molar equivalents of 1	32

Figure 3.3	Time-dependent ThT assay of hIAPP ₁₋₃₇ (10μM) and various molar equivalents of 2	33
Figure 3.4	Time-dependent ThT assay of hIAPP ₁₋₃₇ (10μM) and various molar equivalents of 3	33
Figure 3.5	Time-dependent ThT assay of hIAPP ₁₋₃₇ (10μM) and various molar equivalents of 4	34
Figure 3.6	Time-dependent ThT assay of hIAPP ₁₋₃₇ (10μM) and various molar equivalents of 5	35
Figure 3.7	Time-dependent ThT assay of hIAPP ₁₋₃₇ (10μM) and various molar equivalents of 6	36
Figure 3.8	Time-dependent ThT assay of hIAPP ₁₋₃₇ (10μM) and various molar equivalents of 7	36
Figure 3.9	Time-dependent ThT assay of hIAPP ₁₋₃₇ (10μM) and various molar equivalents of 8	37
Figure 3.10	Time-dependent ThT assay of hIAPP ₁₋₃₇ (10μM) and various molar equivalents of HW-155	38
Figure 3.11	Time-dependent ThT assay of the disruption of hIAPP ₁₋₃₇ (10μM) preformed fibrils by 5 (100μM)	39
Figure 3.12	AFM image the disruption of hIAPP ₁₋₃₇ (10μM) preformed fibrils by 5 (100μM)	39
Figure 3.13	TEM images of hIAPP ₁₋₃₇ alone and in the presence of equimolar amount 2,3,4,5, and HW-155	40
Figure 3.14	Effects of peptides 2,3,4,5 and HW-155 on NIH-3T3 cells in CCK-8 cell viability assay	41
Figure 3.15	Evaluation of the potential of peptides 2,3,4,5 and HW-155 to improve the chances of cell survival in the presence of hIAPP ₁₋₃₇ amyloid.	42

Figure 3.16	Synthesis of γ -AApeptide building block/monomeric unit.	43
Figure 3.17	Solid Phase synthesis scheme for HW-155,C1 and 1-8.....	45
Figure 3.18	HPLC spectra of peptides 1-8 and HW-155	50
Figure 4.1	A sample L-peptide and its analogues	55
Figure 4.2	Congo red spectra of retro-peptides at time t = 0h	60
Figure 4.3	Congo red spectra of retro-peptides at time t = 28h	60
Figure 4.4	Congo red spectra of retro-peptides at time t = 43h	61
Figure 4.5	ThT assay for aggregation of retro-peptides	61
Figure 4.6	TEM images of hIAPP ₂₂₋₂₉ , and peptides r1 – r8.....	62
Figure 4.7	CD spectra of peptides consisting of alternating L- and D-amino acid units	63
Figure 4.8	CD spectra of peptides consisting of all D-amino acid units (r5, r6, and r8)	63
Figure 4.9	CD spectra of peptides consisting of all D-amino acid units (r7).....	64
Figure 4.10	Kinetic aggregation assay for all peptides.	64
Figure 4.11	ThT inhibition assay for r1.	65
Figure 4.12	ThT inhibition assay for r2.	65
Figure 4.13	ThT inhibition assay for r3.	66
Figure 4.14	ThT inhibition assay for r4.	66
Figure 4.15	ThT inhibition assay for r5.	67

Figure 4.16	ThT inhibition assay for r6.	67
Figure 4.17	ThT inhibition assay for r7.	68
Figure 4.18	ThT inhibition assay for r8.	68
Figure 4.19	ThT inhibition assay for hIAPP ₂₂₋₂₉	69
Figure 5.1	Peptides designed to disrupt H3K9me3-MPP8 interaction.	78
Figure 5.2	Western blot from cell fractionation studies (PJ-164-13 – PJ-164-17).	79
Figure 5.3	Structure of designed cell-penetrating and cyclic peptides.....	80
Figure 5.4	Structure of designed cyclic peptides.	81
Figure 5.5	Western blot of cell fractionation assay for peptides PJ 164-18 – PJ 164-24.....	82
Figure 5.6	Synthetic scheme for the reductive alkylation of Lysine.....	86

LIST OF ABBREVIATIONS

HIV	Human immunodeficiency virus
TFA	Trifluoroacetic acid
TIS	Triisopropylsilane
HPLC	High-performance liquid chromatography
ACN	Acetonitrile
MALDI-TOF	Matrix-assisted laser desorption ionization time of flight
HOBt	1-hydroxybenzotriazole monohydrate
DIC	Diisopropylcarbodiimide
DMF	Dimethylformamide
DIPEA	Diisopropylethylamine
Fmoc	Fluorenylmethyloxycarbonyl (chloride)
Alloc	Allyl chloroformate
CCK-8	Cell counting kit 8
TEM	Transmission electron microscopy
AFM	Atomic force microscopy
ThT	Thioflavin-t
OBOC	One-bead-one-compound
DMSO	Dimethyl sulfoxide
CDCl ₃	Deuterated chloroform

NMR	Nuclear magnetic resonance
PCR	Polymerase chain reaction
CD	Circular dichroism
RCM	Ring-closing metathesis
DCE	Dichloroethane
EtOAc	Ethyl acetate
Boc	tert-Butyloxycarbonyl
Cbz	Benzyl chloroformate
LC/MS	Liquid chromatography-mass spectrometry
AZT	Azidothymidine
N-HR	N-heptad repeat
C-HR	C-heptad repeat
6-HB	Six helical bundle
PPI	Protein-protein interaction
SPPS	Solid phase peptide synthesis
CO ₂	Carbon dioxide
DMEM	Dulbecco's modified eagle's medium
T2DM	Type 2 diabetes mellitus
PBS	Phosphate buffered saline
DNA	Deoxyribonucleic acid
RNA	Ribonucleic acid
PTM	Post – translational modifications
EMT	Epithelial- mesenchymal transition

MPP8	M-phase phosphoprotein 8
NE	Nuclear extract
NP	Nuclear pellet
TBTU	2-(1H-Benzotriazole-1-yl)-1,1,3,3-tetramethylaminium tetrafluoroborate
MEOH	Methanol
HCl	Hydrochloric acid
M	Molarity

ABSTRACT

Proteins can be described as the “machineries” responsible for almost all tasks in the levels of organizational complexity in multi-cellular organisms namely: the cells, tissues, organs and systems. Any disorder in the function of a protein at any of these levels could result in disease, and a study of protein function is critical to understanding the pathological features of the disease at the molecular level. A quick glance at these abundantly present proteins reveals two striking features: large diversity of biological function, and the variations in structural complexity, which varies from simple random coils, to turns and helices, and on to structured assemblies of turns, helices and sheets.

Over the past few years, more research efforts have been channeled to the application of synthetic research to protein dynamics, most especially in disease conditions. This provides insight into the design and development of chemical tools capable of modulating protein functions .Some of such tools include small molecules, peptides and peptidomimetics.

In this work, we have described the application of these tools to three (3) different disease systems topping the list of incurable diseases: HIV, Diabetes, and Cancer. We have designed and developed chemical probes to facilitate a better understanding of major “culprit” proteins underlying the pathological conditions associated with these diseases. Our designed chemical probes were capable of modulating protein functions by producing the desired effects: inhibition of protein-protein interactions.

CHAPTER 1 : INTRODUCTION

1.1 Peptidomimetics

In the last three decades, peptides have gained a broader application, especially for therapeutic interventions.¹ The relevant application of these macromolecules to nature, and their facile and well-established solid phase synthesis (SPPS) have encouraged their study, and proven applicability in medicinal chemistry and drug discovery.^{2,3} Even though the solubility of peptides is strictly sequence-dependent, they generally exhibit better solubility profiles than classical medicinal chemistry therapeutics, including low molecular weight compounds and small molecules.⁴ Despite their abundance and relative ease of accessibility, their application is limited by major drawbacks including protease degradation, poor oral availability, short plasma half-life.¹

However, several strategies have been explored to fully or partially address these concerns. These include backbone modification,^{5, 6, 7} cyclization,⁸⁻¹¹ PEGylation,¹² lipidation,^{13, 14} and stapling.^{15, 16} Another very effective approach is the concept of peptidomimetics.¹⁷

Peptidomimetics are small, protein-like chains that are capable of mimicking native analogs with presumably better pharmacokinetic and pharmacological profiles.^{18, 19}

1.2 Protein-Protein Interactions (PPIs)

Protein-protein interactions (PPIs) are short-lived interactions between protein partners. The driving force for these interactions could be one or more of these: electrostatic and hydrophobic interactions, hydrogen bonding, and Van der Waals attraction. Compared to enzyme-substrate interactions, the druggability of PPIs is very poor because they lack well defined binding

pockets.²⁰ For instance, two proteins can interact with each other over large areas and in a less defined way as seen in transcription factors and their co-activators.

PPIs form the basis of a wide range of crucial cellular processes, hence, they are indispensable to human existence.²⁰ An appealing and innovative strategy to drug discovery is the disruption and destabilization of PPIs. However, this comes with a lot of challenges including difficulty in screening assays due to lack of measurable output, and poor druggability.²¹ These bottlenecks have limited research in this area as many small molecules cannot span the entire length of the interacting flat surfaces in PPIs. In addition, large molecules cannot gain access to PPIs targets in cell compartments.²⁰ The short-term nature of these interactions also makes quantitative evaluations difficult.

Due to these challenges, only one small molecule PPI inhibitor have been approved till date: Venetoclax (Venclexta).^{22, 23} Venetoclax (Venclexta) is a BH3-mimetic developed by AbbVie and Genentech, and approved for the treatment of Chronic Lymphocytic Leukaemia (CLL). This was approved in 2016 and works by inhibiting the interaction between BCL-2, a BH3-only protein, and the pro-apoptotic proteins, BAK and BAX. This inhibition results in the apoptosis of CLL cells bearing the 17p deletion.²⁴

Despite these shortcomings, intensive and vigorous research in finding inhibitors of protein-protein interactions has provided a ray of hope over the past few years. In fact, the recent successes recounted in this area has indicated that protein-protein interfaces might be easier to manipulate than previously thought. These studies unraveled the ‘hotspots’ on protein contact surfaces and developed compact small molecules that bind tighter and deeper within the contact surface than the contact atoms of the natural protein partner.²⁵⁻²⁹ High-throughput methods that

enhance easy screening and accurate qualitative characterization of protein-protein interactions have been developed.³⁰⁻³²

The identification of epitopes on the interacting surface of proteins (hotspots) have paved way for the design of peptides and peptidomimetic inhibitors of protein-protein interactions. In recent times, Peptide fragments consisting of the contact amino acid residues on partner proteins have been designed.³³ On several occasions, alanine scanning has been used to further detect the most relevant amino acid in the hotspot.²⁹ A similar but more effective approach in identifying protein-protein interactions modulators is peptidomimetics. Peptidomimetics that mimic the functional epitope of protein complexes have been developed.³⁴⁻³⁹

The application of peptides and peptidomimetics has advanced the course of medicinal chemistry and drug discovery as it unlocks potential agents that could target a broad spectrum of proteins that are implicated in many pathogenic diseases.

1.3 γ -AApeptides

Over the past two decades, peptidomimetics have found important applications in chemical biology and drug discovery.¹⁹ Our recently developed peptidomimetics, γ -AApeptides are oligomers of N-acylated-N-aminoethyl amino acids, and are capable of accommodating a second side chain functional group, in addition to the chiral side chain (Figure 1.1).⁴⁰ This means that a γ -AApeptide monomer is similar to a canonical dipeptide residue. In addition to having other desirable features of a typical peptidomimetic, a unique advantage that γ -AApeptides offer is their limitless derivatization potential, which is not commonly found in most reported peptidomimetics.

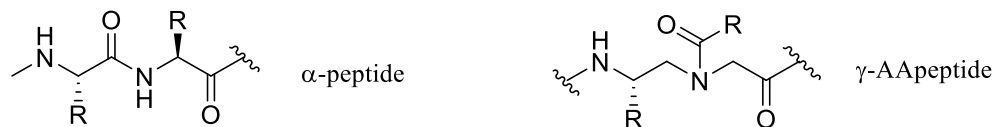


Figure 1.1 General structure of α -peptide and γ -AApeptide

1.4 Outline of the Dissertation

In this dissertation, we discuss the design, synthesis, and therapeutic applications of peptides and our recently developed peptidomimetic scaffold, γ -AApeptides, and its derivatives as chemical probes for protein interactions in disease conditions.

In chapter 2, we describe the design of a modified peptide that shows great HIV-fusion inhibitory activity.

In chapter 3, we discuss the design of γ -AApeptide –based small molecule ligands that inhibit the formation of pancreatic amyloid deposits in Type 2 diabetes mellitus.

In chapter 4, we describe the design of retro-D peptides based on the amyloid forming unit in amylin, the Type 2 diabetes amyloid. We also evaluated their aggregation propensity and fibril morphology, and tested their inhibitory activity.

In chapter 5, we describe the design and development of short peptide antagonists of the MPP8-H3K9me interaction, which is implicated in many cancers.

In chapter 6, we summarize our research findings and gave the future directions of all studies conducted in this research.

1.5 References

1. P. Vlieghe, V. Lisowski, J. Martinez and M. Khrestchatisky, *Drug discovery today*, 2010, **15**, 40-56.
2. R. B. Merrifield, *Journal of the American Chemical Society*, 1963, **85**, 2149-2154.
3. B. L. Bray, *Nature Reviews Drug Discovery*, 2003, **2**, 587.
4. Z. Antosova, M. Mackova, V. Kral and T. Macek, *Trends in Biotechnology*, 2009, **27**, 628-635.
5. R. W. Cheloha, A. Maeda, T. Dean, T. J. Gardella and S. H. Gellman, *Nature Biotechnology*, 2014, **32**, 653.
6. B. D. Welch, A. P. VanDemark, A. Heroux, C. P. Hill and M. S. Kay, *Proceedings of the National Academy of Sciences*, 2007, **104**, 16828-16833.
7. M. Liu, C. Li, M. Pazgier, C. Li, Y. Mao, Y. Lv, B. Gu, G. Wei, W. Yuan, C. Zhan, W.-Y. Lu and W. Lu, *Proceedings of the National Academy of Sciences*, 2010, **107**, 14321-14326.
8. R. M. Freidinger, *Journal of Medicinal Chemistry*, 2003, **46**, 5553-5566.
9. M. L. Huang, S. B. Y. Shin, M. A. Benson, V. J. Torres and K. Kirshenbaum, *ChemMedChem*, 2012, **7**, 114-122.
10. L. H. J. Kleijn and N. I. Martin, Springer Berlin Heidelberg, Berlin, Heidelberg, DOI: 10.1007/7355_2017_9, pp. 1-27.
11. A. Zorzi, K. Deyle and C. Heinis, *Current Opinion in Chemical Biology*, 2017, **38**, 24-29.
12. F. M. Veronese, *Biomaterials*, 2001, **22**, 405-417.
13. K. R. Meena and S. S. Kanwar, *BioMed Research International*, 2015, **2015**, 9.
14. Y. Hu, M. N. Amin, S. Padhee, R. E. Wang, Q. Qiao, G. Bai, Y. Li, A. Mathew, C. Cao and J. Cai, *ACS medicinal chemistry letters*, 2012, **3**, 683-686.
15. G. H. Bird, N. Madani, A. F. Perry, A. M. Princiotto, J. G. Supko, X. He, E. Gavathiotis, J. G. Sodroski and L. D. Walensky, *Proceedings of the National Academy of Sciences*, 2010, **107**, 14093-14098.
16. G. H. Bird, A. Irimia, G. Ofek, P. D. Kwong, I. A. Wilson and L. D. Walensky, *Nature structural & molecular biology*, 2014, **21**, 1058-1067.
17. I. Avan, C. D. Hall and A. R. Katritzky, *Chemical Society Reviews*, 2014, **43**, 3575-3594.
18. G. Andreas and K. Burkhard, *European Journal of Organic Chemistry*, 2009, **2009**, 5099-5111.
19. A. Jung-Mo, A. B. Nicholas, T. M. Mary and D. J. Kim, *Mini-Reviews in Medicinal Chemistry*, 2002, **2**, 463-473.
20. J. A. Wells and C. L. McClendon, *Nature*, 2007, **450**, 1001.
21. A. A. Ivanov, F. R. Khuri and H. Fu, *Trends in Pharmacological Sciences*, 2013, **34**, 393-400.
22. D. R. Green, *Cell*, 2016, **165**, 1560.
23. A. C. King, T. J. Peterson, T. Z. Horvat, M. Rodriguez and L. A. Tang, *Annals of Pharmacotherapy*, 2017, **51**, 410-416.
24. Y. Zhu, S. Su, L. Qin, Q. Wang, L. Shi, Z. Ma, J. Tang, S. Jiang, L. Lu, S. Ye and R. Zhang, *Sci Rep*, 2016, **6**, 31983.
25. C. D. Thanos, W. L. DeLano and J. A. Wells, *Proceedings of the National Academy of Sciences*, 2006, **103**, 15422-15427.

26. M. R. Arkin, M. Randal, W. L. DeLano, J. Hyde, T. N. Luong, J. D. Oslob, D. R. Raphael, L. Taylor, J. Wang, R. S. McDowell, J. A. Wells and A. C. Braisted, *Proceedings of the National Academy of Sciences*, 2003, **100**, 1603-1608.
27. D. Fayne, *Drug Discovery Today: Technologies*, 2013, **10**, e467-e474.
28. J. W. Tilley, L. Chen, D. C. Fry, S. D. Emerson, G. D. Powers, D. Biondi, T. Varnell, R. Trilles, R. Guthrie, F. Mennona, G. Kaplan, R. A. LeMahieu, M. Carson, R.-J. Han, C. M. Liu, R. Palermo and G. Ju, *Journal of the American Chemical Society*, 1997, **119**, 7589-7590.
29. M. I. S., F. P. A. and R. M. J., *Proteins: Structure, Function, and Bioinformatics*, 2007, **68**, 803-812.
30. Y. Du, Z. Nikolovska-Coleska, M. Qui, L. Li, I. Lewis, R. Dingleline, J. A. Stuckey, K. Krajewski, P. P. Roller, S. Wang and H. Fu, *Assay and Drug Development Technologies*, 2011, **9**, 382-393.
31. J. T. Heeres and P. J. Hergenrother, *Chemical Society Reviews*, 2011, **40**, 4398-4410.
32. D. D. Dudgeon, S. N. Shinde, T. Y. Shun, J. S. Lazo, C. J. Strock, K. A. Giuliano, D. L. Taylor, P. A. Johnston and P. A. Johnston, *Assay and Drug Development Technologies*, 2010, **8**, 437-458.
33. J. Eichler, *Current Opinion in Chemical Biology*, 2008, **12**, 707-713.
34. J. Garner and M. M. Harding, *Organic & biomolecular chemistry*, 2007, **5**, 3577-3585.
35. J. M. Mason, *Future Medicinal Chemistry*, 2010, **2**, 1813-1822.
36. H. Sun, Z. Nikolovska-Coleska, C.-Y. Yang, D. Qian, J. Lu, S. Qiu, L. Bai, Y. Peng, Q. Cai and S. Wang, *Accounts of Chemical Research*, 2008, **41**, 1264-1277.
37. D. Seebach and J. Gardiner, *Accounts of Chemical Research*, 2008, **41**, 1366-1375.
38. J. A. Robinson, *Current Opinion in Chemical Biology*, 2011, **15**, 379-386.
39. J. A. Robinson, *Accounts of Chemical Research*, 2008, **41**, 1278-1288.
40. Y. Niu, Y. Hu, X. Li, J. Chen and J. Cai, *New Journal of Chemistry*, 2011, **35**, 542-545.

CHAPTER 2 : SULFONO- Γ -AA MODIFIED PEPTIDES THAT INHIBIT HIV-1 FUSION

2.1 Introduction

The global HIV statistics of 2015 revealed that approximately 36.7 million people worldwide are living with human immunodeficiency virus (HIV) and over 2.1 million new cases of HIV infection was recorded¹ annually. The envelope glycoprotein of human immunodeficiency virus type 1 (HIV-1) encoded by the HIV *env* gene, is a somewhat stable membrane fusion machine which exists as a trimeric complex (gp160)₃. This precursor trimer is proteolytically processed by furin into gp120 and gp41 heterodimers². During the membrane fusion process, gp41 forms a fusion active six-helix bundle (6-HB) with a hydrophobic pocket^{3 4}. In this six-helix bundle, the amino-terminal heptad repeat (N-HR) forms a central trimeric coiled-coil core whereas the trimeric helical carboxyl terminal repeat (C-HR) wraps around and interact with it in an antiparallel fashion⁵. This six-helix bundle brings into close proximity and facilitates the fusion of the viral and host cell membranes (Figure 2.1)^{6,7}. The mutual dependence of N-HR and C-HR on each other in the 6-HB formation during viral entry makes them very important targets for fusion inhibitor design. Indeed, Targeting viral entry and fusion process of enveloped virus remains a very appealing therapeutic strategy due to its relative accessibility. Potent inhibitors which block these specific interactions that are mandatory for HIV-1 viral entry, including small molecules⁸⁻¹⁰, engineered peptides¹¹, artificially designed peptidomimetics¹²⁻¹⁵, etc., have been discovered. However, peptides derived from N-HR mostly show weak inhibitory activity if the design does not promote trimerization of N-HR peptides^{5, 16}. Only typical N-HR constructs forming stable trimers can efficiently target HIV-1 fusion¹⁷⁻²⁰. As a result, C-HR derived peptides have been studied

extensively in the therapeutic search for potential fusion inhibitors. Examples include α -helical peptides such as enfuvirtide (T20)^{21, 22} and C34²³⁻²⁶. Enfuvirtide got market approval as the only HIV-1 fusion inhibitor for clinical use and works by competitively binding the N-HR thereby blocking the formation of the six-helical bundle required for fusion. It is very active against various HIV-1 strains including those resistant to reverse transcriptase and protease inhibitors^{22, 27}. It is similar in design to a segment of C-HR comprising amino acids 127 to 162 of the C-terminal end²⁸²⁹. Although T20 has great anti-HIV activity, it is prone to induce drug resistance through mutations within the N-HR sites. Additionally, its poor bioavailability and large dose requirements complicate its therapeutic use^{30, 31}. Similar to T20, C34 also has sequence homology to the C-HR. Due to a 22-amino acid overlap between T-20 and C34 peptides, HIV-1 has also developed major mutations for C34 resistance in vitro³¹. Meanwhile, its bioavailability was still a concern due to its canonical peptide backbone.

To overcome the problems posed by T20 and other similar HIV fusion inhibitors, great efforts have been made to optimize the fusion inhibitors derived from the C-HR helical region of gp41 to suppress the emergence of resistant strains and increase the in-vivo stability and N-HR binding affinity³²⁻³⁴³⁵. One approach is to introduce electrostatic constraints into peptides to improve helicity and antiviral activity profile. This entails the substitution of charged and hydrophilic amino acids such as glutamic acid (E) and Lysine (K) at *i* and *i*+4 positions in the solvent-accessible site of C34 and its short variants^{4, 36-39}. In a six helix bundle, C-HR interact with N-HR with amino acid residues at their *a* and *d* positions of the heptad repeat (Figure 2.1). These residues are known to be critical for molecular recognition between both heptad repeats while residues at positions *b*, *c*, *f* and *g* are exposed to the solution and are almost non-crucial for gp41 C-HR and N-HR interaction⁶.

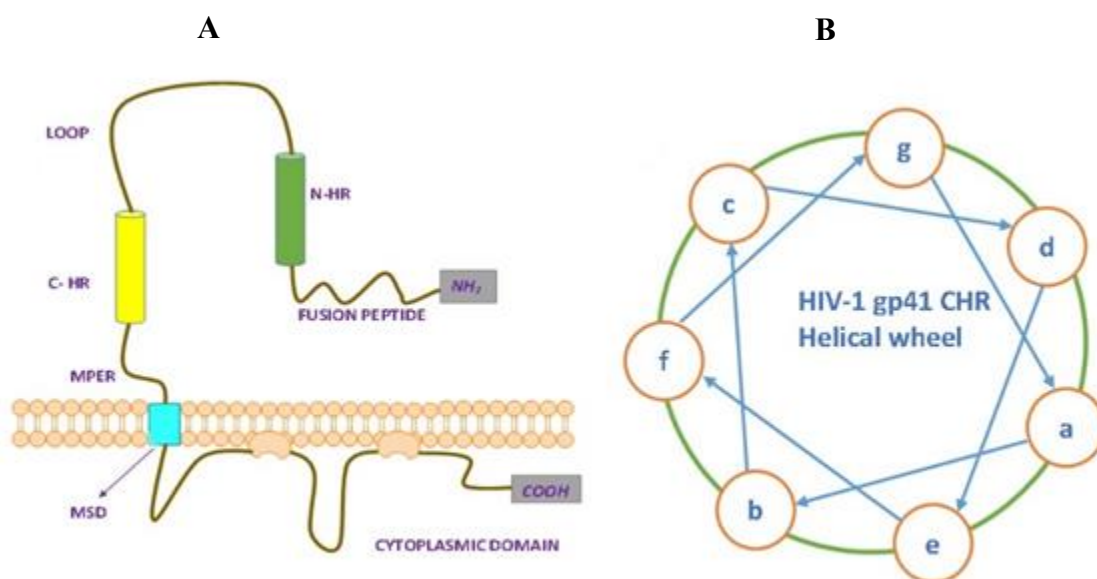


Figure 2.1 (A) Schematic illustration of the different regions of HIV-1 gp41. N-HR: N Heptad Repeat, C-HR: C Heptad Repeat, MPER: Membrane Proximal Ectodomain Region, MSD: Membrane Spanning Domain and. (B) Schematic illustration of the helical wheel of gp41 C-HR.

However, the residues at these positions are very critical for solubility and stability and they have great effects on the in-vivo activity and druggability of peptide fusion inhibitors. These engineered electrostatic interactions are helix enhancers and have significantly improved the solubility, helicity and potency of such derived peptides^{4, 36, 37, 40}. An additional approach is to introduce conformational restraints and substitution with non-proteinogenic amino acids in C-HR derived peptide mimics. For instance, peptidomimetics with unnatural amino acids and building blocks have been reported to successfully mimic the molecular interaction between gp41 C-HR and N-HR^{12-15, 29, 33, 34, 41-46}. Peptide mimics that targets gp41 N-HR include D-peptides^{15, 17}, unnatural foldamers^{44, 45}, and covalently restrained α -helices^{13, 14, 46}. These peptide mimics have generated highly potent fusion inhibitors with outstanding in-vivo stability..

Sulfono- γ -AApeptides are a sub-class of γ -AApeptides that are oligomers of *N*-acylated-*N*-aminoethyl amino acids⁴⁷⁻⁴⁹. The replacement of carboxylic acids with sulfonyl chlorides in γ -AApeptides produces sulfono- γ -AApeptides (Figure. 2.2). They have enormous potential in functional group diversity. Like γ -AApeptides, sulfono- γ -AApeptides are able to display the same number of side chains as conventional peptides of equal length, endowing them with the ability to mimic bioactive peptides. As evidenced by their crystal structures, sulfono- γ -AApeptides possess an intrinsic folding propensity which is most likely a result of the bulkiness of the tertiary sulfonamide group besides intramolecular hydrogen bonding⁵⁰. Their optical analysis by circular dichroism and 2D-NMR also supports their well-crafted helical conformation⁵⁰. To explore the potential of sulfono- γ -AApeptides for their ability to modulate HIV-1 fusion at the cell entry stage, we designed a few peptides containing sulfono- γ -AA residues. Our previous findings suggested that replacement of amino acid residues with sulfono- γ -AA residues could retain sequence helicity⁵¹. Thus, we envisioned these sequences were still capable of mimicking gp41.

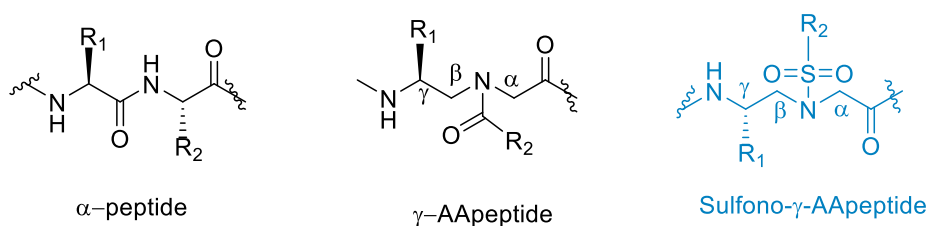


Figure 2.2 General structures of α -peptide, γ -AApeptides, and Sulfono- γ -AApeptides

Peptide **1** is a 24-residue electrostatically constrained C-HR derived peptide with MT-hook, which was previously reported to be an active fusion inhibitor³³. Thus it was used as the template sequence for modification (Figure 2.3)³³. As the initial attempt, we employed a combination of

sulfono γ -AA residue substitution and single hydrocarbon stapling to identify three peptides: **2**, **3** and **4**. **3** and **4** contain a sulfono- γ -AA1 residue at the 22nd position while only **2** and **4** contain hydrocarbon stapling between residues X at the 4th and 8th position (Figure 2.3).

2.2 Results and Discussion

We first assessed the helicity of the sequences by CD. As shown in Figure 2.4, interestingly, both **1** and **3** exhibited comparable helical folding propensity with characteristic minima at both 207 and 222 nm suggesting the existence of probable α -helical conformation. This suggests that incorporation of sulfono- γ -AA residue did not alter helicity significantly. As expected, after hydrocarbon stapling, both **2** and **4** clearly showed a significant increase in helicity compared to their unstapled counterparts, **1** and **3** (Figure 2.4). This is consistent with the previous findings that $i, i+4$ hydrocarbon stapling enhances the α -helicity of peptides.^{46, 52, 53} These findings are corroborated by the thermal stability studies (Figure 2.5). **1** and **3** showed similar behavior at low temperature. However, **3** is more stable than **1** at temperature higher than 42°C. Also, **2** demonstrated increased stability than **4**. Overall, hydrocarbon stapling improved the helicity and thermal stability profiles of **2** and **4**

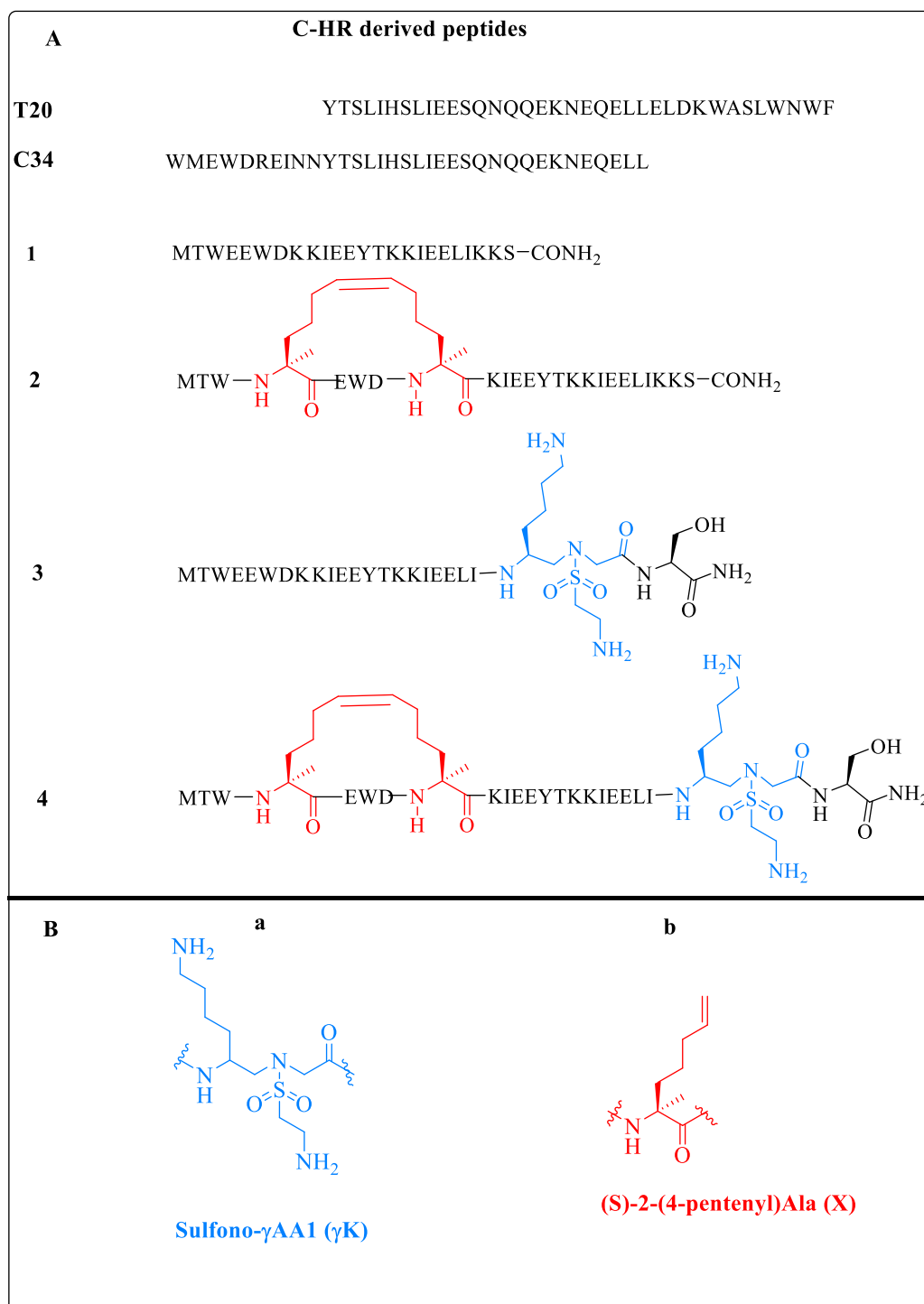


Figure 2.3 (A) C-HR derived peptides. **Peptide 1** is MT-SC22EK and was first reported in ref. ³³; (B) The structure of **sulfono- γ AA1(γ K)** (S)-N-((2-aminoethyl)sulfonyl)-N-(2,6-diaminoethyl)glycine and **(S)-2-(4-pentenyl)Ala residue (X)** substituted at *i* and *i*+4 positions.

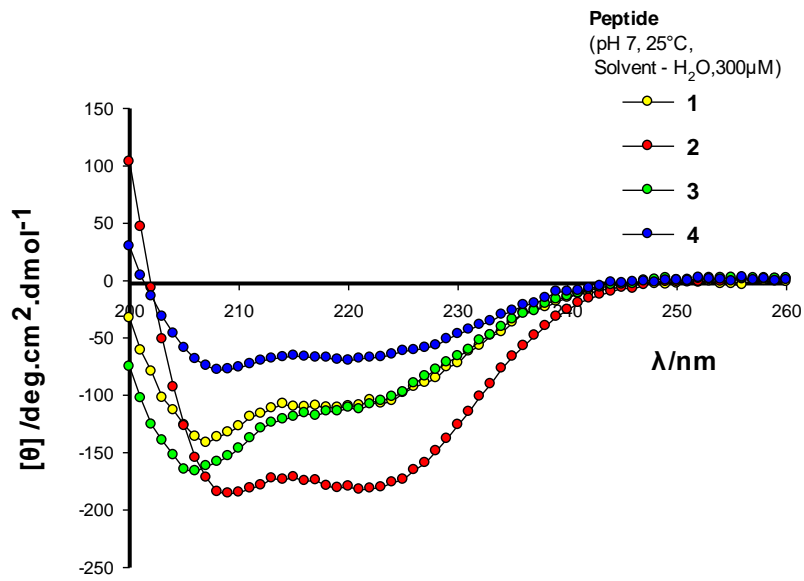


Figure 2.4 CD spectra of peptides 1 – 4

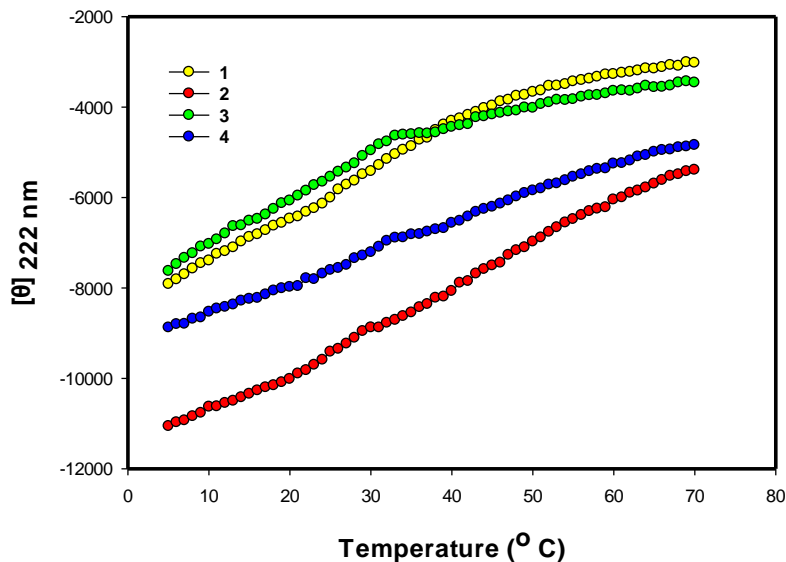


Figure 2.5 Melting curve of peptides 1-4

We next examined the antiviral activity of these sulfono- γ -AA containing peptides by viral infection assay⁵⁴. Conformationally stabilized pre-formed recombinant *env* trimers derived from various subtypes of HIV-1 strains⁵⁵ were used in the assay. Both (enfuvirtide) T20 and AZT were

also tested for comparison. Intriguingly, both **3** and **4** displayed more potent antiviral activity in most tested subtypes including CZA97, B41, BG505, SF162 and DU422 than the unsubstituted peptide **1**(control) and stapled peptide **2**. This indicates that the introduction of the peptidomimetic monomer, sulfono- γ -AA1, improved the interaction of peptide 3 and 4 with the N-HR of gp41, resulting in the inhibition of six-helical bundle formation. It is noteworthy that antiviral activity is not strictly dependent on secondary structures as evidenced by the obtained results (Table 2.1), as **3** and **4** exhibited comparable antiviral activity. All tested peptides showed comparable or greater anti-HIV activity than enfuvirtide (T20), a fusion inhibitor and AZT, a reverse transcriptase inhibitor which are currently being used in the clinics for the treatment of the symptomatic disease (Table 2.1). Thus, **3** and **4** emerged to be the most active with the best antiviral activity across all strains tested.

Table 2.1 Antiviral activity from Viral infection assay

IC50 (nM)	CZA97	B41	BG505	SF162	MN	DU422
1	6.8±1.6	181.1±89.1	15.2±0.2	11.3±2.2	102.4±29.9	14.8±0.3
2	7.6±1.0	210.8±58.9	14.0±0.5	15.6±0.9	67.1±9.1	16.0±1.1
3	4.6±0.1	118.8±4.0	9.0±0.2	7.2±1.8	77.9±2.4	6.0±2.7
4	6.5±0.8	171.3±4.6	9.7±2.6	11.4±0.8	51.2±10.2	11.3±0.1
T20	941.0±328.3	214.6±16.2	18.4±10.1	23.9±2.1	6.5±0.6	56.0±1.6
AZT	184.6±26.4	106.4±16.8	84.0±1.8	109.6±23.5	194.1±1.6	183.3±1.9

To directly interrogate the effect of sulfono- γ AA1 substitution and hydrocarbon stapling on proteolytic cleavage, we used LC/MS to identify proteolytic fragments generated by the digestion of our peptide panels with chymotrypsin (Figure 2.6). After 10 mins, **2** and **4**

demonstrated greater stability to chymotrypsin than **1** and **3**, suggesting stapling lead to sequences with increased stability. It is noted that **1** proved better than **3** (Figure 2.6 and Table 2.2), which may be because the inclusion of sulfono- γ -AA residue slightly altered the helicity, making it easier to be hydrolyzed. However, after backbone stapling, still possessing one sulfono- γ -AA residue, **4** exhibited almost similar resistance to proteolytic degradation as **1**, indicating that the introduction of unnatural residue could enhance stability of the sequence.

Table 2.2 Enzymatic hydrolysis assay with chymotrypsin

Peptide	% remaining after 10 mins
1	53.3
2	69.3
3	17.6
4	57.2

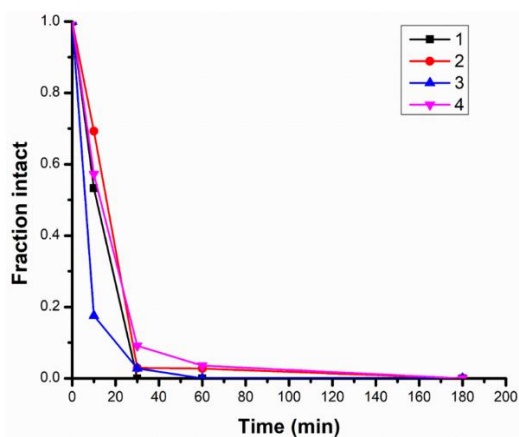


Figure 2.6 The degradation curves of 1-4

2.3 Conclusion

To summarize, although the daunting challenges hampering the clinical applications of enfuvirtide (T20) has limited the repository of active peptide-fusion inhibitors, the possibility of incorporating non-natural scaffolds may ultimately usher in new generation of peptide –fusion inhibitors with great therapeutic potential and improved protease resistance. Although our current design did not yield peptides with enhanced stability toward proteolysis, our study reveals that sulfono- γ -AA modified peptides could be used for the development of more potent anti-HIV agents. Furthermore, it is known that homogeneous sulfono- γ -AApeptides are completely resistant to enzymatic degradation and they possess remarkable helical propensity, we envision that we could use homogeneous sulfono- γ -AApeptides to design GP41 mimetics in the future. Additionally, the strategy implemented herein not only provide ideas for future HIV-1 inhibitor design, but may also be explored for the protein-protein interaction inhibitor (PPII) design.

2.4 General Information

Peptide Synthesis

All peptides used in this study were synthesized by the standard Fmoc-based solid phase peptide synthesis protocol using the Burrell Wrist-Action shaker. All Fmoc protected α -amino acids and Rink amide resin (0.7mmol/g, 200-400 mesh) were purchased from Chem-Impex International, Inc. All other Solvents and reagents were purchased from either Sigma Aldrich or Fisher Scientific and used without further purification. The peptides were analyzed and purified on a Waters Breeze 2 HPLC System, and then lyophilized on a Labconco Lyophilizer

Synthesis of sulfono- γ -AApeptides

Synthesis of Cbz-aminoethanesulfonyl chloride

Taurine (5g) and NaOH (2.5 eq) were dissolved in water and was kept stirring at 0°C. Benzylchloroformate (5.8 eq) was mixed with Dioxane and added dropwise to the solution. The ice bath was then removed and the reaction was stirred for 1h. The solution was washed with

EtOAc three times. The aqueous layer was co-evaporated with Toluene (2 times), Ethanol (once) and DCM (3 times). The resulting white solid, Cbz-protected aminoethane sodium sulfonate was suspended in EtOAc and filtered. To the white solid, Thionyl Chloride (10eq) and DMF (3 drops) were added and the reaction was refluxed for three hours and then concentrated on rotavap to obtain the Cbz-protected aminoethanesulfonyl chloride (Figure 2.7).

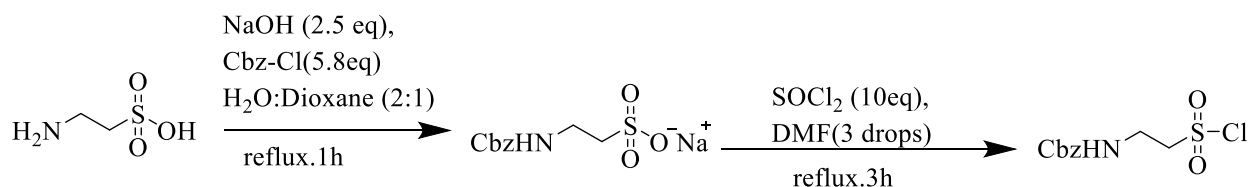


Figure 2.7 Synthesis of Cbz-aminoethanesulfonylchloride

Synthesis of Fmoc-sulfonyl- γ -AA1

Fmoc-Lysine amino aldehyde and Glycine benzyl ester were dissolved in methanol. Triethylamine was added and the reaction was stirred for one hour. Sodium cyanoborohydride was then added to the reaction and left to stir for another hour. The solution was concentrated, extracted with EtOAc and further concentrated on the rotavap. The crude secondary amine was purified on silica gel with Hexanes/EtOAc (1:1) as eluent. After that, the secondary amine was dissolved in DCM, to which Cbz-protected aminoethanesulfonylchloride and DIPEA were added. The reaction was stirred overnight and the resulting product was purified on silica gel (eluent was hexanes/EtOAc 2:1). Next, hydrogenation was done in methanol and under hydrogen with 20% Pd-C for 1 h to remove the benzyl and carbamate group to yield the mono-Boc protected Fmoc-sulfonyl- γ -AA1. Boc protection of the amino group on the sulfonyl side chain was achieved by adding Boc anhydride in THF to a stirred solution of Fmoc-sulfonyl- γ -AA1 (Boc) and NaHCO₃ in water in a dropwise manner. The reaction was allowed to continue overnight at room temperature. 1N citric acid was added, followed by extraction with EtOAc and drying over

Na₂SO₄. The solution was then concentrated and purified on silica gel. The product, Fmoc-sulfonyl- γ -AA1 was eluted with Hexanes/EtOAc 1:1 to give a white solid (Figure 2.8).

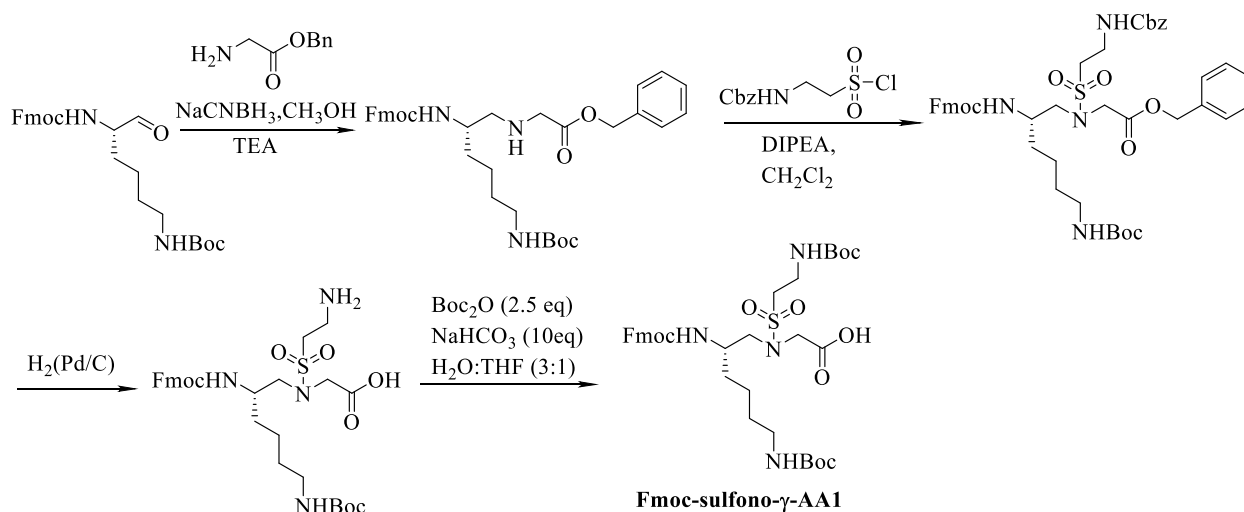


Figure 2.8 Synthesis of Fmoc-sulfonyl- γ -AA1.

Solid Phase synthesis.

The synthesis was conducted on 200 mg Rink amide resin (0.7 mmol/g) at room temperature and atmospheric pressure. The Fmoc protecting group was removed by treatment with 3mL 20% Piperidine in DMF solution for 15 mins(x2). The resin was washed with DCM and DMF (three times each). A solution of Fmoc-aa-OH/ Fmoc-sulfonyl- γ -AA1/ Fmoc-(S)-2-(4-pentenyl)Ala-OH (2 eq), HOBt (4 eq) and DIC (4 eq) was first premixed in 2mL DMF and then transferred into the peptide vessel containing the deprotected resin. The mixture was allowed to shake for 4h. The resin is then washed with DCM and DMF (3x each) and capped with acetic anhydride (1mL) and Pyridine (2mL) for another 15 min. After capping, deprotection was done and the cycle was repeated until the desired product was obtained (Figure 2.9).

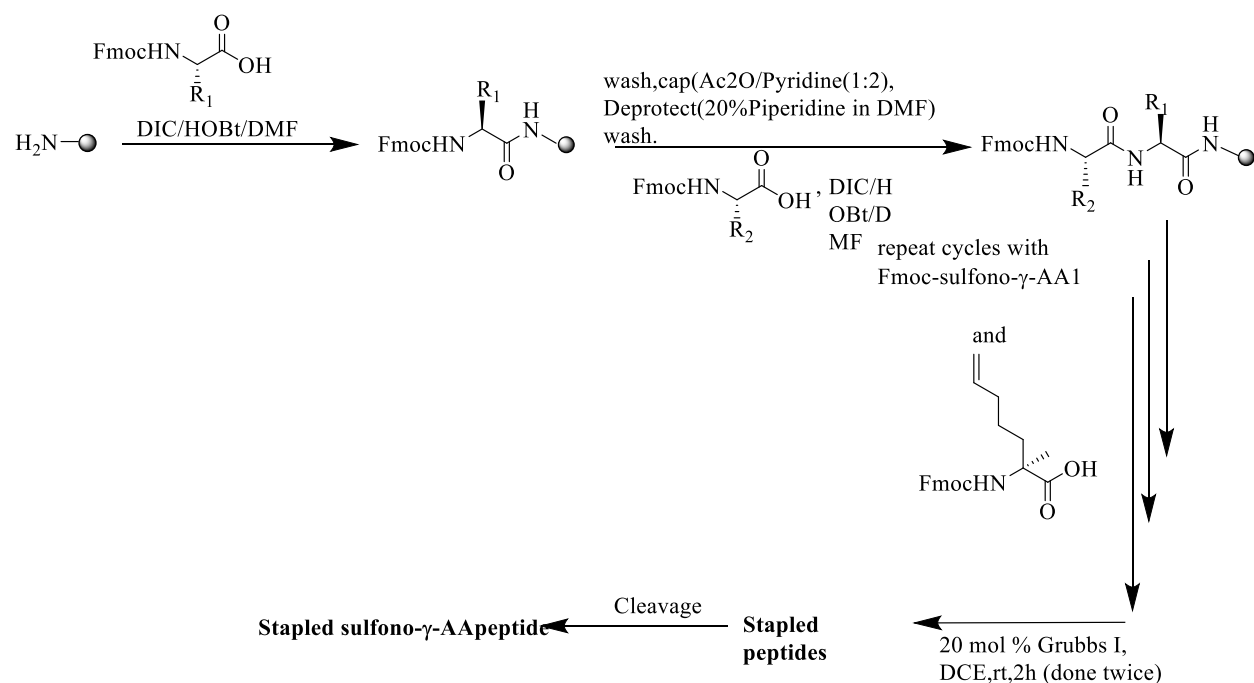


Figure 2.9 Solid phase synthesis of stapled peptides.

Olefin Metathesis and Purification.

Ring-closing metathesis (RCM) of resin-bound N-Fmoc, side chain protected peptides was performed using 20 mol% of Grubbs I catalyst in degassed DCE for 2 hours at room temperature. The resin-bound peptide was washed in the peptide vessel and filtered. The RCM reaction was repeated once again to complete the cross-linking reaction. The reaction was monitored by LC/MS after cleavage of peptide from an aliquot of resin. The resulting stapled peptide was deprotected and cleaved from the resin with a cleavage cocktail mixture of TFA/Phenol/H₂O/thioanisole/1, 2-ethanedithiol (82.5%/5% /5% / 5%/2.5% v/v) for 3h and then precipitated with diethyl ether. The crude peptides(stapled and unstapled) were analyzed and purified on an analytical(1mL/min) and a preparative (16mL/min) RP-HPLC respectively.5% to 100% linear gradient of solvent B(0.1% TFA in acetonitrile) in A(0.1 % TFA in water) over 40 min was used. The HPLC traces were

detected at 215nm. The fraction containing the desired peptides/stapled peptide was collected, confirmed on an Applied Biosystems 4700 Proteomics Analyzer and lyophilized.

Circular Dichroism Analysis.

Circular dichroism (CD) spectra were measured on an Aviv 215 circular dichroism spectrometer using a 1 nm bandwidth and 1nm step resolution from 200 to 260nm at 25°C. 3 scans were averaged for each sample. Peptide solutions were prepared in water to a final concentration of 300µM. The samples were loaded in a 1mm path length quartz cell, and the CD spectra were acquired with an averaging time of 1s; Settling time of 0.333s and multi-scan wait time of 1s. The final spectra were normalized by subtracting the average blank spectra. The data unit was converted from machine units (millidegree, θ) into mean residue ellipticity [θ]. Mean Residue Ellipticity [θ] ($\text{deg.cm}^2.\text{dmol}^{-1}$) was calculated using the equation:

$$[\theta] = \theta_{\text{obs}} / (p \times c \times 10 \times n) \quad (\text{i})$$

Where θ_{obs} is the measured ellipticity in millidegrees, while p is the path length in centimeter, n is the number of side chains and c is the concentration of the peptide in Molar.

The temperature-dependent unfolding was carried out by monitoring the change in ellipticity [θ] at 222nm at increasing temperature (5-70°C) after 1.6 mins equilibration at the desired temperature and an integration time of 1s. The temperature was increased at the rate of 1°C per min; data acquisition was done with the following parameters: 1-nm bandwidth; $\lambda = 222\text{nm}$

HIV-1 Neutralization Assay.

The preparation of Env-pseudotyped virus stocks in 293T cells by calcium phosphate transfection and the use of the engineered HIV-1 coreceptor-bearing cell line U87-CD4⁺-CCR5⁺ (3,000 cells per well) for Env-pseudotyped virion infection were described previously.^{56,57} Briefly, the envelope genes were amplified by PCR, cloned into an expression vector and cotransfected

with an envelope-defective proviral plasmid to generate pseudotyped luciferase-encoding viruses. Recombinant viruses were used to infect U87-CD4⁺-CCR5⁺ cells (3,000 cells per well) in the presence of varying concentrations of peptide. The amount of input pseudovirus was normalized by infectivity (virus titer) rather than by p24 antigen content. Luciferase activity in the target cells was measured in relative light units (RLU) 72 h after infection. Data from duplicate measurements were fit to the variable-slope-sigmoid equation to obtain IC₅₀ values.⁵⁴

Protease Stability Assay.

To evaluate the stability of the peptides against enzyme degradation, the peptides (0.1 mg/ml) were incubated with Chymotrypsin (0.1mg/ml) in 100mM pH 7.8 ammonium bicarbonate buffer for 30 mins. The residual substrate and digested products were quantified by LC-based peak detection at 280nm. Each experiment was done in duplicate.

The NMR Spectrum of Fmoc-sulfonyl-AA1

¹H NMR (400 MHz, CDCl₃): δ 7.71-7.75 (t, *J* = 8.00 Hz, 2H), 7.57 – 7.60 (t, *J* = 8.00 Hz, 2H), 7.34 - 7.37 (t, *J* = 4.00 Hz, 2H), 7.28 – 7.3 (d, *J* = 8.00 Hz, 2H), 7.24 (s, 1H), 5.65 – 5.67 (d, *J* = 8.00 Hz, 1H), 5.22 – 5.27 (m, *J* = 8.00 Hz, 1H), 4.60 – 4.73 (dd, *J* = 4.00, 16.00 Hz, 1H), 4.38 – 4.43 (t, *J* = 12.00 Hz, 1H), 4.33 – 4.35 (d, *J* = 8.00 Hz, 1H), 4.25 – 4.29 (t, *J* = 8.00 Hz, 1H), 4.18 – 4.21 (t, *J* = 8.00 Hz, 1H), 3.76 (s, 2H), 3.57 – 3.65 (dd, *J* = 4.00 Hz, 1H), 3.27 – 3.33 (t, *J* = 16.00 Hz, 2H), 3.20 (s, 1H), 3.07 (s, 2H), 1.50 (s, 4H), 1.41 (s, 18H), 1.25 (s, 1H).

¹³C NMR (400MHz, DMSO-*d*₆): δ 156.4, 155.9, 155.7, 144.4, 141.4, 127.9, 127.45, 125.6, 120.5, 78.4, 77.7, 70.2, 65.7, 65.3, 51.5, 47.2, 40.5, 40.3, 40.1, 39.9, 39.7, 39.5, 39.3, 35.3, 31.8, 29.8, 28.7, 23.2. HRMS (ESI): ([M+H]⁺) calculated for C₃₅H₅₀N₄O₁₀S, 719.3281; found, 719.3336.

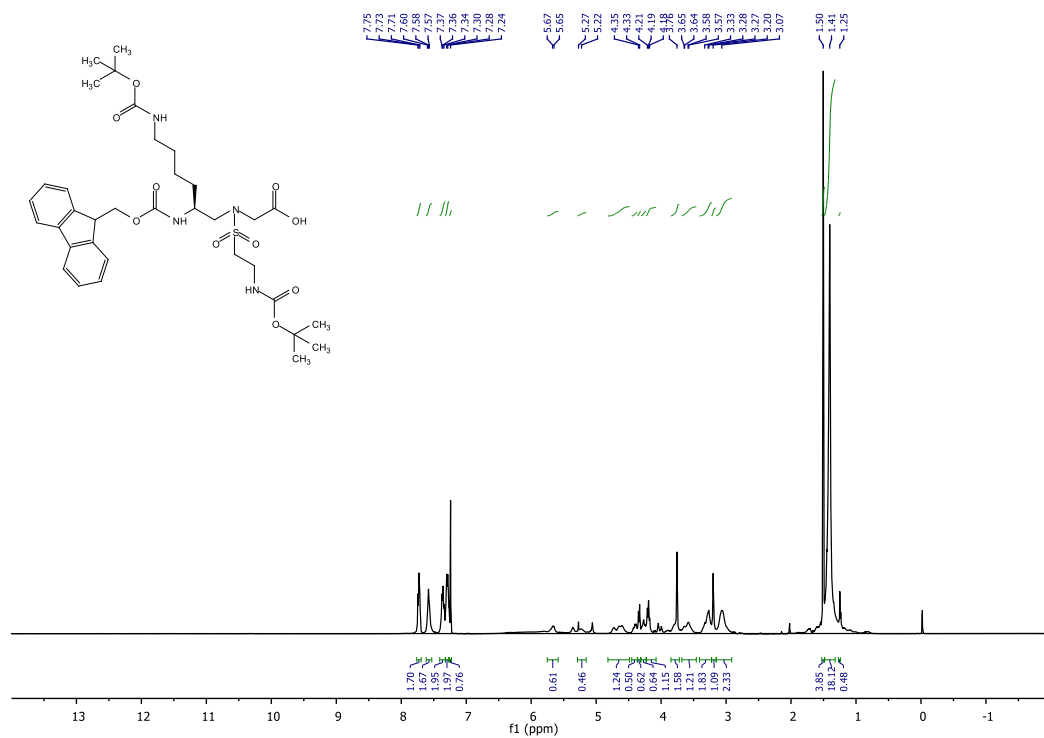


Figure 2.10 ^1H NMR (400 MHz, CDCl_3) and MS of Fmoc-sulfonyl- γ -AA1

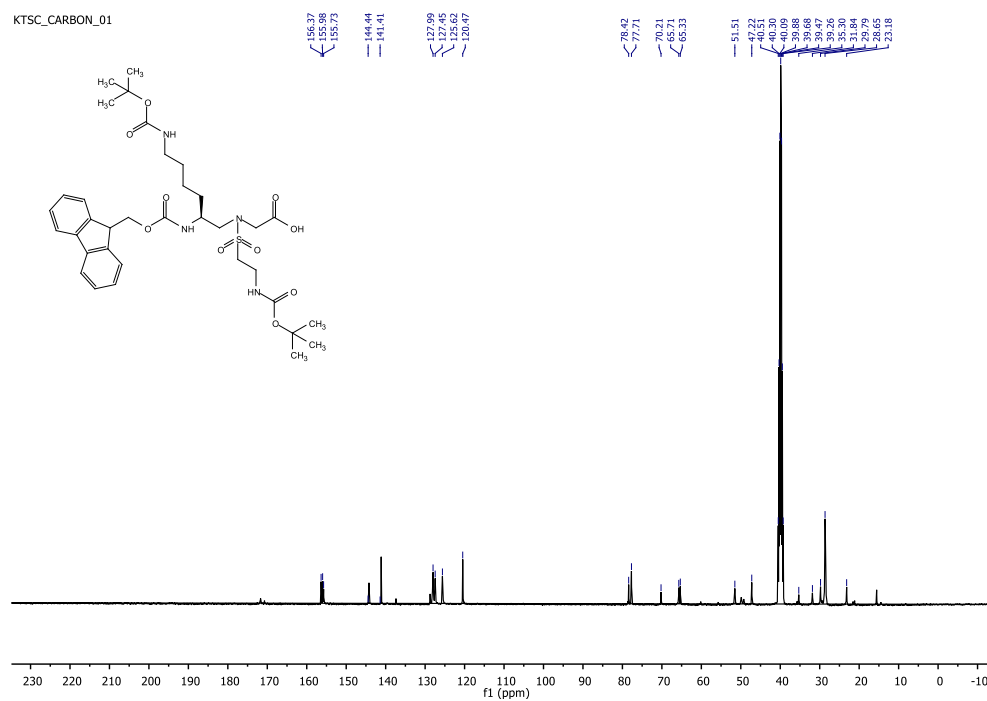


Figure 2.11 ^{13}C NMR (400 MHz, $\text{DMSO}-d_6$) of Fmoc-sulfonyl- γ -AA1.

Table 2.3 HPLC purities and retention time of peptides 1-4

Peptide	Molecular Mass [M+H] ⁺ (expected/observed)	Purity (based on HPLC) %	Retention Time (min)	Yield (%)
1	3125.6431/3125.8845	93.55	19.99	67
2	3118.6494/3118.3872	95.45	21.53	54
3	3147.5702/3147.8384	93.62	19.82	63
4	3140.6007/3140.3728	98.89	20.02	48

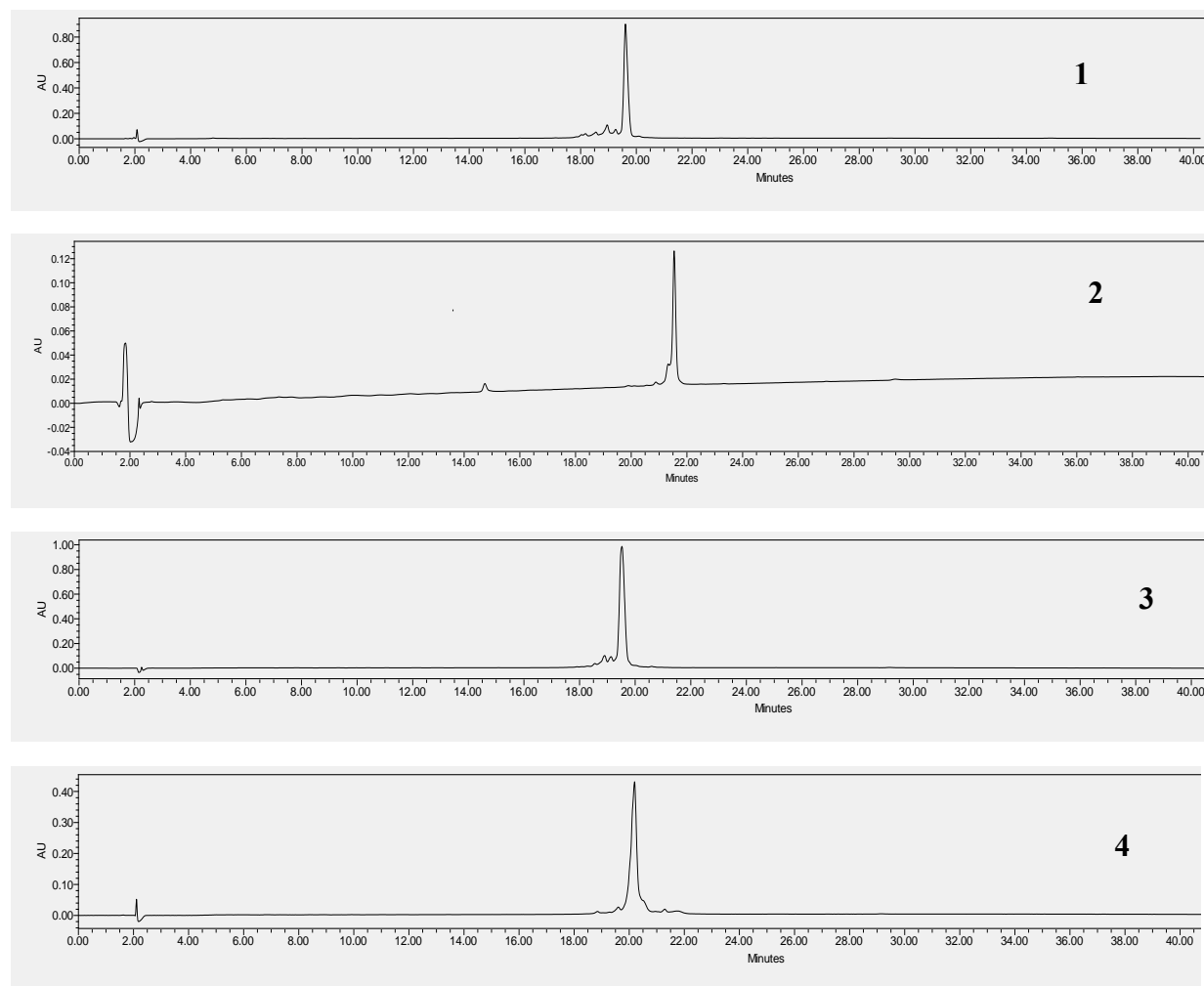


Figure 2.12 HPLC spectra of peptides 1-4

2.5 References

1. J. U. N. P. O. HIV/AIDS, *Biomedical AIDS Research: Recent and Upcoming Advances*. Retrieved May, 2015, **12**, 2015.
2. S. Hallenberger, V. Bosch, H. Angliker, E. Shaw, H. D. Klenk and W. Garten, *Nature*, 1992, **360**, 358-361.
3. S. Su, Q. Wang, W. Xu, F. Yu, C. Hua, Y. Zhu, S. Jiang and L. Lu, *AIDS (London, England)*, 2017, DOI: 10.1097/qad.0000000000001415.
4. T. Naito, K. Izumi, E. Kodama, Y. Sakagami, K. Kajiwara, H. Nishikawa, K. Watanabe, S. G. Sarafianos, S. Oishi, N. Fujii and M. Matsuoka, *Antimicrobial agents and chemotherapy*, 2009, **53**, 1013-1018.
5. M. Lu, S. C. Blacklow and P. S. Kim, *Nat Struct Mol Biol*, 1995, **2**, 1075-1082.
6. D. C. Chan, D. Fass, J. M. Berger and P. S. Kim, *Cell*, 1997, **89**, 263-273.
7. H. J. Ryser and R. Fluckiger, *Drug discovery today*, 2005, **10**, 1085-1094.
8. W. Li, L. Lu, W. Li and S. Jiang, *Expert opinion on therapeutic patents*, 2017, DOI: 10.1080/13543776.2017.1281249, 1-13.
9. L. Lu, F. Yu, L. Cai, A. K. Debnath and S. Jiang, *Current topics in medicinal chemistry*, 2016, **16**, 1074-1090.
10. G. Frey, S. Rits-Volloch, X. Q. Zhang, R. T. Schooley, B. Chen and S. C. Harrison, *Proceedings of the National Academy of Sciences of the United States of America*, 2006, **103**, 13938-13943.
11. M. T. Augusto, A. Hollmann, M. A. R. B. Castanho, M. Porotto, A. Pessi and N. C. Santos, *Journal of Antimicrobial Chemotherapy*, 2014, **69**, 1286-1297.
12. W. S. Horne, L. M. Johnson, T. J. Ketas, P. J. Klasse, M. Lu, J. P. Moore and S. H. Gellman, *Proceedings of the National Academy of Sciences*, 2009, **106**, 14751-14756.
13. D. Wang, M. Lu and P. S. Arora, *Angewandte Chemie International Edition*, 2008, **47**, 1879-1882.
14. S. K. Sia, P. A. Carr, A. G. Cochran, V. N. Malashkevich and P. S. Kim, *Proceedings of the National Academy of Sciences*, 2002, **99**, 14664-14669.
15. D. M. Eckert, V. N. Malashkevich, L. H. Hong, P. A. Carr and P. S. Kim, *Cell*, 1999, **99**, 103-115.
16. M. Lu and P. S. Kim, *J Biomol Struct Dyn*, 1997, **15**, 465-471.
17. D. M. Eckert and P. S. Kim, *Proceedings of the National Academy of Sciences of the United States of America*, 2001, **98**, 11187-11192.
18. M. J. Root, M. S. Kay and P. S. Kim, *Science (New York, N.Y.)*, 2001, **291**, 884-888.
19. L. Cai, E. Balogh and M. Gochin, *Antimicrobial agents and chemotherapy*, 2009, **53**, 2444-2449.
20. X. Jiang, Q. Jia, L. Lu, F. Yu, J. Zheng, W. Shi, L. Cai, S. Jiang and K. Liu, *Amino acids*, 2016, **48**, 2867-2873.
21. C. V. Fletcher, *The Lancet*, 2003, **361**, 1577-1578.
22. J. P. Lalezari, K. Henry, M. O'Hearn, J. S. G. Montaner, P. J. Piliero, B. Trottier, S. Walmsley, C. Cohen, D. R. Kuritzkes, J. J. J. Eron, J. Chung, R. DeMasi, L. Donatucci, C. Drobnes, J. Delehanty and M. Salgo *New England Journal of Medicine*, 2003, **348**, 2175-2185.
23. J. M. Louis, J. L. Baber and G. M. Clore, *Biochemistry*, 2015, **54**, 6796-6805.
24. M. Sugaya, O. Hartley, M. J. Root and A. Blauvelt, *Journal of Investigative Dermatology*, 2007, **127**, 1436-1443.

25. C. Hashimoto, W. Nomura, A. Ohya, E. Urano, K. Miyauchi, T. Narumi, H. Aikawa, J. A. Komano, N. Yamamoto and H. Tamamura, *Bioorganic & medicinal chemistry*, 2012, **20**, 3287-3291.
26. X. Ma, J. Tan, M. Su, C. Li, X. Zhang and C. Wang, *PloS one*, 2014, **9**, e111923.
27. A. Lazzarin , B. Clotet , D. Cooper , J. Reynes , K. Arastéh , M. Nelson , C. Katlama , H.-J. Stellbrink , J.-F. Delfraissy , J. Lange , L. Huson , R. DeMasi , C. Wat , J. Delehanty , C. Drobnes and M. Salgo *New England Journal of Medicine*, 2003, **348**, 2186-2195.
28. C. Wild, T. Greenwell and T. Matthews, *AIDS Research and Human Retroviruses*, 1993, **9**, 1051-1053.
29. S. Xiong, P. Borrego, X. Ding, Y. Zhu, A. Martins, H. Chong, N. Taveira and Y. He, *Journal of virology*, 2017, **91**.
30. M. L. Greenberg and N. Cammack, *Journal of Antimicrobial Chemotherapy*, 2004, **54**, 333-340.
31. K. Izumi, E. Kodama, K. Shimura, Y. Sakagami, K. Watanabe, S. Ito, T. Watabe, Y. Terakawa, H. Nishikawa, S. G. Sarafianos, K. Kitaura, S. Oishi, N. Fujii and M. Matsuoka, *Journal of Biological Chemistry*, 2009, **284**, 4914-4920.
32. J. J. Eron, R. M. Gulick, J. A. Bartlett, T. Merigan, R. Arduino, J. M. Kilby, B. Yangco, A. Diers, C. Drobnes, R. DeMasi, M. Greenberg, T. Melby, C. Raskino, P. Rusnak, Y. Zhang, R. Spence and G. D. Miralles, *The Journal of Infectious Diseases*, 2004, **189**, 1075-1083.
33. H. Chong, X. Yao, Z. Qiu, J. Sun, M. Zhang, S. Waltersperger, M. Wang, S.-L. Liu, S. Cui and Y. He, *The FASEB Journal*, 2013, **27**, 1203-1213.
34. H. Chong, Z. Qiu, Y. Su, L. Yang and Y. He, *AIDS (London, England)*, 2015, **29**, 13-21.
35. Y. He, J. Cheng, J. Li, Z. Qi, H. Lu, M. Dong, S. Jiang and Q. Dai, *Journal of virology*, 2008, **82**, 6349-6358.
36. H. Nishikawa, S. Nakamura, E. Kodama, S. Ito, K. Kajiwara, K. Izumi, Y. Sakagami, S. Oishi, T. Ohkubo, Y. Kobayashi, A. Otaka, N. Fujii and M. Matsuoka, *The International Journal of Biochemistry & Cell Biology*, 2009, **41**, 891-899.
37. K. Shimura, D. Nameki, K. Kajiwara, K. Watanabe, Y. Sakagami, S. Oishi, N. Fujii, M. Matsuoka, S. G. Sarafianos and E. N. Kodama, *The Journal of biological chemistry*, 2010, **285**, 39471-39480.
38. K. Shimane, K. Kawaji, F. Miyamoto, S. Oishi, K. Watanabe, Y. Sakagami, N. Fujii, K. Shimura, M. Matsuoka, M. Kaku, S. G. Sarafianos and E. N. Kodama, *Antimicrobial agents and chemotherapy*, 2013, **57**, 4035-4038.
39. F. Miyamoto and E. N. Kodama, *Antiviral Chemistry and Chemotherapy*, 2012, **22**, 151-158.
40. Y. Su, H. Chong, Z. Qiu, S. Xiong and Y. He, *Journal of virology*, 2015, **89**, 5801-5811.
41. H. Chong, X. Yao, J. Sun, Z. Qiu, M. Zhang, S. Waltersperger, M. Wang, S. Cui and Y. He, *The Journal of biological chemistry*, 2012, **287**, 34558-34568.
42. H. Chong, J. Xue, S. Xiong, Z. Cong, X. Ding, Y. Zhu, Z. Liu, T. Chen, Y. Feng, L. He, Y. Guo, Q. Wei, Y. Zhou, C. Qin and Y. He, *Journal of virology*, 2017, **91**, e00288-00217.
43. H. Chong, Z. Qiu, J. Sun, Y. Qiao, X. Li and Y. He, *Retrovirology*, 2014, **11**, 40-40.
44. O. M. Stephens, S. Kim, B. D. Welch, M. E. Hodsdon, M. S. Kay and A. Schepartz, *Journal of the American Chemical Society*, 2005, **127**, 13126-13127.

45. A. D. Bautista, O. M. Stephens, L. Wang, R. A. Domaoal, K. S. Anderson and A. Schepartz, *Bioorganic & Medicinal Chemistry Letters*, 2009, **19**, 3736-3738.
46. G. H. Bird, N. Madani, A. F. Perry, A. M. Princiotta, J. G. Supko, X. He, E. Gavathiotis, J. G. Sodroski and L. D. Walensky, *Proceedings of the National Academy of Sciences*, 2010, **107**, 14093-14098.
47. Y. Niu, Y. Hu, X. Li, J. Chen and J. Cai, *New Journal of Chemistry*, 2011, **35**, 542-545.
48. P. Teng, Y. Shi, P. Sang and J. Cai, *Chemistry – A European Journal*, 2016, **22**, 5458-5466.
49. Y. Shi, P. Teng, P. Sang, F. She, L. Wei and J. Cai, *Accounts of Chemical Research*, 2016, **49**, 428-441.
50. H. Wu, Q. Qiao, Y. Hu, P. Teng, W. Gao, X. Zuo, L. Wojtas, R. W. Larsen, S. Ma and J. Cai, *Chemistry – A European Journal*, 2015, **21**, 2501-2507.
51. P. Teng, N. Ma, D. C. Cerrato, F. She, T. Odom, X. Wang, L.-J. Ming, A. van der Vaart, L. Wojtas, H. Xu and J. Cai, *Journal of the American Chemical Society*, 2017, **139**, 7363-7369.
52. H. E. Blackwell, J. D. Sadowsky, R. J. Howard, J. N. Sampson, J. A. Chao, W. E. Steinmetz, D. J. O'Leary and R. H. Grubbs, *The Journal of Organic Chemistry*, 2001, **66**, 5291-5302.
53. C. E. Schafmeister, J. Po and G. L. Verdine, *Journal of the American Chemical Society*, 2000, **122**, 5891-5892.
54. S. Beddows, N. Schülke, M. Kirschner, K. Barnes, M. Franti, E. Michael, T. Ketas, R. W. Sanders, P. J. Maddon, W. C. Olson and J. P. Moore, *Journal of virology*, 2005, **79**, 8812-8827.
55. M. G. Joyce, I. S. Georgiev, Y. Yang, A. Druz, H. Geng, G. Y. Chuang, Y. D. Kwon, M. Pancera, R. Rawi, M. Sastry, G. B. E. Stewart-Jones, A. Zheng, T. Zhou, M. Choe, J. G. Van Galen, R. E. Chen, C. R. Lees, S. Narpala, M. Chambers, Y. Tsybovsky, U. Baxa, A. B. McDermott, J. R. Mascola and P. D. Kwong, *Cell Rep*, 2017, **21**, 2992-3002.
56. C. J. Gordon, M. A. Muesing, A. E. I. Proudfoot, C. A. Power, J. P. Moore and A. Trkola, *Journal of virology*, 1999, **73**, 684-694.
57. C. Herrera, C. Spenlehauer, M. S. Fung, D. R. Burton, S. Beddows and J. P. Moore, *Journal of virology*, 2003, **77**, 1084-1091.

CHAPTER 3 : I-AAPEPTIDES –BASED SMALL MOLECULE LIGANDS THAT DISAGGREGATE HUMAN ISLET AMYLOID POLYPEPTIDE

3.1 Introduction

The human islet amyloid polypeptide (hIAPP), also known as amylin, is a unique amyloidogenic precursor peptide, and a critical pathogenic feature of Type II diabetes. Amylin is co-secreted with insulin by the β -cells of the pancreas, and co-stored in the secretory granules.¹ As a matter of fact, there is an overwhelming evidence of the useful role of soluble amylin in glucose metabolism, however, the insoluble aggregates resulting from the misfolding of this protein is implicated in type II diabetes.²⁻⁴ Just like the amyloid deposits formed in neurodegenerative disorders (e.g., Alzheimer's, Parkinson's and Huntington's diseases)⁵ and progressive diseases (e.g., Type II diabetes and cystic fibrosis)^{6, 7}, amylin aggregates consist of stacked protofilaments, leading to a structural architecture known as the cross- β structure.⁸⁻¹⁰ The oligomerization of amylin into amyloid fibrils has been suggested to be a stepwise process: first, the aggregation of monomers into colloidal spheres, which stop growing after reaching a uniform diameter ; second, the association of the spheres to form linear chains of toxic, mature fibrils of pore-like morphology.⁸ The extent of these oligomerization process is strongly correlated to pancreatic β -cell dysfunction and death in Type II diabetic patients,¹¹⁻¹³ therefore, an impairment of the initial monomer aggregation process is an appealing therapeutic approach to diabetes drug discovery and development.

So far, there is no treatment for pancreatic amyloidosis, and there is only a few approved therapeutic strategies for its prevention. Hence, the need for channelling intense research efforts to the search for potent inhibitors of the process producing these pathogenic fibrils. In line with this, some inhibitors have been reported including the peptides derived from the various secondary recognition elements along the amylin peptide chain,¹⁴⁻¹⁶ engineered peptides,¹⁷⁻¹⁹ constrained peptides²⁰⁻²⁶, small molecules^{27, 28} and natural products.²⁹⁻³¹ Although, many of these inhibitors are specific in their activity, a few of them have exhibited dual inhibitory activity.³¹⁻³⁴

In order to advance the application of peptidomimetics in chemical biology and drug discovery, we have recently introduced our new class of peptidomimetic scaffold, γ -AApeptide. γ -AApeptide contain *N*-acylated-*N*-aminoethyl amino acid units, and are derived from γ -PNAs.³⁵ Each monomeric unit of the γ -AApeptide is equivalent to a dipeptide residue in a conventional peptide. This means that they are able to project an identical number of functional groups as canonical peptides of the equal length.

In our previous work, we reported on a small molecule A β ₄₀ aggregation inhibitor, HW-155, which was identified from a peptidomimetic OBOC (one-bead-one-compound) library.³⁶ **HW-155** is a γ -AApeptide³⁵ tetramer with little structural similarity to KLVFF, the core amyloid-forming unit of A β . Inspired by the findings on dual inhibitors, and based on the fact that **HW-155** was from an OBOC library, we hypothesized that **HW-155** could be a non-specific amyloid inhibitor. To critically evaluate this hypothesis, we synthesized **HW-155** and eight (8) analogues (**1 - 8**), and investigated their ability in preventing the fibrillation of amylin (hIAPP), and the disruption of preformed hIAPP aggregates. We also

examined the effect of **HW-155** and its analogues (Figure 3.1) on the toxicity of hIAPP aggregates towards the cell.

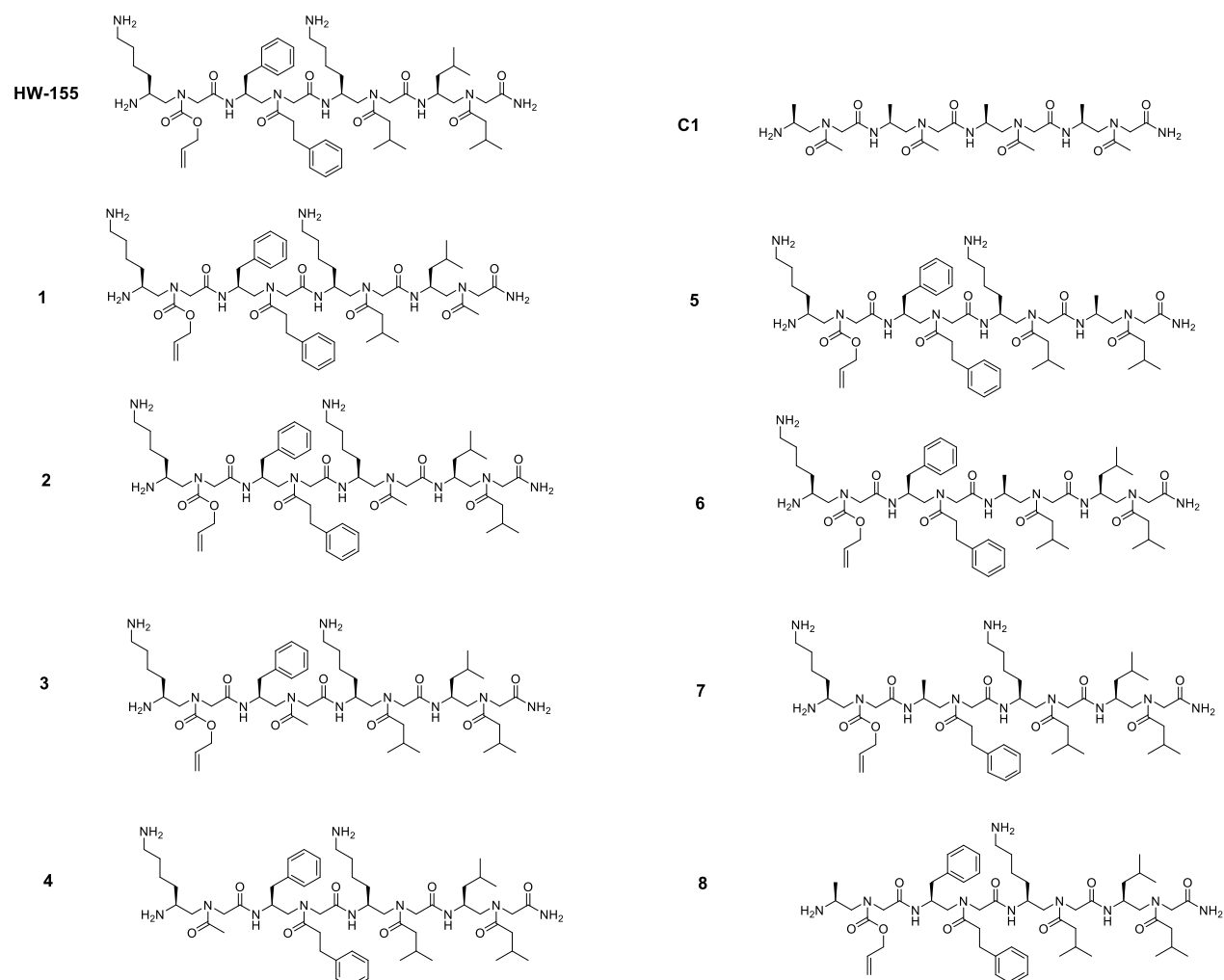


Figure 3.1 Peptide Sequences HW-155, control C1 and 1-8

3.2 Results and Discussion

We have previously reported a γ -AApeptide oligomer, **HW-155**, as a potent inhibitor of A β aggregation. In this study, we investigated the effectiveness of **HW-155** in the inhibition of amyloid formation by hIAPP₁₋₃₇. First, we studied the aggregation

behaviour of hIAPP₁₋₃₇ in the presence of a 2.5-, 5-, and 10- fold molar excesses of **HW-155**. Time-dependent ThT assay revealed a significantly enhanced fluorescent intensity with hIAPP₁₋₃₇ (10 μ M) alone.

Table 3.1 Percent Inhibition (Based on ThT Fluorescence assay) of HW-155, C1 and 1-8.

Peptides (%)	100 μ M	50 μ M	25 μ M	12.5 μ M	6.25 μ M	3.13 μ M	1.56 μ M
1	50.6	67.9	44.1	42.7	54.7	43.2	71.8
2	59.2	49.3	55.0	70.6	49.5	43.3	50.1
3	55.1	55.9	60.0	62.3	54.1	54.1	50.7
4	60.5	64.4	63.6	67.4	67.1	58.2	48.7
5	50.0	56.7	73.2	74.1	67.8	66.5	59.6
6	66.0	65.7	64.5	59.0	59.5	65.8	60.2
7	50.4	58.8	48.1	48.8	51.6	50.5	46.7
8	51.9	48.7	51.7	55.0	57.3	47.0	34.4
HW-155	52.0	51.6	45.8	40.2	44.2	45.6	36.5
C1	21.1	-2.3*	-21.9*	-11.9*	0.4	-8.9*	-1.6*

* no inhibition

Surprisingly, **HW-155** was able to prevent hIAPP₁₋₃₇ aggregation by ~50% at the 2.5-, 5- and 10-fold molar excesses tested (Figure 3.10).

Encouraged by this result, we further studied the aggregation formation by hIAPP₁₋₃₇ in the presence of equimolar or lesser concentration of **HW-155**. To our surprise, a significant reduction in the fluorescent intensity of hIAPP₁₋₃₇ was observed at these tested

concentrations of **HW-155**, even with 0.2-fold molar excess of **HW-155**. This implies that **HW-155** could not only inhibit A β aggregation, but also prevent amyloid formation in hIAPP₁₋₃₇. This was further confirmed by the TEM images that were captured (Figure 3.13). A characteristic feature of amyloidogenic peptides is the presence of fibrillary morphology under the electron microscope.³⁷

Inspired by this new development, we sought to pinpoint the role and effect of each monomeric unit in **HW-155** on inhibitory activity. Using **HW-155** as a template, we designed and performed a functional analysis of eight (8) analogues of **HW-155** namely peptides **1-8** (Figure 3.1). In four analogues (**1-4**), we substituted each of the *N*-side chains in **HW-155** with an acetyl group, while alanine scanning was performed on the chiral side chains (**5-8**). We also designed a control peptide, **C1**, which consists of both modifications. Our intention was to carefully evaluate the effects of a change in the molecular interface of **HW-155** on inhibition.

Amyloid aggregation kinetics of hIAPP₁₋₃₇ in the presence of **1-8** was monitored by time-dependent ThT assay. In an initial attempt, we studied the anti-aggregation activity of 2.5-, 5-, and 10-fold molar excesses of **1-8**. Interestingly, peptides 1-8 were able to suppress the fluorescence by over 40% at 2.5-fold and over 50% at 5- and 10-fold molar excesses. Further investigation of equimolar or lesser concentrations of **1-8** resulted in a minimum inhibitory activity of 30% (Figures 3.2 – 3.10).

We identified peptides **3**, **5**, and **6** (Figures 3.4, 3.6, and 3.7) with over 50% inhibition across all molar equivalents tested. In fact, **5** (Figure 3.6) showed more than 65% inhibition at 1-, 0.6- and 0.3-fold molar excesses. Also, our control peptide, **C1**, only prevented hIAPP₁₋₃₇ aggregation at a 10-fold molar excess (Table 3.1).

To evaluate the ability of our designed analogues to disaggregate preformed hIAPP₁₋₃₇ fibrils, we performed a time – dependent ThT assay and monitored the fluorescent intensity for over twenty four (24) hours. Interestingly, only **5** was able to disrupt preformed hIAPP₁₋₃₇ fibrils at a tested concentration of 100μM (Figure 3.11).

Further evidence of hIAPP₁₋₃₇ aggregation inhibition by the designed analogues and **HW-155** was obtained from the TEM morphological studies of hIAPP₁₋₃₇ that was pre-incubated with equimolar amount of peptides **2,3,4,5** and **HW-155**.

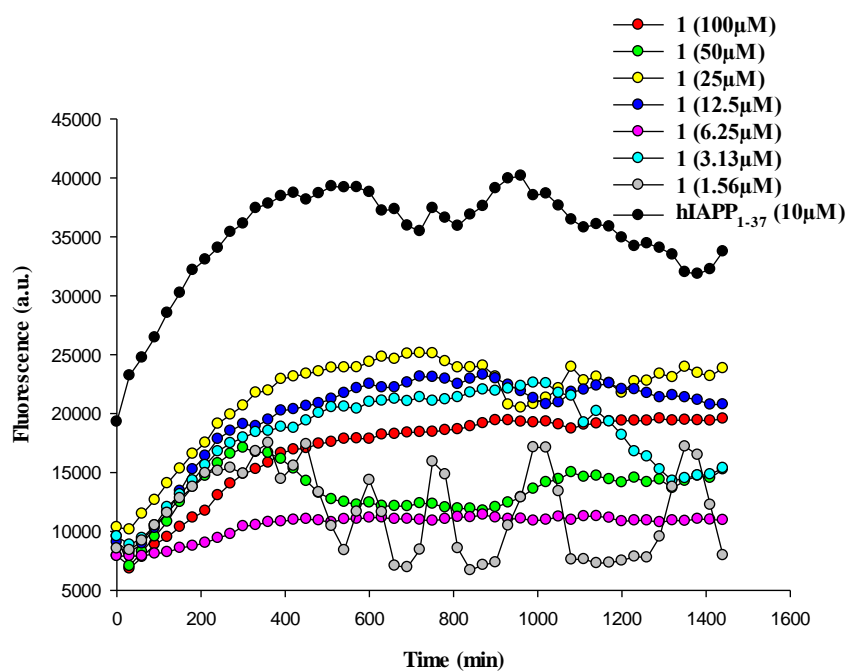


Figure 3.2 Time-dependent ThT assay of hIAPP₁₋₃₇ (10μM) and various molar equivalents of 1

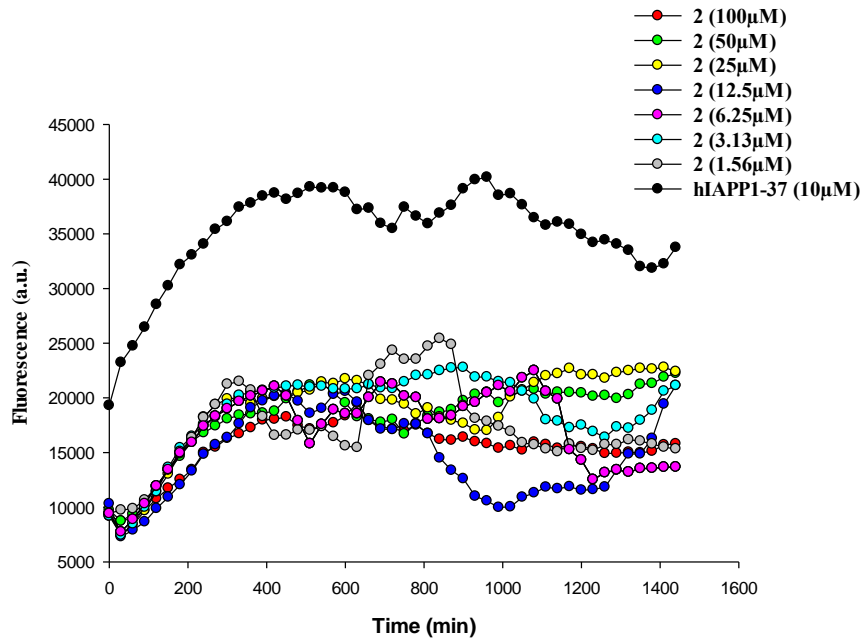


Figure 3.3 Time-dependent ThT assay of hIAPP₁₋₃₇ (10µM) and various molar equivalents of 2

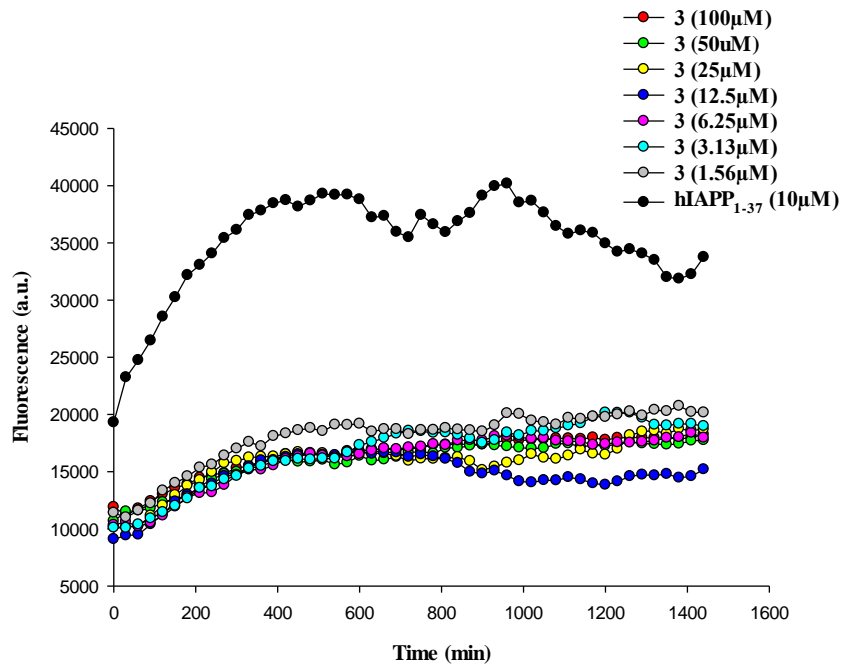


Figure 3.4 Time-dependent ThT assay of hIAPP₁₋₃₇ (10µM) and various molar equivalents of 3

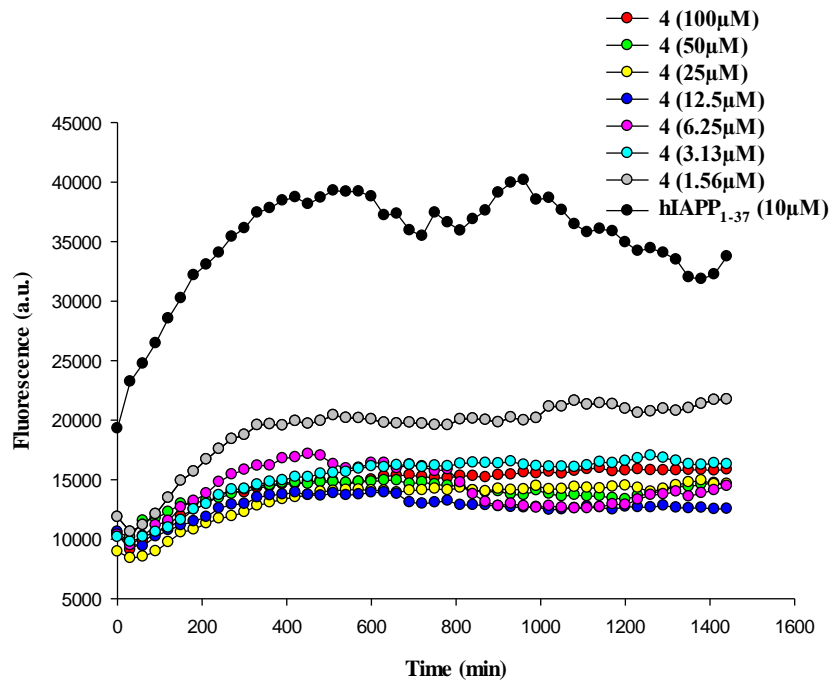


Figure 3.5 Time-dependent ThT assay of hIAPP₁₋₃₇ (10µM) and various molar equivalents of 4

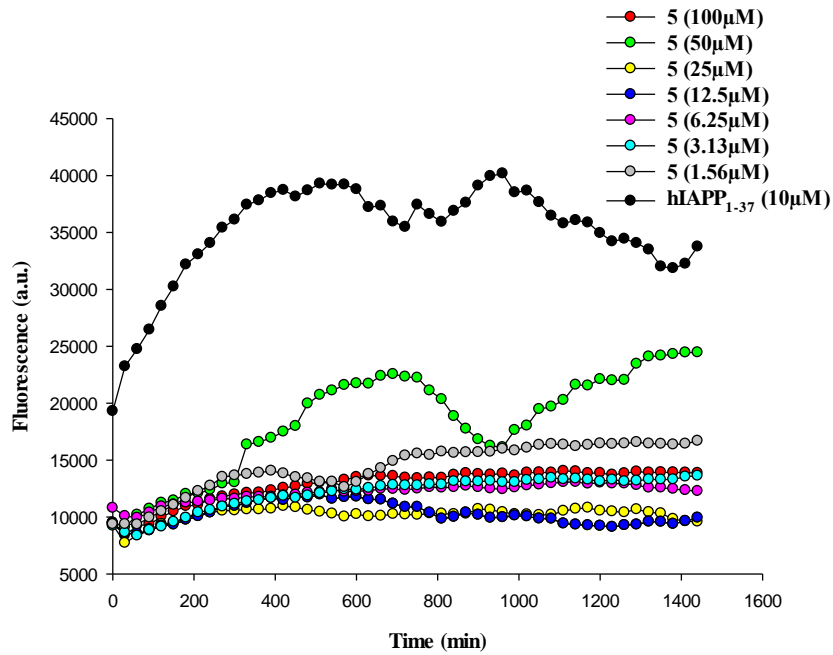


Figure 3.6 Time-dependent ThT assay of hIAPP₁₋₃₇ (10µM) and various molar equivalents of 5

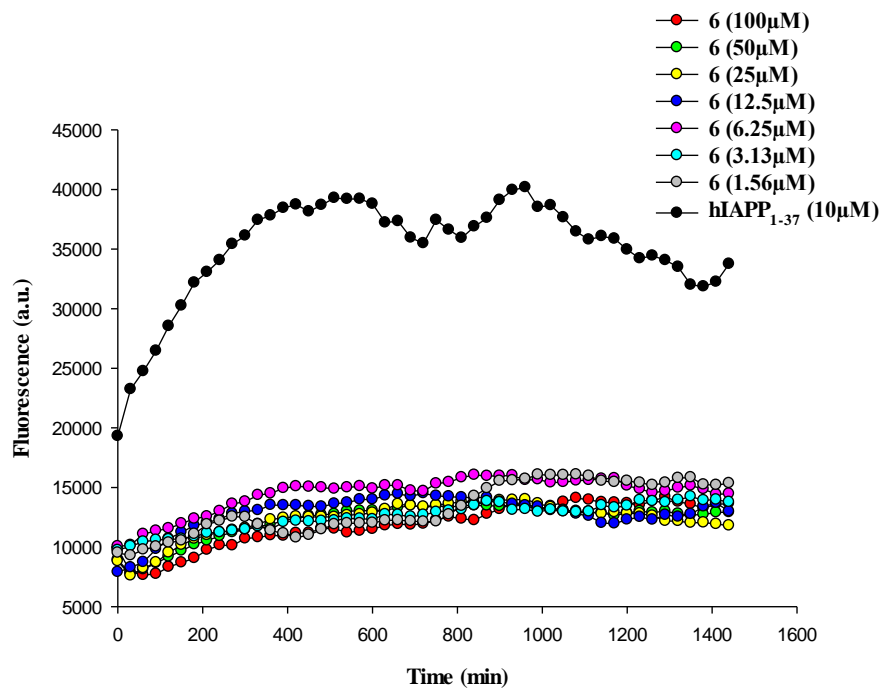


Figure 3.7 Time-dependent ThT assay of hIAPP1-37 (10µM) and various molar equivalents of 6

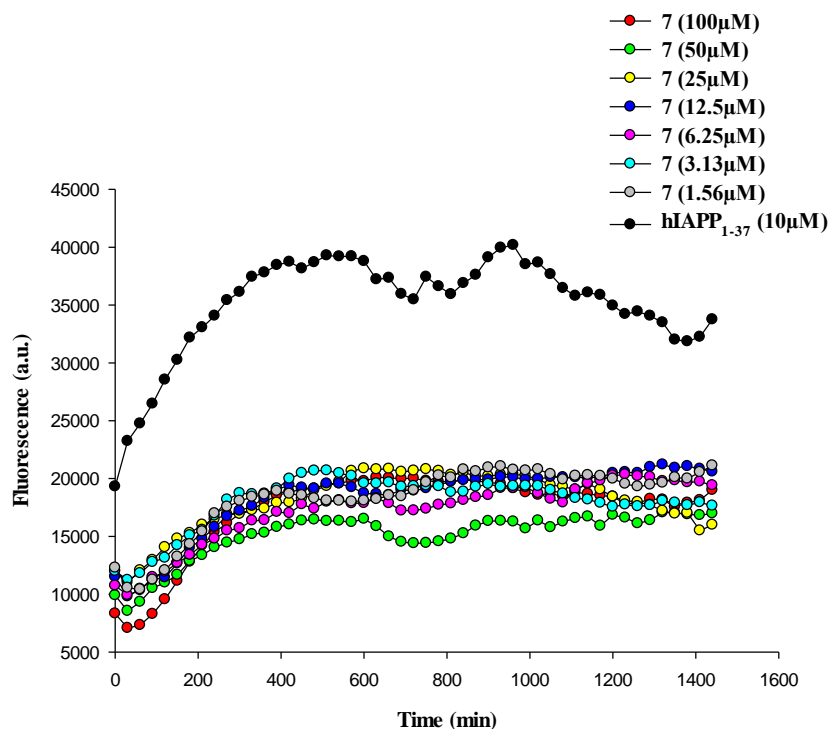


Figure 3.8 Time-dependent ThT assay of hIAPP1-37 (10µM) and various molar equivalents of 7

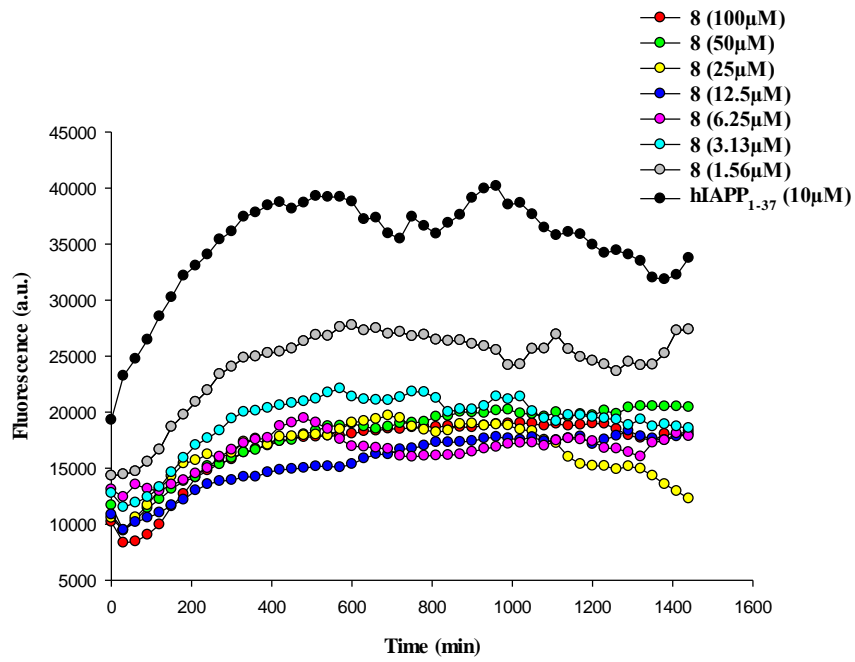


Figure 3.9 Time-dependent ThT assay of hIAPP₁₋₃₇ (10µM) and various molar equivalents of 8

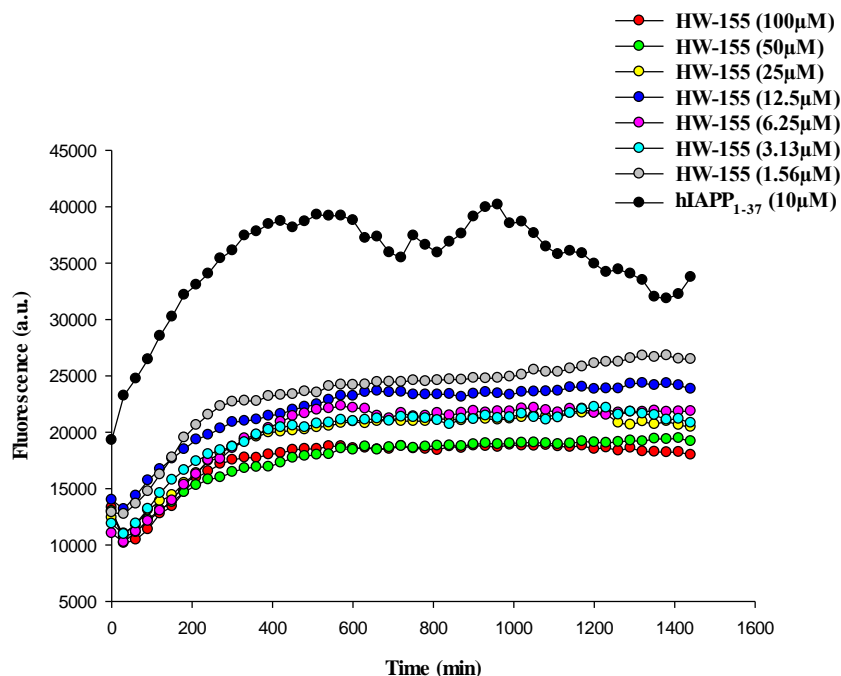


Figure 3.10 Time-dependent ThT assay of hIAPP₁₋₃₇ (10µM) and various molar equivalents of HW-155

The TEM micrographs for hIAPP₁₋₃₇ revealed a dense network of intertwined mature fibrils with linear, and thread-like morphology (Figure 3.13) indicating the presence of hIAPP₁₋₃₇ amyloid. However, no such fibril was observed in the presence of **2,3,4,5** and **HW-155**, indicating a significant prevention of fibril formation by hIAPP₁₋₃₇. A prevention of fibril formation by **2**, and **5** resulted in the monomers observed in the TEM images. Likewise, the oligomers seen in **3**, **4**, and **HW-155** were as a result of the inhibition of formation of mature fibrils.

To visualize the effect of **5** on hIAPP₁₋₃₇ preformed aggregates, we allowed 10µM hIAPP₁₋₃₇ to age for 10h before treatment with a 10 –fold molar excess of **5**. AFM showed a disappearance of mature fibrils (Figure 3.12). However, very few oligomeric hIAPP₁₋₃₇

spheres resulting from the disrupted aggregates were observed. This confirms that **5** is able to disaggregate preformed hIAPP₁₋₃₇ aggregates.

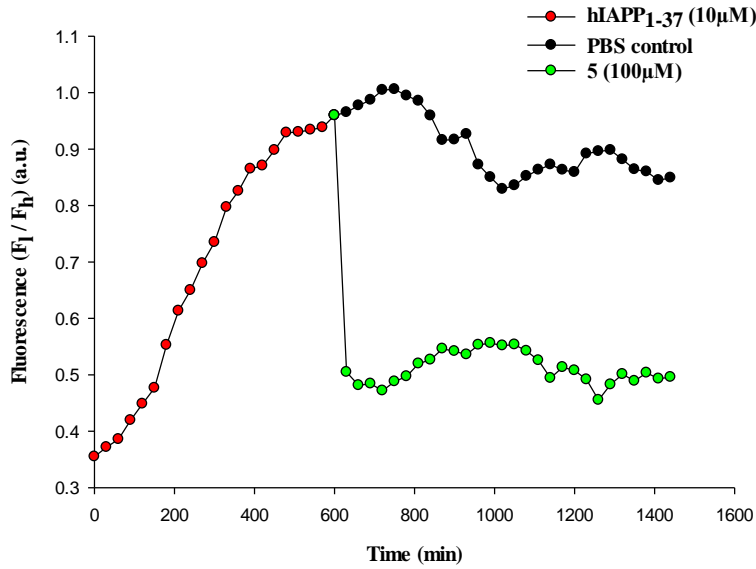


Figure 3.11 Time-dependent ThT assay of the disruption of hIAPP₁₋₃₇ (10µM) preformed fibrils by 5 (100µM)

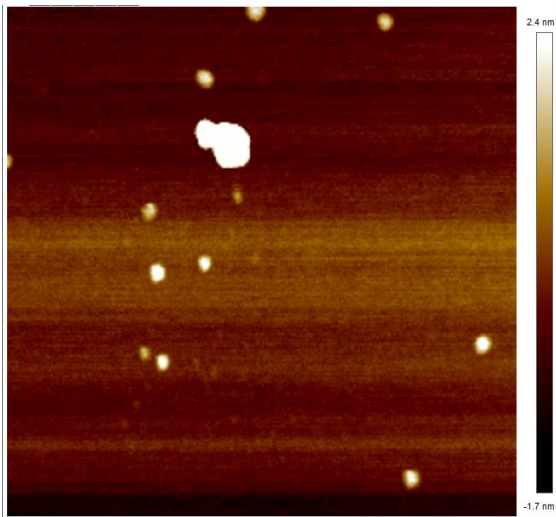


Figure 3.12 AFM image the disruption of hIAPP₁₋₃₇ (10µM) preformed fibrils by 5 (100µM)

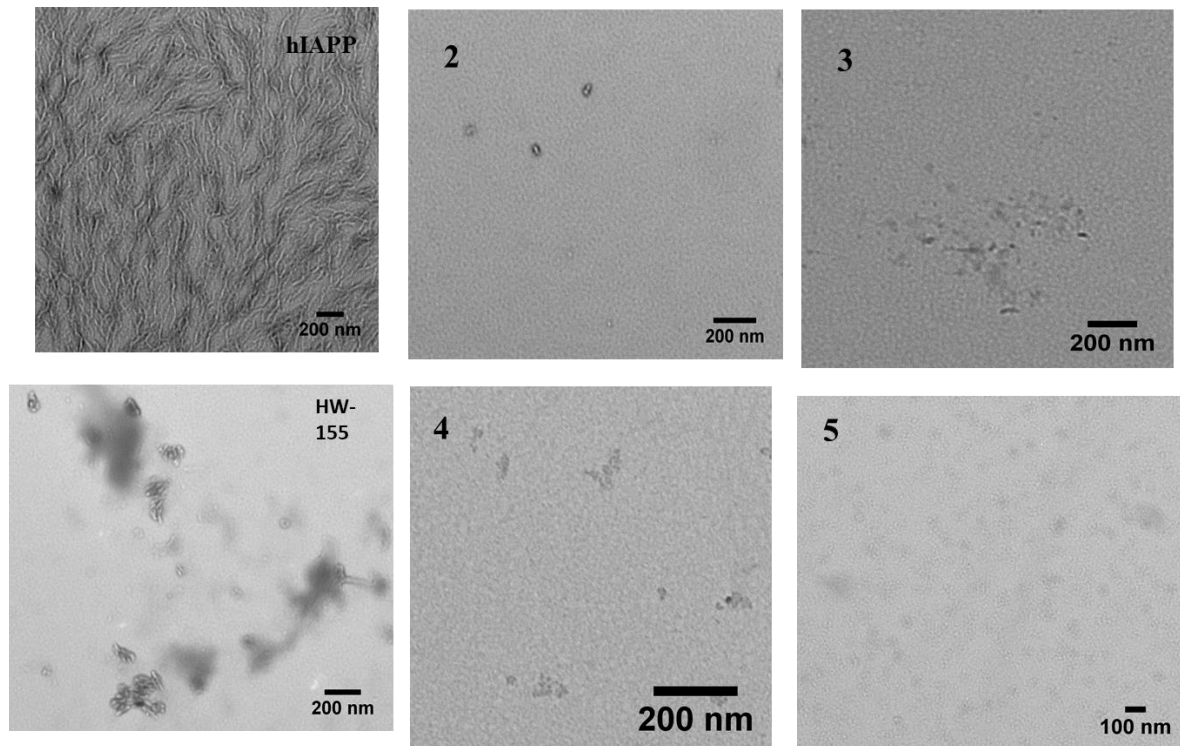


Figure 3.13 TEM images of hIAPP₁₋₃₇ alone and in the presence of equimolar amount 2,3,4,5, and HW-155.

Based on our findings on the inhibition of hIAPP₁₋₃₇ fibrillation by **2,3,4,5** and **HW-155**, we further assessed their safety index in mammalian cells by CCK-8 assay. We tested the toxic effects of 1 μ M and 5 μ M concentrations of **2,3,4,5**, and **HW-155** on NIH-3T3 cells (Figure 3.14). At 1 μ M concentration, only peptide **2** altered the viability of the cell (~10% reduction). However, at a peptide concentration of 5 μ M, peptides **3, 4, 5**, and **HW-155** reduced the cell viability by at least 10%, while peptide **2** showed a significant cell viability reduction of about 20%. At both concentrations tested, peptide **2** exhibited some cytotoxic effect on the NIH-3T3 cells.

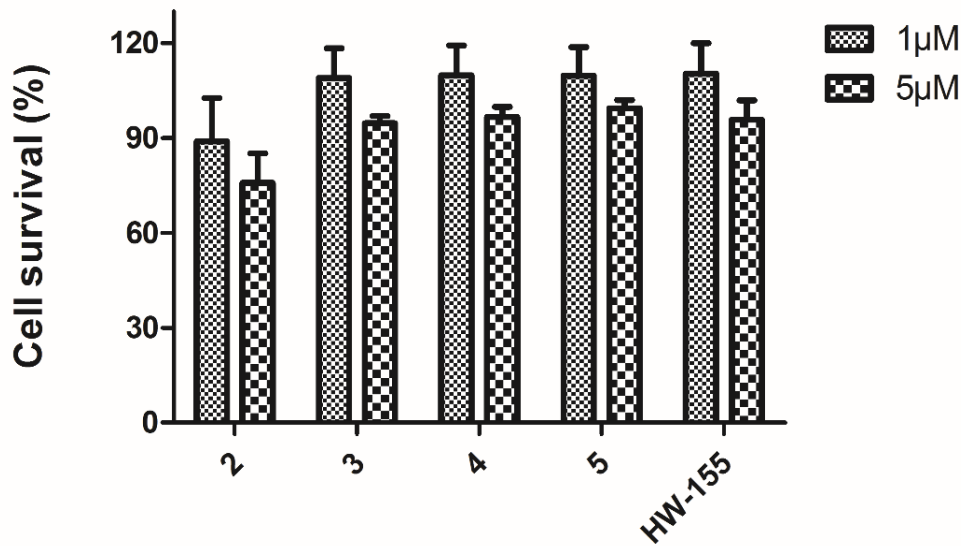


Figure 3.14 Effects of peptides 2,3,4,5 and HW-155 on NIH-3T3 cells in CCK-8 cell viability assay

To study the ability of peptides **2,3,4,5** and **HW-155** to modulate the hIAPP₁₋₃₇ amyloid – induced cytotoxicity, we treated NIH-3T3 cells with hIAPP₁₋₃₇ (10µM) and 5µM peptide as described in the general information section. Results showed that cells treated with only hIAPP₁₋₃₇ exhibited a significant reduction in survival, whereas, treatment with 5µM concentration of peptides **2,3,4,5** and **HW-155** was able to rescue the cells from hIAPP₁₋₃₇ amyloid assembly cytotoxicity (Figure 3.15). However, it is noteworthy that peptides **3,4**, and **5** were better at reducing cell death due to hIAPP₁₋₃₇ amyloid toxicity than **2** and **HW-155**.

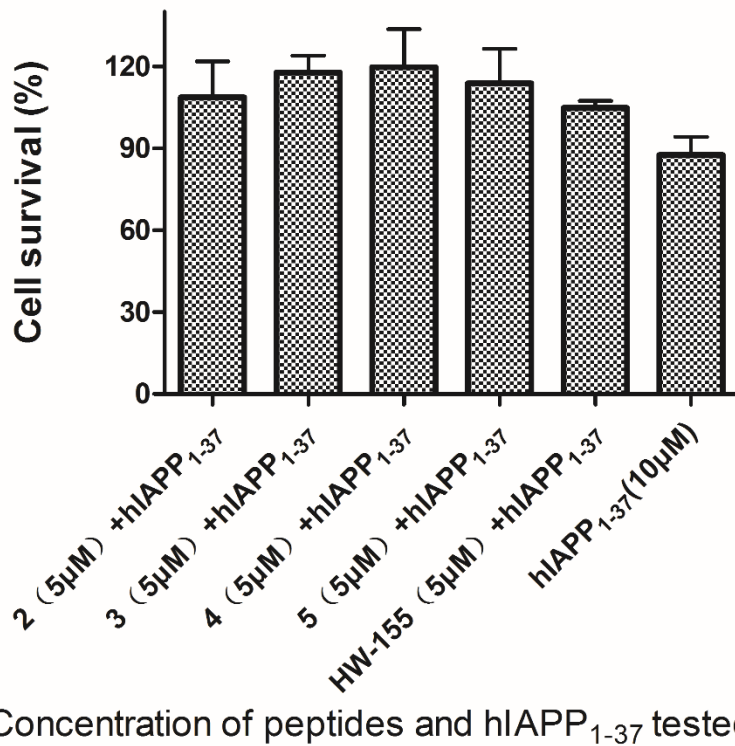


Figure 3.15 Evaluation of the potential of peptides 2,3,4,5 and HW-155 to improve the chances of cell survival in the presence of hIAPP₁₋₃₇ amyloid.

3.3 Conclusion

Altogether, this study provides experimental support to the dual action of **HW-155** in preventing amyloid fibril formation by A β ³⁶ and hIAPP₁₋₃₇. We have utilized a simple, but effective approach for designing potential inhibitors of hIAPP₁₋₃₇ fibrillation. We have also demonstrated the ability of **HW-155** analogues to effectively disaggregate preformed hIAPP₁₋₃₇ fibrils. The truncation/substitution of side chains in **HW-155** resulted in analogues that proved more effective in amyloid prevention, and disaggregation of preformed hIAPP₁₋₃₇ amyloid than **HW-155**. **HW-155** as a dual inhibitor compound, does not only have greater advantages over other known inhibitors of amyloid formation that only target a specific amyloid system, it also provides a template for the design of potent

analogues that could be next-generation therapeutic agents for the treatment of Type 2 diabetes mellitus.

3.4 Materials and Methods

Peptides Synthesis

General Information Fmoc –protected α -amino acids and Rink amide resin used for γ -AApeptide synthesis were purchased from Chem-Impex International, Inc.. All chemicals and solvents used were purchased from Aldrich or Fisher and were used without further purification.

γ -AApeptide Monomer Synthesis

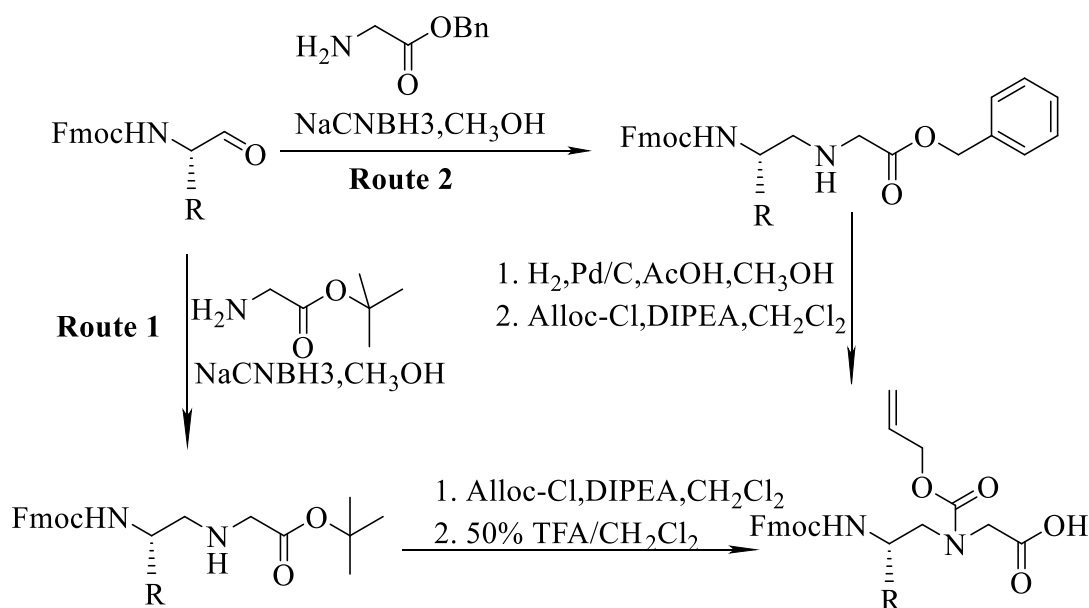


Figure 3.16 Synthesis of γ -AApeptide building block/monomeric unit.

Solid Phase Peptide Synthesis Peptides were synthesized on the rink amide resin (0.6mmol/g) on a Burrell Wrist-action shaker (Figure 3.2). 200 mg resin was treated twice (15 mins each time) with 3ml 20% Piperidine in DMF to deprotect the Fmoc group. The beads were then washed thrice with 3ml each of DCM and DMF. The desired *N*-alloc

protected γ -AApeptide building blocks were prepared (Figure 3.16) and are combined (2 equivalents) with 4 equivalents each of HOBt and DIC in 3ml DMF. The solution was then added to the deprotected resin and was allowed to react for 4 hours. Ninhydrin test³⁵ was used to confirm the success of the coupling and depending on the Ninhydrin test result, a second round of coupling was done. On reaction completion, the beads were washed with DMF and DCM, followed by a fifteen minutes (15 min) capping reaction with 500uL Acetic Acid. After capping, the beads were washed and alloc-deprotection reaction was done by reacting the beads with Pd (PPh₃)₄ (1 equivalent) and Me₂NH BH₃ (6 equivalents) (10 mins each time). The beads were then washed with DCM and DMF, followed by the reaction of the deprotected beads with acyl chloride (4 equivalents) and DIPEA (6 equivalents) in 3ml DCM for 1h or with the carboxylic acid (4 equivalents), HOBt (8 equivalents), and DIC (8 equivalents) for 6h (x2).

The above steps were repeated to assemble the desired sequence on the resin (Figure 3.17). After these, the resin was washed and the peptide was cleaved from the resin with the cocktail: TFA/H₂O/TIS (95/2.5/2.5) for 2.5h. The solvent evaporated to obtain the crude peptide which was analysed and purified on an analytical (1ml/min) and a preparative (20ml/min) Waters HPLC systems, respectively. 5-100% linear gradient of 0.1% TFA/ACN in 0.1 % TFA/H₂O over 50 min was used. The HPLC traces were detected at 215 nm. The products were confirmed by MALDI-TOF MS. The product fractions were then collected and lyophilized.

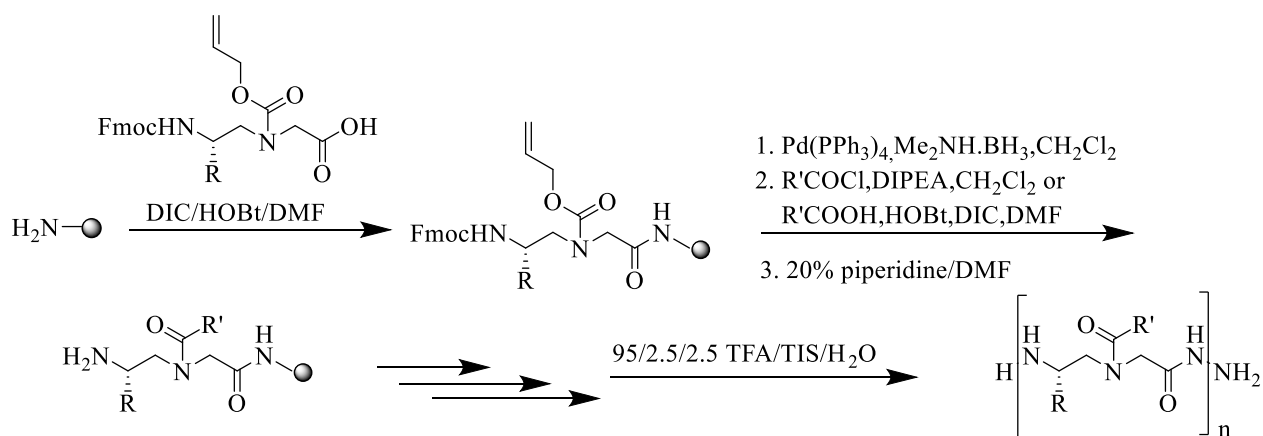


Figure 3.17 Solid Phase synthesis scheme for HW-155,C1 and 1-8.

hIAPP Sample Preparation

This was done according to previously published protocol.^{24, 38} 3.1mg of hIAPP₁₋₃₇ was dissolved in minimal amount of HFIP (50ul) to remove aggregated hIAPP and the HFIP was removed over a gentle stream of Nitrogen gas. The process was done twice and 5ml of Milli Q pure water was added to the disaggregated hIAPP film. The solution was then divided into 25 aliquots of 200ul each. The 25 aliquots were lyophilized and reconstituted in 800μL of PBS prior to use to obtain a hIAPP stock solution of 40μM. The stock solution was always sonicated prior to use.

Thioflavin T Fluorescence Assay

Inhibition of hIAPP aggregate formation Different peptide concentrations were made in PBS (x1, pH 7.4). hIAPP stock solution (40μM) was also prepared as described above. The peptide, hIAPP and 15μM ThT were added into a 96-well black plate. Equal volume of hIAPP solution was added into the 96-well black plate to make the final concentration of hIAPP in each well to be 10μM. Time-dependent fluorescent change was monitored for

24h by the Biotek Synergy H1 hybrid plate reader at excitation and emission wavelengths of 435 and 490 nm respectively.

Disruption of preformed aggregates Similar to the protocol described above for the inhibition studies, hIAPP and ThT were added to PBS in a 96-well black plate and at concentrations of 10 μ M and 15 μ M respectively. Time dependent fluorescent change was monitored for 10h after which 5 μ l of peptide was added to make a final peptide concentration of 100 μ M. 5 μ l of PBS was also added to control wells. Each test well containing the peptide has a control well to which equal volume of PBS was added. The fluorescent change was then monitored for another 12h.

Transmission Electron Microscopy (TEM)

Sample preparation was similar to ThT assay. Sample solution containing 10 μ M hIAPP₁₋₃₇ and 12.5 μ M of the respective peptide were incubated at 30°C for 24h. 10 μ L aliquot of the incubated solution was placed on carbon-coated 200-mesh copper grid. After 10 mins, excess solution was wicked away and the grid was allowed to dry. This is then followed by the addition of 2% uranyl acetate solution (10 μ L) which was allowed to float for 5min. The excess solution was then removed using the blotting paper. The copper grid was left to dry at room temperature before imaging with FEI Morgagni 268D TEM operated at 60kV.

Atomic Force Microscopy (AFM)

A droplet (10 μ l) of the sample solution is placed on the freshly cleaved mica disk and let it dry in open air at room temperature. Imaging is performed by Multimode 8 AFM (Bruker, Santa Barbara, CA) and a Nanoscope V controller in Peak Force quantitative nanomechanics (QNM) air mode. Standard silicon cantilever probe, FMVA (Bruker), with

spring constant of 2.8N/m, and tip radius 8nm is used for imaging at room temperature. Images are acquired at scan rate of 1-1.5 Hz and 256pixel/lines.

Percentage inhibition

The percent inhibition was calculated using the formula below:³⁹

Percent inhibition = 100% - (F in the presence of inhibitor / F in the absence of inhibitor X 100) % where F = the average of the ThT signals at 870, 900, 930, 960 and 990 min. These time points were chosen because the maximum ThT signals were observed at these points in the uninhibited hIAPP control experiment.

Cell viability/proliferation assay

The 3T3 cells were seeded in a 96-well flat-bottomed microplate (5000 cells/well) and cultured in 100 μ L of growth medium at 37°C and 5% CO₂ for 24 h. The cell culture medium in each well was then replaced with 100 μ L of cell growth medium containing peptides 2,3,4,5 and HW-155 alone at concentrations of 1 μ M and 5 μ M or 5 μ M peptide with 10 μ M hIAPP₁₋₃₇.

After incubation for 24 hours at 37°C, the peptides were washed with PBS three times. Then, 10 μ L of CCK-8 dye and 100 μ L of DMEM cell culture medium were added to each well, and the cells were incubated for another 1.5 hour at 37°C. The absorbance at 450 nm was measured by a Synergy H1 Hybrid Reader (BioTek, Dallas, TX, USA). Untreated cells served as controls with 100% viability. The results are presented as the mean \pm SD of three measurements.

Table 3.2 HPLC purities and retention time of peptides 1-8 and HW-155

Peptide	Molecular Mass [M+H]⁺ (expected/observed)	Purity (based on HPLC) %	Retention Time (min)	Yield (%)
1	1048.6845/1048.6747	99.01	17.95	80
2	1048.6845/1048.6746	96.48	17.13	83
3	1000.6845/1000.6750	96.59	16.82	70
4	1048.7209/1048.7217	91.42	17.88	78
5	1048.6845/1048.7781	91.61	17.14	90
6	1033.6736/1033.7318	92.47	21.04	87
7	1014.7001/1014.7594	85.32	16.94	95
8	1033.6736/1033.7430	99.1	20.58	96
HW- 155	1090.7314/1090.7928	98.98	18.95	75

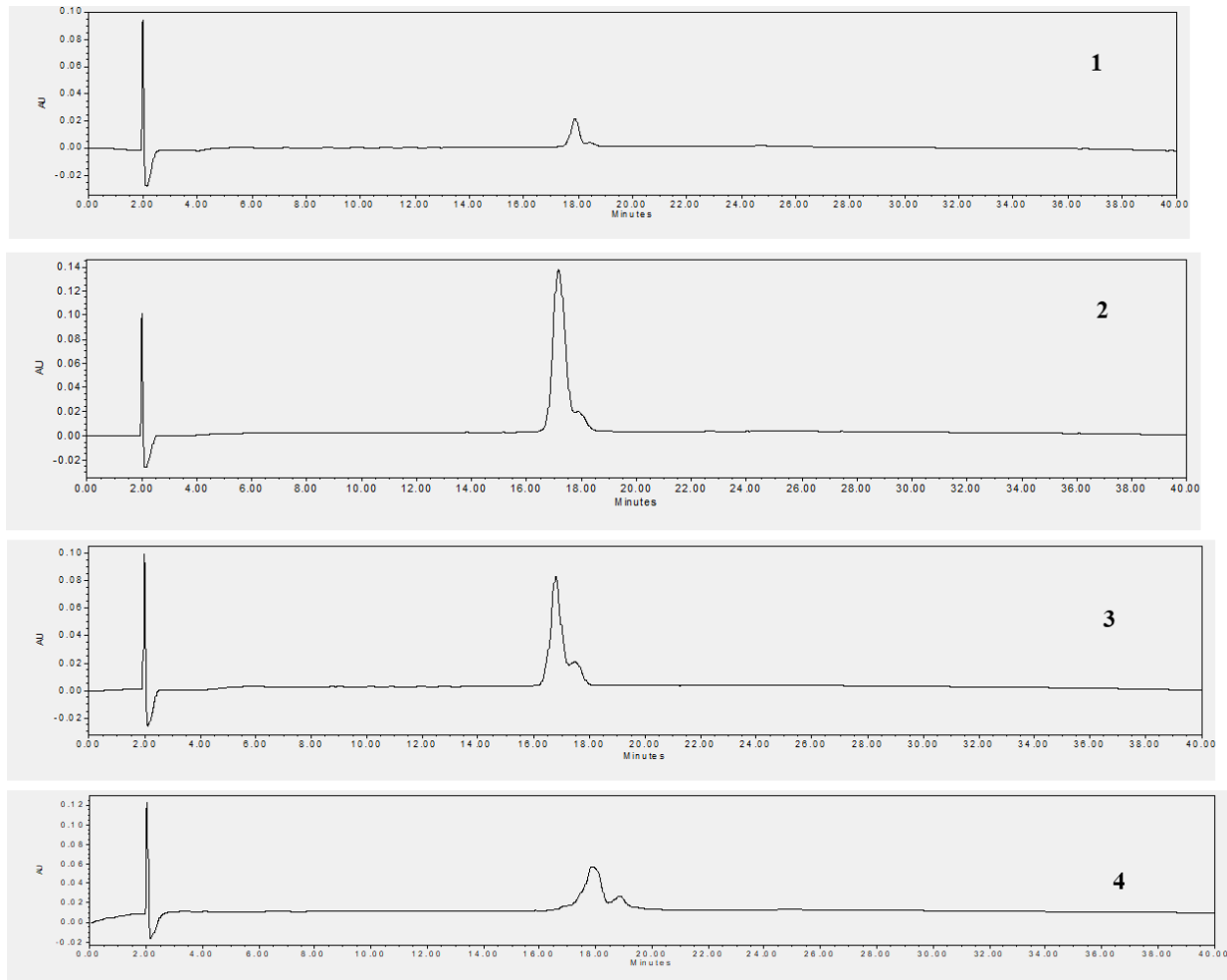


Figure 3.18 HPLC spectra of peptides 1-8 and HW-155

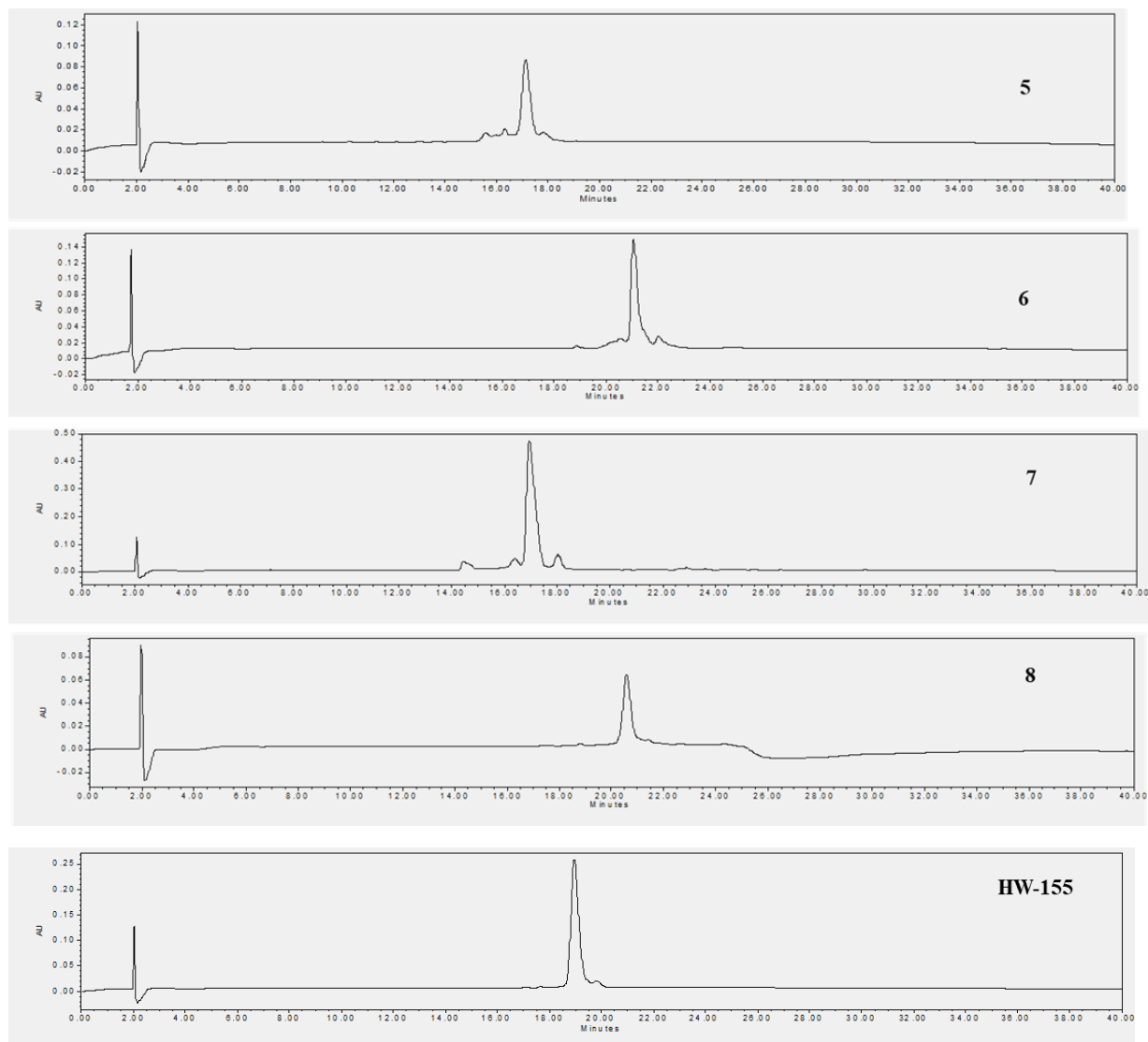


Figure 3.19 HPLC spectra of peptides 1-8 and HW-155 continued

3.5 References

1. S. E. Kahn, D. A. D'Alessio, M. W. Schwartz, W. Y. Fujimoto, J. W. Ensinck, G. J. Taborsky and D. Porte, *Diabetes*, 1990, **39**, 634-638.
2. R. L. Hull, G. T. Westermark, P. Westermark and S. E. Kahn, *The Journal of Clinical Endocrinology & Metabolism*, 2004, **89**, 3629-3643.
3. P. Westermark, A. Andersson and G. T. Westermark, *Physiological Reviews*, 2011, **91**, 795-826.
4. K. Aphrodite, *Peptide Science*, 2001, **60**, 438-459.
5. F. Chiti and C. M. Dobson, *Annual Review of Biochemistry*, 2017, **86**, 27-68.
6. A. Omiste, C. Maldonado-Araque, C. Olveira, J. Mellado and G. Olveira, *AACE Clinical Case Reports*, 2015, **1**, e36-e39.
7. A. Marie Mc Laughlin, T. B Crotty, J. J Egan, A. Watson and C. G Gallagher, *Amyloidosis in cystic fibrosis: A case series*, 2006.

8. S. Xu, *The Journal of Physical Chemistry B*, 2009, **113**, 12447-12455.
9. J. J. W. Wiltzius, S. A. Sievers, M. R. Sawaya, D. Cascio, D. Popov, C. Riekel and D. Eisenberg, *Protein Science : A Publication of the Protein Society*, 2008, **17**, 1467-1474.
10. A. V. Kajava, U. Aebi and A. C. Steven, *Journal of Molecular Biology*, 2005, **348**, 247-252.
11. P. Cao, A. Abedini, H. Wang, L.-H. Tu, X. Zhang, A. M. Schmidt and D. P. Raleigh, *Proceedings of the National Academy of Sciences*, 2013, **110**, 19279-19284.
12. N. B. Last, E. Rhoades and A. D. Miranker, *Proceedings of the National Academy of Sciences*, 2011, **108**, 9460-9465.
13. D. Raleigh, X. Zhang, B. Hastoy and A. Clark, *Journal of Molecular Endocrinology*, 2017, **59**, R121-R140.
14. P. Westermark, U. Engström, K. H. Johnson, G. T. Westermark and C. Betsholtz, *Proceedings of the National Academy of Sciences*, 1990, **87**, 5036-5040.
15. Y. Porat, Y. Mazor, S. Efrat and E. Gazit, *Biochemistry*, 2004, **43**, 14454-14462.
16. L. A. Scrocchi, Y. Chen, S. Waschuk, F. Wang, S. Cheung, A. A. Darabie, J. McLaurin and P. E. Fraser, *Journal of Molecular Biology*, 2002, **318**, 697-706.
17. E. A. Mirecka, L. Gremer, S. Schiefer, F. Oesterhelt, M. Stoldt, D. Willbold and W. Hoyer, *Journal of Biotechnology*, 2014, **191**, 221-227.
18. Y. Mao, L. Yu, R. Yang, C. Ma, L. Qu and P. d. B. Harrington, *European Journal of Pharmacology*, 2017, **804**, 102-110.
19. M. Yexuan, Y. Lanlan, M. Mengfan, M. Chuanguo and Q. Lingbo, *Journal of Peptide Science*, 2018, **24**, e3058.
20. K. Muthusamy, P. I. Arvidsson, P. Govender, H. G. Kruger, G. E. M. Maguire and T. Govender, *Bioorganic & Medicinal Chemistry Letters*, 2010, **20**, 1360-1362.
21. M. Tatarek-Nossol, L.-M. Yan, A. Schmauder, K. Tenidis, G. Westermark and A. Kapurniotu, *Chemistry & Biology*, 2005, **12**, 797-809.
22. L.-M. Yan, M. Tatarek-Nossol, A. Velkova, A. Kazantzis and A. Kapurniotu, *Proceedings of the National Academy of Sciences of the United States of America*, 2006, **103**, 2046-2051.
23. D. Sellin, L.-M. Yan, A. Kapurniotu and R. Winter, *Biophysical Chemistry*, 2010, **150**, 73-79.
24. A. Paul, S. Kalita, S. Kalita, P. Sukumar and B. Mandal, *Scientific Reports*, 2017, **7**, 40095.
25. A. Mishra, A. Misra, T. Sri Vaishnavi, C. Thota, M. Gupta, S. Ramakumar and V. S. Chauhan, *Chemical Communications (Cambridge, England)*, 2013, **49**, 2688-2690.
26. I. Obasse, M. Taylor, N. J. Fullwood and D. Allsop, *Interface Focus*, 2017, **7**.
27. S. Bahramikia and R. Yazdanparast, *European Journal of Pharmacology*, 2013, **707**, 17-25.
28. A. A. Profit, J. Vedad and R. Z. B. Desamero, *Bioconjugate Chemistry*, 2017, **28**, 666-677.

29. B. Cheng, H. Gong, X. Li, Y. Sun, X. Zhang, H. Chen, X. Liu, L. Zheng and K. Huang, *Biochemical and Biophysical Research Communications*, 2012, **419**, 495-499.
30. M. F. M. Sciacca, R. Chillemi, S. Sciuto, V. Greco, C. Messineo, S. A. Kotler, D.-K. Lee, J. R. Brender, A. Ramamoorthy, C. La Rosa and D. Milardi, *Biochimica et Biophysica Acta (BBA) - Biomembranes*, 2018, DOI: <https://doi.org/10.1016/j.bbamem.2018.03.012>.
31. B. Ren, Y. Liu, Y. Zhang, Y. Cai, X. Gong, Y. Chang, L. Xu and J. Zheng, *ACS Chemical Neuroscience*, 2018, **9**, 1215-1224.
32. D. E. Ehrnhoefer, M. Duennwald, P. Markovic, J. L. Wacker, S. Engemann, M. Roark, J. Legleiter, J. L. Marsh, L. M. Thompson, S. Lindquist, P. J. Muchowski and E. E. Wanker, *Human Molecular Genetics*, 2006, **15**, 2743-2751.
33. Q. Wang, X. Yu, K. Patal, R. Hu, S. Chuang, G. Zhang and J. Zheng, *ACS Chemical Neuroscience*, 2013, **4**, 1004-1015.
34. B. Ren, Y. Liu, Y. Zhang, M. Zhang, Y. Sun, G. Liang, J. Xu and J. Zheng, *Journal of Materials Chemistry B*, 2018, **6**, 56-67.
35. Y. Niu, Y. Hu, X. Li, J. Chen and J. Cai, *New Journal of Chemistry*, 2011, **35**, 542-545.
36. H. Wu, Y. Li, G. Bai, Y. Niu, Q. Qiao, J. D. Tipton, C. Cao and J. Cai, *Chemical Communications*, 2014, **50**, 5206-5208.
37. M. R. Nilsson, *Methods*, 2004, **34**, 151-160.
38. H. C. E., J. E. T.A.S., F. P. E., G. Michael and C. Anne, *FEBS Letters*, 2000, **470**, 55-60.
39. K. Sivanesam and N. H. Andersen, *Biochemistry*, 2017, **56**, 5373-5379.

CHAPTER 4 : EVALUATION OF THE SEQUENCE-DEPENDENT AGGREGATION AND INHIBITORY POTENTIAL OF ISLET AMYLOID POLYPEPTIDE-DERIVED RETRO-PEPTIDES.

4.1 Introduction

Amyloid fibrillation of proteins and peptides are underlying causes of a wide range of pathological conditions including Parkinson's, Alzheimer's and Diabetes type II mellitus(T2DM),to mention a few. These pathological conditions are collectively referred to as protein misfolding or amyloid diseases, and over fifty (50) distinct human protein misfolding disorders have been reported.^{1,2} Even though the culprit proteins in these disorders are dissimilar in their primary and tertiary structure, their amyloid fibril morphologies share many similarities in their structure and chemical properties.³ The production of these fibrils have been implicated in loss of protein function and most importantly, a gain of toxic function by the aggregated protein.²

Human amylin, also called human Islet Polypeptide Hormone (hIAPP), is a 37-residue peptide responsible for amyloid formation in Type II diabetes mellitus. hIAPP contains three major regions,the N-terminal region with probable α -helical propensity especially in membrane conditions, the aggregation –prone middle region(20-29),which contains the core molecular recognition sequence and amyloid forming units, and the C-terminal region.⁴ Monomeric hIAPP exhibit random coil conformation, contains a disulfide bridge between cysteine residues at positions 2 and 7, and is amidated at the C-terminus. However, some previous reports have shown evidence that hIAPP monomers may adopt helical conformations.⁵

The step-wise process of hIAPP amyloid formation includes the self-aggregation of monomers, leading to the conversion of the protein secondary structure from its random coil native

state to cross β -sheets. The oligomers formed from this process gradually grow into protofibrils, which eventually matures into full grown toxic fibrils. While it may be true and generally believed that the full grown fibrils are very toxic,⁶⁻⁸ evidences have shown that the soluble oligomer may be more toxic.⁹⁻¹¹ A good understanding of the fibrillation properties and behaviors of hIAPP could provide insights for the development of inhibitors that are capable of interrupting the amyloidogenic process.

To date, sequences derived from the middle region of hIAPP have been reported to show similar aggregation patterns to the full length hIAPP peptide.^{4, 12-14} Variations in this region can significantly impact amyloid formation.¹⁵ Among the core amyloid forming motifs of hIAPP, hIAPP₂₂₋₂₉ (NFGAILSS) have been shown to form amyloid fibrils with great similarities to the full-length peptide.^{13, 16, 17} Hence, it is frequently studied as a simple model for understanding the factors regulating amyloid fibrillation.¹⁸ Modifications in this region have also shed more light on the relationship between sequence patterns and amyloidogenic properties. Common modifications include substitution,^{12, 18} and incorporation of β -sheet breakers.^{14, 19-21}

In line with the above mentioned modifications, we sought to investigate the effects of retro-inversion on the fibrillation behavior and morphology of hIAPP₂₂₋₂₉. This strategy has been previously exploited for inhibitor design for A β .²² Retro-D- peptides (containing retro-inverso- and retro-enantio -isomers of a template peptide) or analogues are obtained by reversing the assembly pattern of parent or template peptides with a simultaneous substitution of L-amino acids with D-amino acids (Figure 4.1). Theoretically, the side chain orientation in retro-inversed peptides are projected in a similar fashion to their parent peptides, except for situations when it is fixed in special secondary structures.²³⁻²⁵ D-amino acids are the stereoisomers of naturally

occurring L-amino acids and are considered unnatural. Some prokaryotic organisms produce and use D-amino acids, but in general D-amino production is during chemical synthesis.²⁶

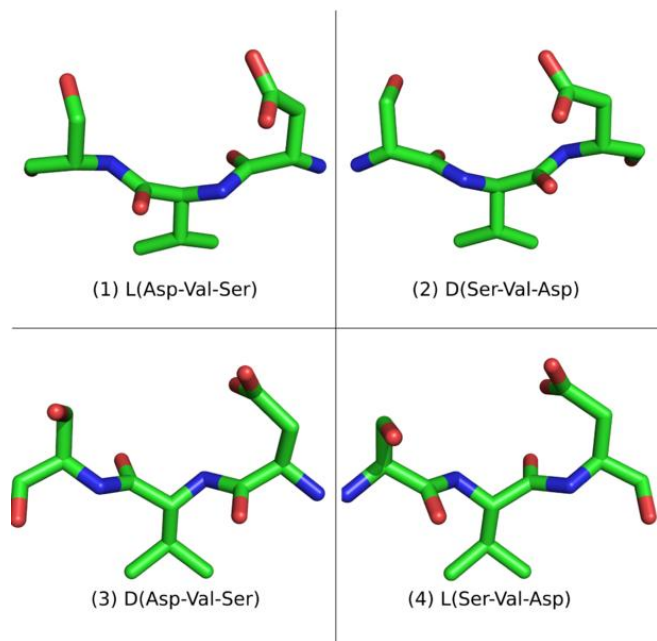


Figure 4.1 A sample L-peptide and its analogues. An L-peptide (1) sequence has three analogues: the D-enantiomer (3) with the same sequence, the retro L-peptide (4) with the inverted sequence, and the retro-inverso D-peptide(2), with all D-amino acids and the inverted sequence. Note that (1) and (2) have similar side chain positions; one is the retro-inverso sequence of the other. The same applies to (3) and (4). <https://commons.wikimedia.org/wiki/File:L-peptideD-peptideAnalogues.png>

In the present study, eight retro-analogues of hIAPP₂₂₋₂₉ including four (4) retro-inverso analogues and four (4) retro-analogues with alternating L and D were designed, and their aggregation propensity and amyloid morphology were systematically characterized using transmission electron microscopy (TEM), Thioflavin T (ThT) fluorescence assay, Congo red Spectrophotometric assay, Kinetic aggregation assay and Circular dichroism (CD). We also evaluated the inhibitory potential of these peptides on hIAPP amyloid aggregation.

Table 4.1 Peptide sequences of designed retro-peptides.

Retro - peptides	Sequence
r1	RG-sSIIaGfN-GR
r2	Ac-RG-sSIIaGfN-GR
r3	RG-NfGailSs-GR
r4	Ac-RG-NfGailSs-GR
r5	rG-nfgailss-Gr
r6	Ac-rG-nfgailss-Gr
r7	rG- ssliaGfn-Gr
r8	Ac-rG- ssliaGfn-Gr
hIAPP ₂₂₋₂₉	NFGAILSS

4.2 Results and Discussion

In this work, we sought to determine the effect of D-amino acid substitution and retro inversion on the self-assembly behavior and fibril morphology of peptides derived from hIAPP₂₂₋₂₉. hIAPP₂₂₋₂₉ was previously reported to form fibrils with similar morphological features as the full length hIAPP₁₋₃₇.

At first, we investigated the presence of amyloid fiber in our retro-peptides. Since the peptides were derived from an amyloid-prone region of full length hIAPP₁₋₃₇, we hypothesized that they should possess inherent self-aggregation properties. We employed various amyloid-detecting strategies including fluorophore binding – Congo red and ThT, and kinetic aggregation assay to verify our hypothesis.

Congo red is an amyloidogenic dye with interesting spectrophotometric properties. In aqueous solution, its maximum absorption wavelength is 490nm. Congo red is able to bind various

amyloid morphologies ranging from innocuous soluble monomers to toxic mature fibrils. When bound to amyloid fibrils that are rich in β -sheet, it assumes an orientation which induces torsional restrictions with a consequent increase in absorption and a red – shift in the maximum absorption from 490nm to 540nm.²⁷ We observed a gradual red shift in absorbance maxima for our retro-peptides over 43 hours (Figure 4.2, Figure 4.3, and Figure 4.4). This indicates the presence of some amyloid fibers, most especially in peptides comprising alternating L- and D-amino acids. However, this red-shift is accompanied by an increase in absorption in **r1**, **r8**, **r2**, and **r4**.

In order to fully understand the aggregation potential of the various retro-peptides, and the effect of chirality on aggregation patterns, we performed a turbidity assay, using hIAPP₂₂₋₂₉ as a control. The turbidity of the peptide solutions was monitored in a kinetic aggregation assay by monitoring the absorbance at 405nm as a function of time (Figure 4.10). hIAPP₂₂₋₂₉ displayed higher absorption, which is indicative of the presence of amyloid. Retro-peptides **r5**, and **r7** exhibited a nucleation-dependent aggregation mechanism while **r6**, displayed a seeded aggregation kinetics with a maximum absorption similar to hIAPP₂₂₋₂₉. However, hIAPP₂₂₋₂₉ is non-nucleation-dependent. We observed that the retro-inverso peptides **r5**, **r6**, **r7** and, **r8** consisting mainly of D-amino acids showed a higher aggregation potential than peptides comprising alternating L- and D- amino acids.

Amyloid formation kinetics is a multi-step process comprising many distinctive features including a lag phase, rapid growth/elongation phase and steady state/equilibrium phase. In a bid to confirm our results on Kinetic aggregation and Congo red assays, we performed Thioflavin T fluorescence assay to assess the time-dependence of the aggregation of the retro-peptides.

The curve obtained for the ThT assay for the retro-peptides showed that hIAPP₂₂₋₂₉, **r5** and **r6** displayed a seeded aggregation kinetics consisting of a short elongation phase leading to the steady state. hIAPP₂₂₋₂₉ showed a higher fluorescent signal than the retro-peptides (Figure 4.5)

Amyloid fibrils consist majorly of β -sheet conformation, hence, UV Circular Dichroism studies proves useful in determination of the secondary structure of the retro-peptides. A CD signal around 195nm typically indicates random coil. The signal is negative if it's due to L-amino acids and positive for D-amino acids.²⁸ The presence of a maximum and minimum near 195nm and 215 nm respectively signals the presence of a β -sheet. As seen in Figure 4.7, the spectra acquired for peptides **r1** and **r2** revealed that both retropeptides have some β -character, with a characteristic maximum around 200nm and a corresponding minimum at 220nm. **r1** and **r2** are composed of alternating units of L- and D- amino acids in a retroinversed arrangement, and an acetylated N-terminus in **r2**. Surprisingly, **r3** and **r4** comprising of alternating units of L- and D-amino acids, but with no retro inversion, exhibited characteristic β -sheets spectra with maxima around 200nm and minima of 220nm (Figure 4.7). Peptides **r5**, **r6**, **r7** and **r8**, which are all D-peptides displayed positive signals around 200nm (Figure 4.8 and Figure 4.9). This is very typical unstructured conformers termed random coils. The CD result corroborates previous findings that d-amino acids possess inherent secondary structure destabilizing properties.²⁹

Having confirmed the amyloidogenic potential of our designed retro-peptides, we decided to investigate the morphological features of the aggregates formed. We obtained TEM micrographs of all our retropeptides and hIAPP₂₂₋₂₉. In line with previous reports, hIAPP₂₂₋₂₉ formed mature fibrillary bundles similar to full length hIAPP₁₋₃₇ (Figure 4.6).^{13, 16, 17} **r1** formed amorphous aggregates while **r2**, **r3**, and **r4** formed protofibrillar structures (Figure 4.6), however, hIAPP monomers were seen in **r5**, **r6** and **r8**.

Encouraged by these results, we proceeded to evaluate the possibility of inhibition of hIAPP₁₋₃₇ amyloid fibrillation by our designed peptides, using Thioflavin T assay. 0.6-, 2.5-, and 10-fold molar excesses of peptides r1 – r8, 15µM ThT and 10µM hIAPP₁₋₃₇ were added to sample wells (black 96-well plates), and the relative rise in fluorescent intensity was recorded. The measurement was done in duplicates. **r1** exhibited a dose-dependent relationship, in which the lowest suppression of fluorescent signal was observed with 10-fold molar excess of peptide. **r5** is suspected to promote aggregation due to an increase in the observed fluorescence signal. At all concentrations tested, **r5** showed similar or higher fluorescent signal than hIAPP₁₋₃₇. Results also revealed **r6** and **r7** inhibited hIAPP₁₋₃₇ fibril formation at 10-fold and 0.6-fold molar excess respectively. **r2** also displayed some inhibitory effect at 2.5- and 0.6-fold molar excesses, whereas, **r3** showed moderate inhibition at all peptide concentrations tested. **r8** exhibited weak inhibition at 2.5-fold molar excess and a strong inhibitory effect at 10- and 0.6-fold molar excess. At 10- and 2.5-fold molar excesses, **r4** also showed strong inhibitory effect. Contrary to previous reports, hIAPP₂₂₋₂₉ promoted aggregation at all concentrations tested¹³

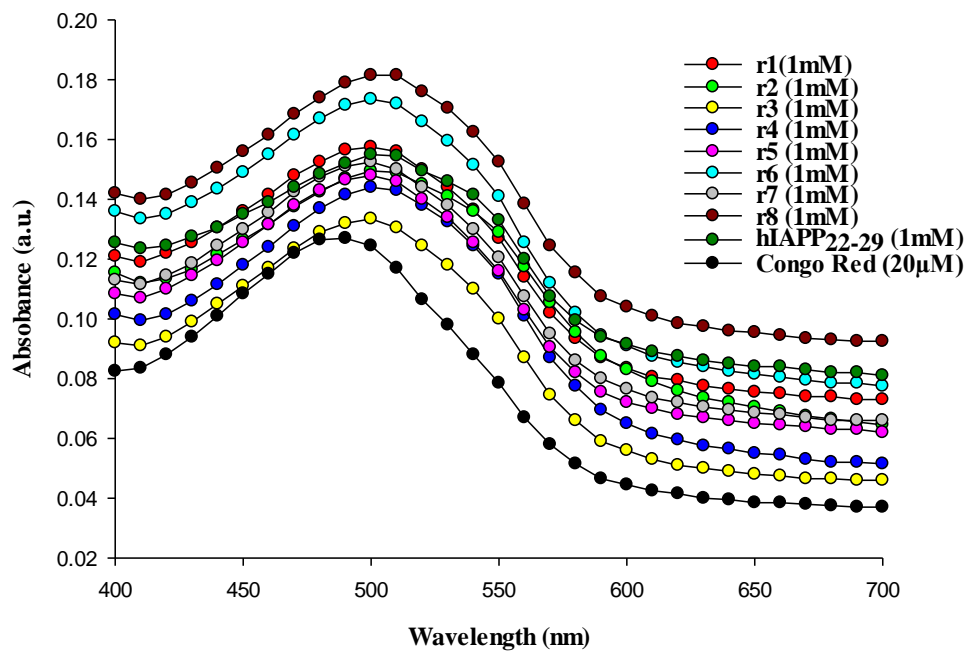


Figure 4.2 Congo red spectra of retro-peptides at time $t = 0h$

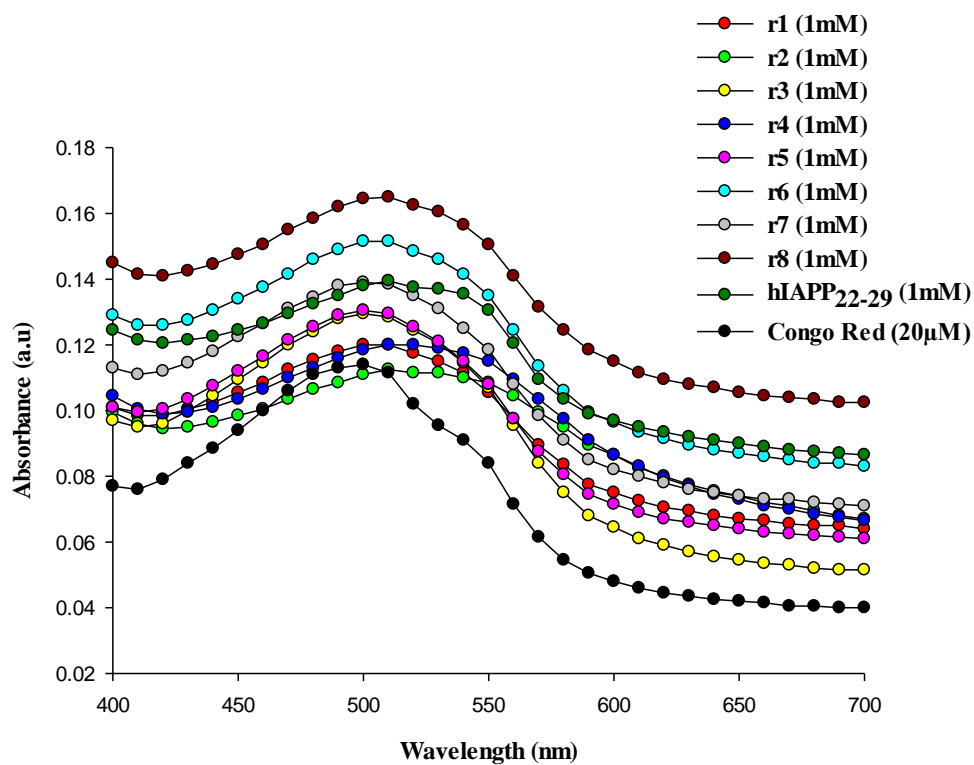


Figure 4.3 Congo red spectra of retro-peptides at time $t = 28h$

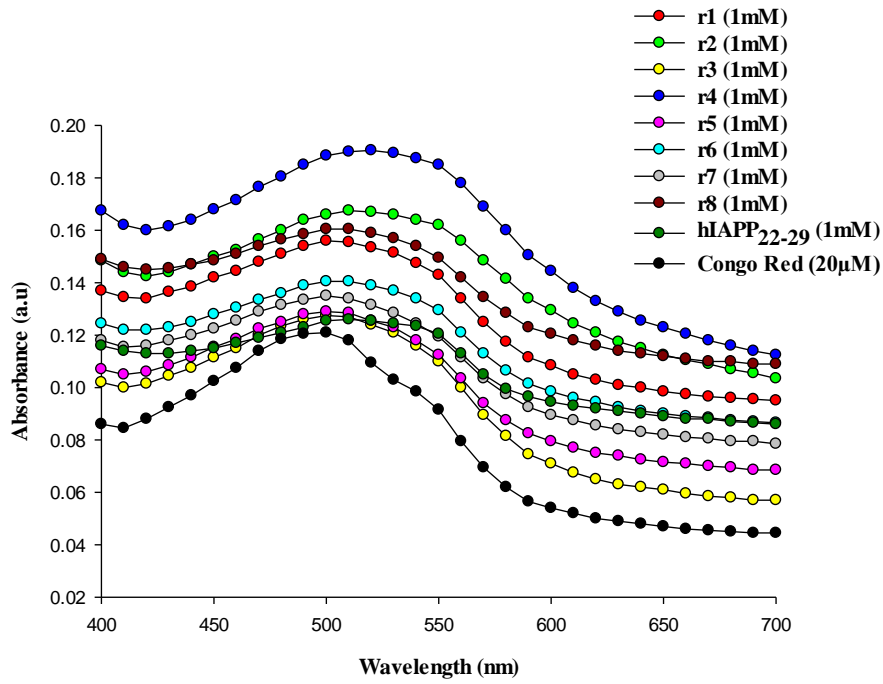


Figure 4.4 Congo red spectra of retro-peptides at time $t = 43h$

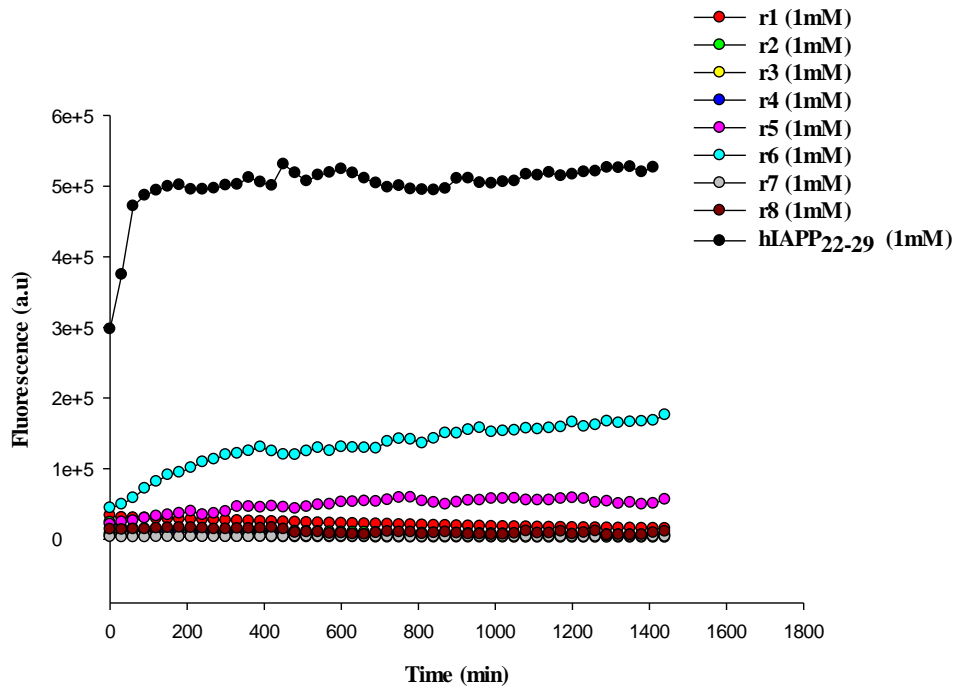


Figure 4.5 ThT assay for aggregation of retro-peptides

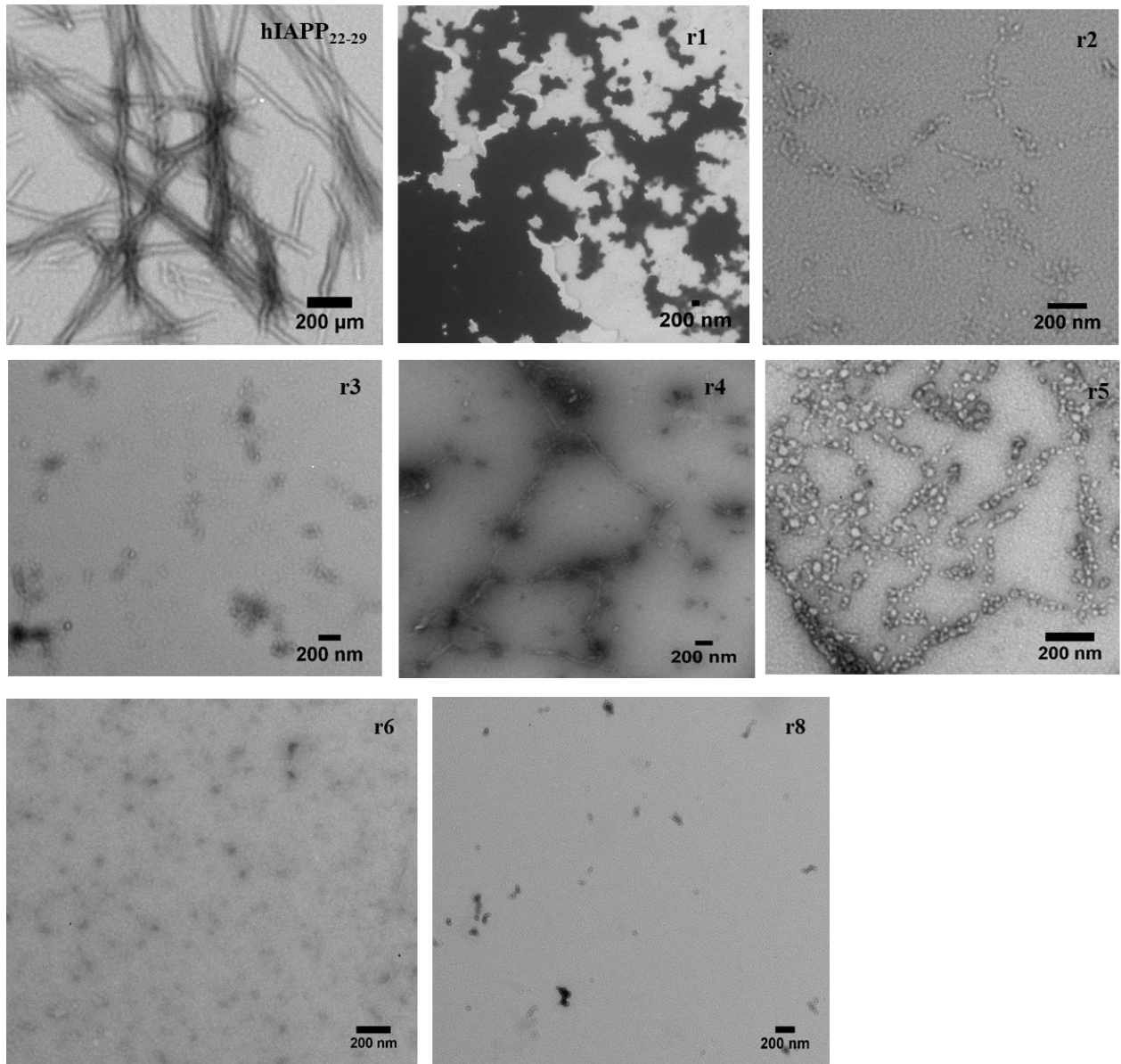


Figure 4.6 TEM images of hIAPP₂₂₋₂₉, and peptides r1 – r8

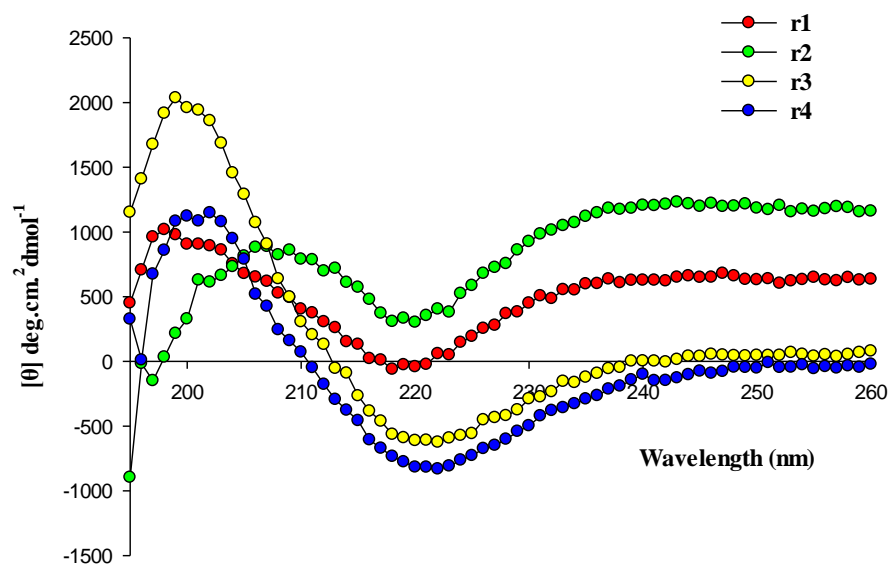


Figure 4.7 CD spectra of peptides consisting of alternating L- and D-amino acid units

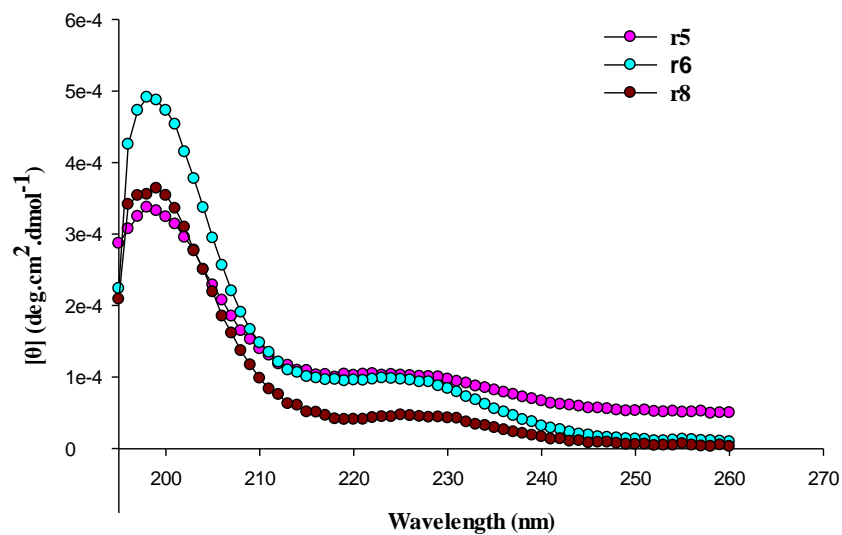


Figure 4.8 CD spectra of peptides consisting of all D-amino acid units (r5, r6, and r8)

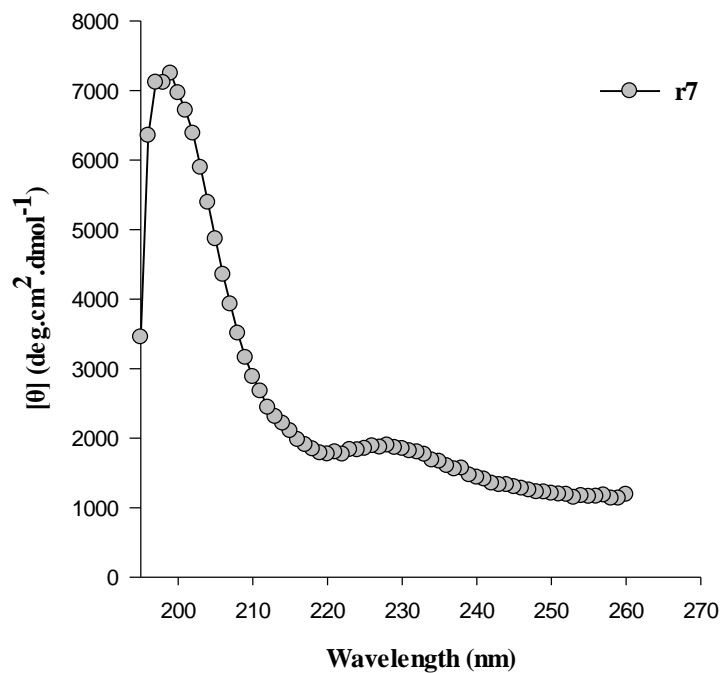


Figure 4.9 CD spectra of peptides consisting of all D-amino acid units (r7)

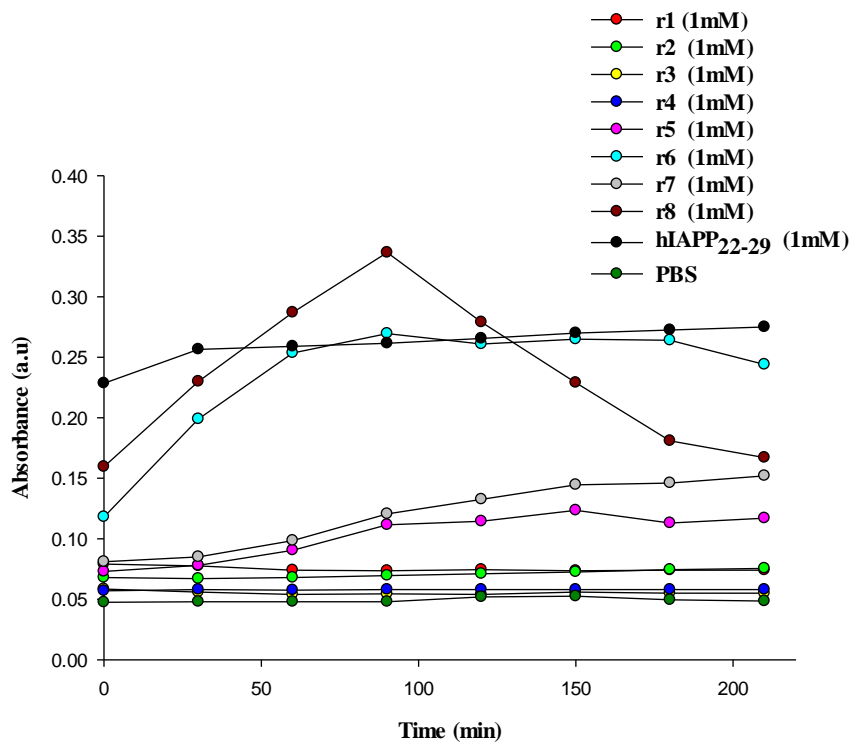


Figure 4.10 Kinetic aggregation assay for all peptides.

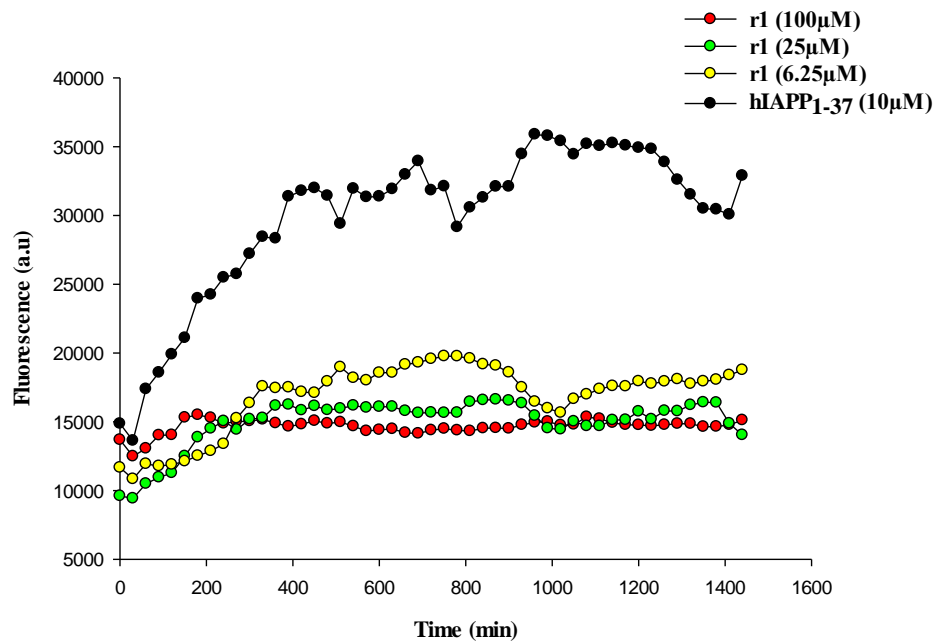


Figure 4.11 ThT inhibition assay for r1.

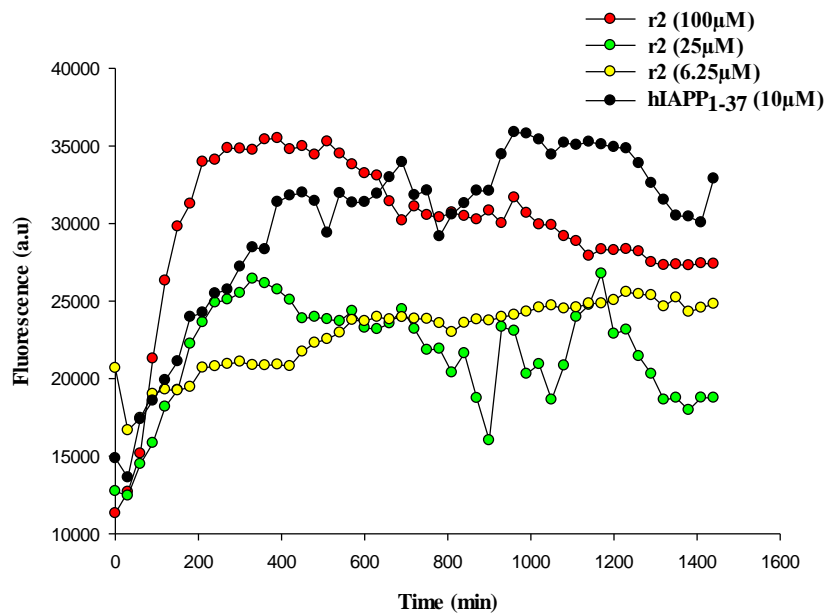


Figure 4.12 ThT inhibition assay for r2.

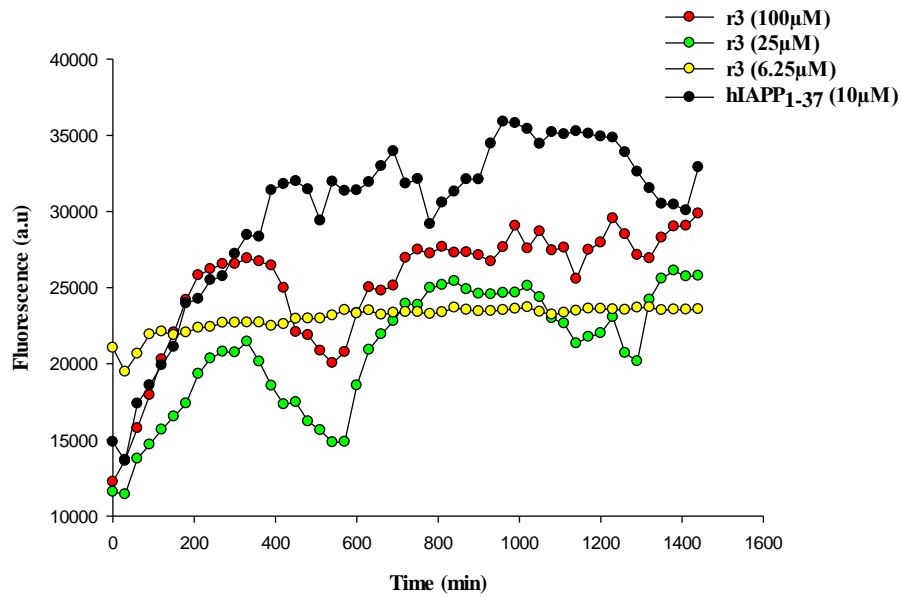


Figure 4.13 ThT inhibition assay for r3.

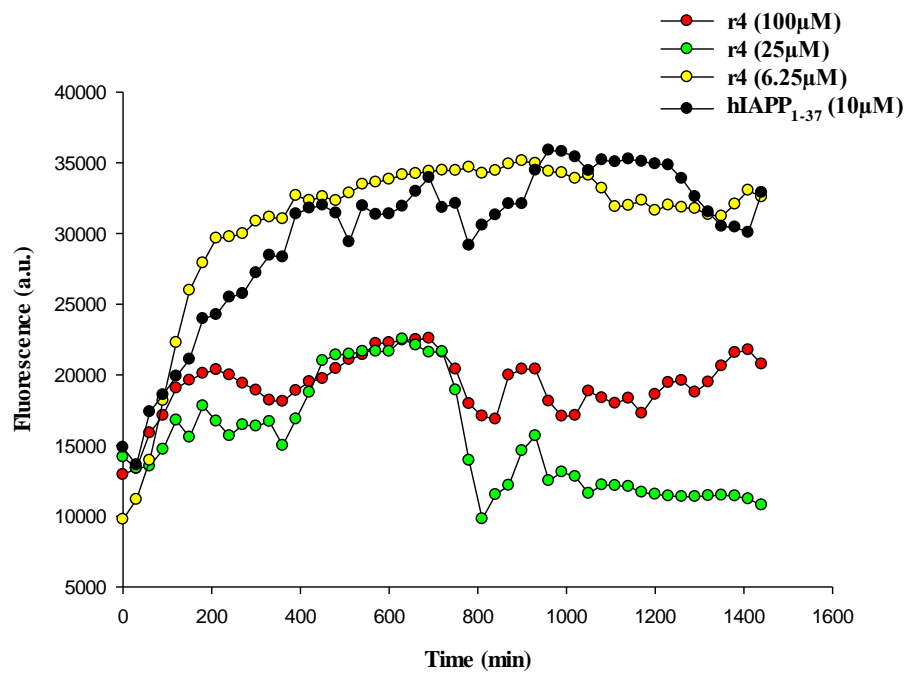


Figure 4.14 ThT inhibition assay for r4.

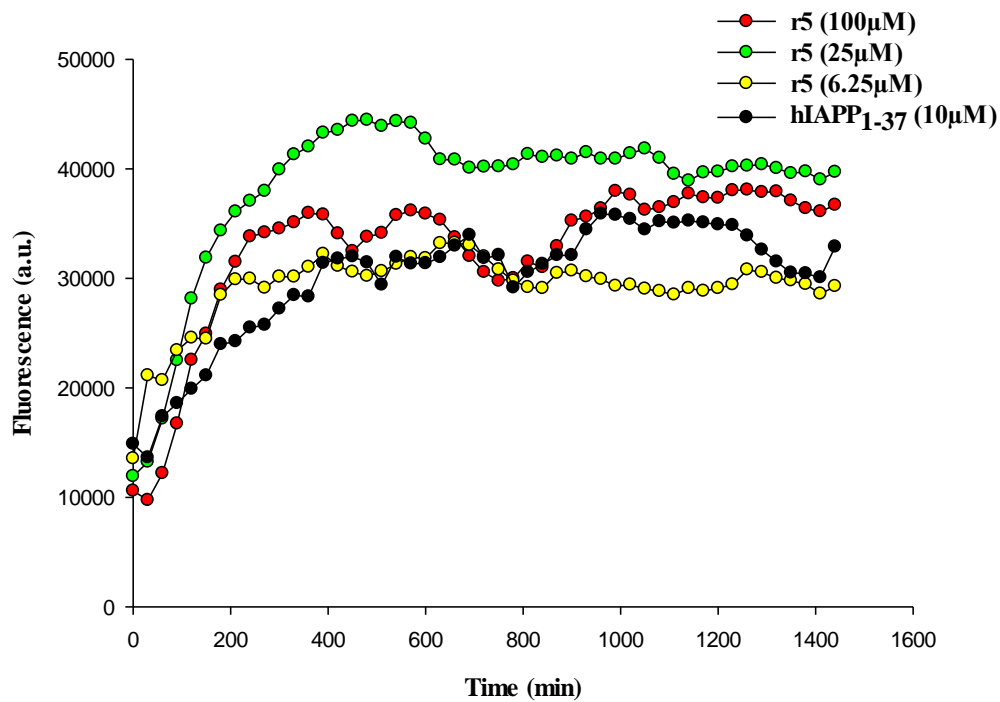


Figure 4.15 ThT inhibition assay for r5.

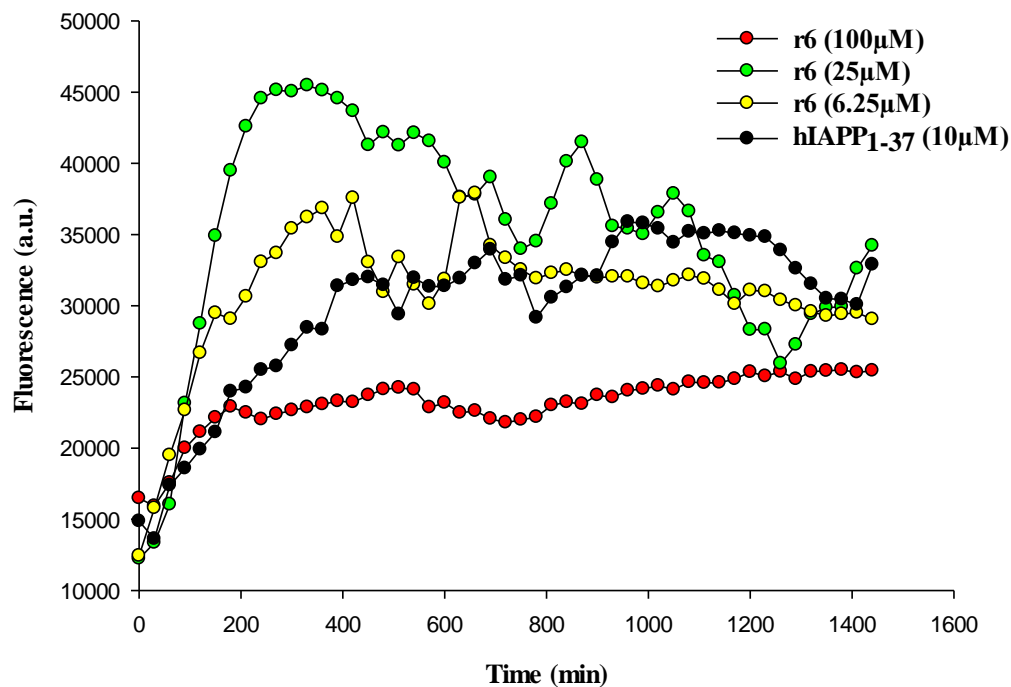


Figure 4.16 ThT inhibition assay for r6.

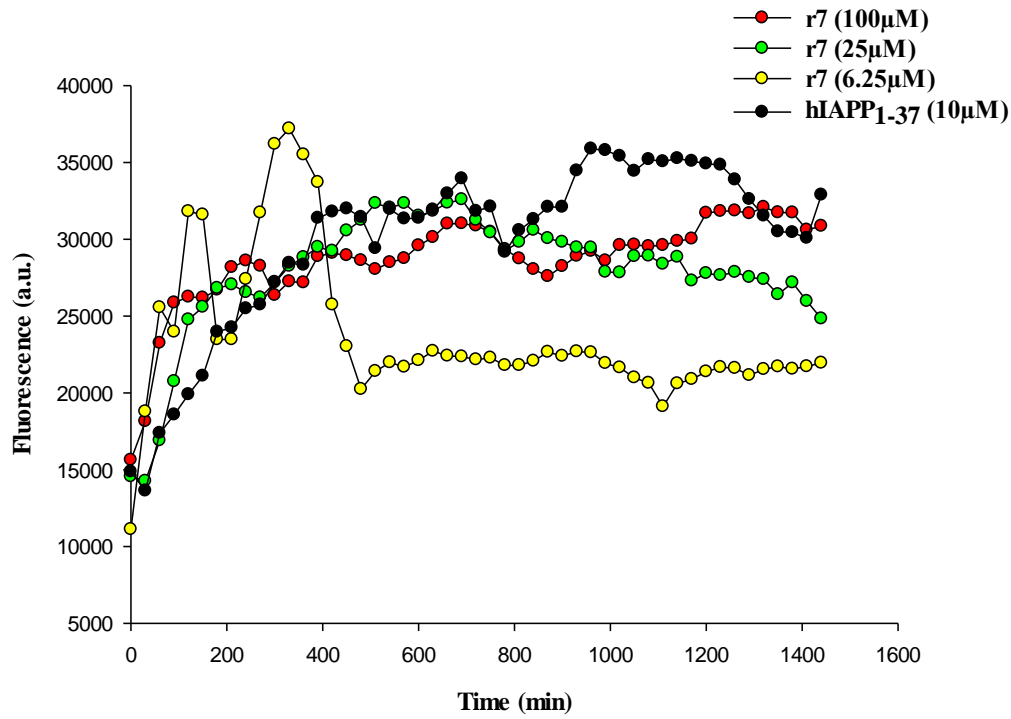


Figure 4.17 ThT inhibition assay for r7.

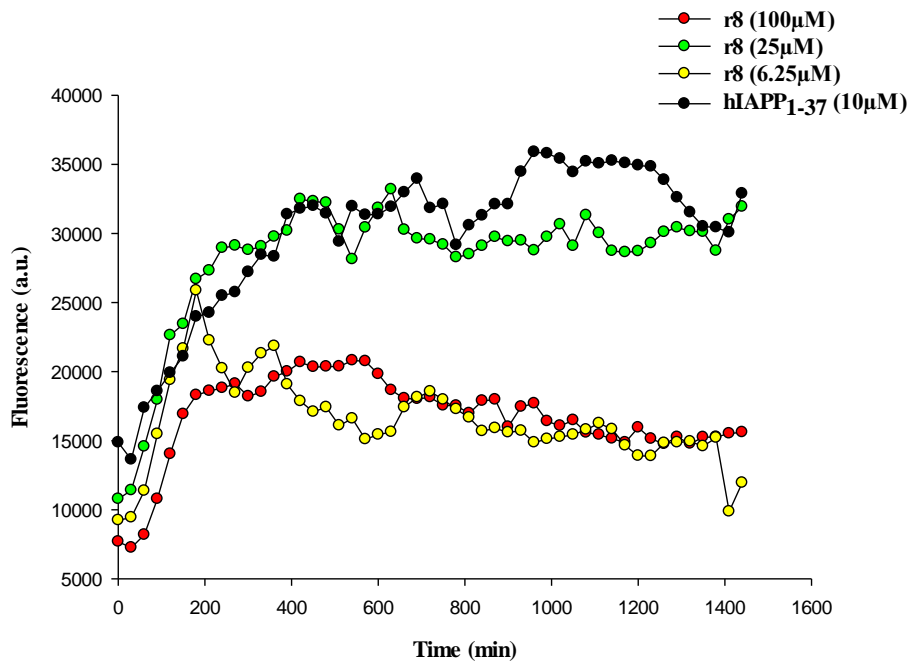


Figure 4.18 ThT inhibition assay for r8.

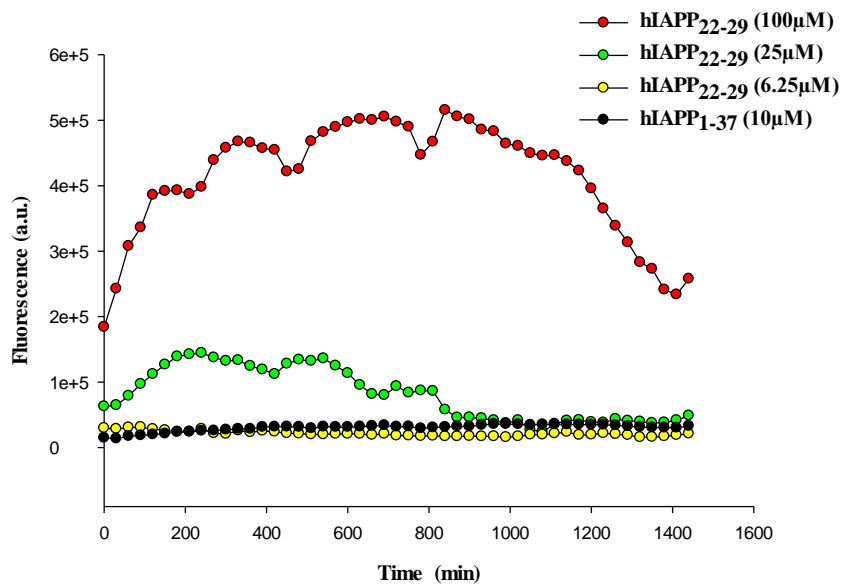


Figure 4.19 ThT inhibition assay for hIAPP₂₂₋₂₉.

4.3 Conclusion

In this study, we evaluated the effects of alternating L- and D-amino acids, retro-inversion and all D-peptides on the self-aggregation potential and amyloid morphology of peptides derived from hIAPP₂₂₋₂₉. Our results showed the complete incorporation of D-peptides in hIAPP₂₂₋₂₉ (all D-peptides) dramatically changed the secondary structure from the known cross β -sheet to random coil, whereas, alternating L- and D-amino acids did not significantly alter the β -sheet conformation. We also observed that aggregation behavior is strictly dependent on the nature and chirality of constituent amino acids rather than N-terminus acetyl capping.

We anticipate that this strategy may provide a template for the understanding of different amyloid systems, thereby providing insights into the design of novel inhibitors of amyloid aggregation for various amyloidogenic diseases.

4.4 General information

Peptide Synthesis

All peptides used in this study were synthesized by the standard Fmoc-based solid phase peptide synthesis protocol using the Burrell Wrist-Action shaker. All Fmoc protected α -L-amino acids, α -D-amino acids, and Rink amide resin (0.7mmol/g, 200-400 mesh) were purchased from Chem-Impex International, Inc. All other Solvents and reagents were purchased from either Sigma Aldrich or Fisher Scientific and used without further purification.

For each amino acid coupling, 2 equivalents of Fmoc-amino acid, 4equivalents each of DIC and HOBt were used and the coupling cycle was repeated, followed by capping with 1 equivalent of acetic anhydride and 2 equivalents of pyridine. Fmoc-deprotection was done with 20%piperidine in DMF. The final peptide was cleaved from the resin using a cleavage cocktail:95% TFA,2.5% TIS,2.5% Water for 3h. TFA was removed by evaporation and the crude peptide was dissolved in acetonitrile and water. The peptides were analyzed and purified on a Waters Breeze 2 HPLC System, and then lyophilized on a Labconco Lyophilizer

Congo red binding assay.

Congo red was dissolved in PBS buffer (X 1) to make a stock solution of 100 μ M. The stock solution was sonicated and filtered through a 0.4micron filter membrane to remove any insoluble aggregate. 20 μ M Congo red solution was then incubated with 1mM retro-peptides in duplicate wells in a clear 96-well plate for 30 minutes at room temperature before measurement. The absorption spectra was acquired at a wavelength range of 400nm – 700nm using a Biotek Synergy H1 hybrid plate reader. The reaction solution in each well was mixed with a pipette before measurement.

Circular Dichroism studies.

Circular dichroism (CD) spectra were measured on an Aviv 215 circular dichroism spectrometer using a 1 nm bandwidth and 1nm step resolution from 200 to 260nm at 25°C. 3 scans were averaged for each sample. Control water blank scans were run, averaged and then subtracted from the sample spectra. Retro-peptide solutions were prepared in water to a final concentration of 200µM and allowed to age for 5 days at 37°C. The samples were loaded in a 1mm path length quartz cell, and the CD spectra were acquired with an averaging time of 1s, Settling time of 0.333s and multi-scan wait time of 1s. The data unit was converted from machine units (millidegree, θ) into mean residue ellipticity $[\theta]$. Mean Residue Ellipticity $[\theta]$ ($\text{deg.cm}^2.\text{dmol}^{-1}$) was calculated using the equation:

$$[\theta] = \theta_{\text{obs}} / (p \times c \times 10 \times n)$$

Where θ_{obs} is the measured ellipticity in millidegrees, while p is the path length in centimeter, n is the number of side chains and c is the concentration of the peptide in Molar.

Thioflavin T Fluorescence Assay

Detection of amyloid fiber 1mM peptide concentrations were incubated with 15µM ThT in duplicate wells in a 96-well black plate at a total volume of 100µL. Time-dependent fluorescent change was monitored for 24h by the Biotek Synergy H1 hybrid plate reader at excitation and emission wavelengths of 435 and 490 nm respectively.

Inhibition of hIAPP aggregate formation Different peptide concentrations were made in PBS (x1, pH 7.4). hIAPP stock solution (40µM) was also prepared as described above. The peptide, hIAPP and 15µM ThT were added into a 96-well black plate. Each reaction solution was duplicated. Equal volume of hIAPP solution was added into the 96-well black plate to make the final concentration of hIAPP in each well to be 10µM. Time-dependent fluorescent change was monitored for 24h by

the Biotek Synergy H1 hybrid plate reader at excitation and emission wavelengths of 435 and 490 nm respectively

Transmission Electron Microscopy (TEM)

10 μ L of 1mM retro peptide solution was placed on carbon-coated 200-mesh copper grid. After 10 mins, excess solution was wicked away and the grid was allowed to dry. This is then followed by the addition of 2% uranyl acetate solution (10 μ L) which was allowed to float for 5min. The excess solution was then removed using the blotting paper. The copper grid was left to dry at room temperature before imaging with FEI Morgagni 268D TEM operated at 60kV.

Kinetic aggregation assay

Freshly prepared 3mM stock of retro-peptides were used in the assay. The stock solution was sonicated and a volume equivalent to 1mM retro-peptide was added to clear 96-well plate. PBS (X1) buffer was added to make the total volume 100 μ L. The absorption spectra was acquired for 3h 30min at 30 min interval, and at a wavelength of 405nm, using a Biotek Synergy H1 hybrid plate reader.

Table 4.2 Molecular weight of peptides and their percent yield.

Peptide	Molecular Mass [M+H] ⁺ (expected/observed)	Yield (%)
r1	1233.6738/1233.8107	90
r2	1275.6844/1275.8912	89
r3	1233.6738/1233.8312	92
r4	1275.6844/1275.7228	91
r5	1233.6738/1233.8624	89
r6	1275.6844/1275.8861	93
r7	1233.6738/1233.7389	90
r8	1275.6844/1275.7449	95

4.5 References

1. C. M. Dobson, *Trends in Biochemical Sciences*, 1999, **24**, 329-332.
2. F. Chiti and C. M. Dobson, *Annual Review of Biochemistry*, 2017, **86**, 27-68.
3. S. Xu, *The Journal of Physical Chemistry B*, 2009, **113**, 12447-12455.
4. K. Sivanesam and N. H. Andersen, *Biochemistry*, 2017, **56**, 5373-5379.
5. J. A. Williamson and A. D. Miranker, *Protein Science : A Publication of the Protein Society*, 2007, **16**, 110-117.
6. A. Lorenzo, B. Razzaboni, G. C. Weir and B. A. Yankner, *Nature*, 1994, **368**, 756.
7. K. Aphrodite, B. Jürgen, G. Norma, A. A. Yousef, T. Saul, F. R. W., V. Wolfgang and B. Richard, *European Journal of Biochemistry*, 1998, **251**, 208-216.
8. Y. Li - Mei, V. Aleksandra, T. N. Marianna, A. Erika and K. Aphrodite, *Angewandte Chemie International Edition*, 2007, **46**, 1246-1252.
9. J. Janson, R. H. Ashley, D. Harrison, S. McIntyre and P. C. Butler, *Diabetes*, 1999, **48**, 491-498.
10. J. F. Aitken, K. M. Loomes, D. W. Scott, S. Reddy, A. R. J. Phillips, G. Prijic, C. Fernando, S. Zhang, R. Broadhurst, P. L'Huillier and G. J. S. Cooper, *Diabetes*, 2010, **59**, 161-171.
11. K. Barbara, A. J. F., K. Joerg, Z. Shaoping and C. G. J. S., *The FEBS journal*, 2006, **273**, 3614-3624.

12. S.-T. Wang, Y. Lin, R. K. Spencer, M. R. Thomas, A. I. Nguyen, N. Amdursky, E. T. Pashuck, S. C. Skaalure, C. Y. Song, P. A. Parmar, R. M. Morgan, P. Ercius, S. Aloni, R. N. Zuckermann and M. M. Stevens, *ACS Nano*, 2017, **11**, 8579-8589.
13. Y. Porat, Y. Mazor, S. Efrat and E. Gazit, *Biochemistry*, 2004, **43**, 14454-14462.
14. A. Mishra, A. Misra, T. Sri Vaishnavi, C. Thota, M. Gupta, S. Ramakumar and V. S. Chauhan, *Chemical Communications (Cambridge, England)*, 2013, **49**, 2688-2690.
15. A. Abedini and D. P. Raleigh, *Journal of Molecular Biology*, 2006, **355**, 274-281.
16. K. Tenidis, M. Waldner, J. Bernhagen, W. Fischle, M. Bergmann, M. Weber, M.-L. Merkle, W. Voelter, H. Brunner and A. Kapurniotu, *Journal of Molecular Biology*, 2000, **295**, 1055-1071.
17. P. Westermark, U. Engström, K. H. Johnson, G. T. Westermark and C. Betsholtz, *Proceedings of the National Academy of Sciences*, 1990, **87**, 5036-5040.
18. D. Zanuy, B. Ma and R. Nussinov, *Biophysical Journal*, 2003, **84**, 1884-1894.
19. A. Kapurniotu, A. Schmauder and K. Tenidis, *Journal of Molecular Biology*, 2002, **315**, 339-350.
20. A. Abedini, F. Meng and D. P. Raleigh, *Journal of the American Chemical Society*, 2007, **129**, 11300-11301.
21. A. Paul, S. Kalita, S. Kalita, P. Sukumar and B. Mandal, *Scientific Reports*, 2017, **7**, 40095.
22. B. Matharu, O. El-Agnaf, A. Razvi and B. M. Austen, *Peptides*, 2010, **31**, 1866-1872.
23. M. Goodman and M. Chorev, *Accounts of Chemical Research*, 1979, **12**, 1-7.
24. M. Chorev and M. Goodman, *Accounts of Chemical Research*, 1993, **26**, 266-273.
25. M. D. Fletcher and M. M. Campbell, *Chemical Reviews*, 1998, **98**, 763-796.
26. J. Kumar and V. Sim, *Prion*, 2014, **8**, 119-124.
27. C. Wu, J. Scott and J.-E. Shea, *Biophysical Journal*, 2012, **103**, 550-557.
28. J. Kellock, G. Hopping, B. Caughey and V. Daggett, *Journal of Molecular Biology*, 2016, **428**, 2317-2328.
29. E. B. Martin, A. Williams, T. Richey, C. Wooliver, A. Stuckey, J. S. Foster, S. J. Kennel and J. S. Wall, *Journal of Translational Medicine*, 2017, **15**, 247.

<https://commons.wikimedia.org/wiki/File:L-peptideD-peptideAnalogues.png>

CHAPTER 5 : DEVELOPMENT OF POTENT CHEMICAL PROBES TARGETING MPP8-H3K9ME INTERACTION.

5.1 Introduction

Cancer is a process of multistep cellular transformation, which consequently lead to abnormal and uncontrolled cell growth.¹ It is mostly characterized by a series of alterations in the genome and epigenetic network. In higher organisms, the epigenetic network can undergo four major modifications including chromatin remodeling, microRNAs, DNA methylation and histones posttranslational modifications (acetylation, methylation, ubiquitination, phosphorylation, sumoylation and so on).² Being a major player in the regulation of the chromatin, histone octamers wrapped with 147 base pairs of DNA, forming the nucleosome. The nucleosome is also subjected to various post-translational modifications (PTM) such as acetylation and methylation.³ These posttranslational modifications are collectively known as the histone code which is identified by histone “PTM-reader” protein complexes.⁴⁻⁶

Over the past few decades, lysine methylation of histone tails has attracted tremendous attention in drug discovery research.^{7,8} Histone methylation mostly occurs on Lysine and Arginine residues and can be easily identified by effector protein complexes bearing different binding domains for methylated histones. Previous studies have reported some of these binding motifs including chromodomain, tudor domain, WD40 repeat domain, MBT domain PHD fingers and ankyrin-repeats domain, PWWP domain and chromobarrel domain.⁹⁻¹⁷ The common code for recognition by these domains is the coordination of methylated lysine residue via a conserved aromatic cage. The first identified example of the chromodomain binding motif was in *Drosophila*

melanogaster namely heterochromatin protein-1(HP-1) and Polycomb. The HP-1 proteins identifies H3K9me (histone 3 that is methylated at Lysine 9) through its N-terminal domain. The Polycomb chromodomain recognizes H3K27me (Histone 3 that is methylated at Lysine at position 27).¹⁸⁻²⁰

Recently, more research efforts has been invested in understanding the diverse function of H3K9 methylation and identifying more H3K9me-binding chromodomain. MPP8 (M-Phase Phosphoprotein 8) has been identified and characterized as a novel methyl-H3K9 binding protein.^{21, 22} Using their chromodomain, MPP8 binds tri- and di-methylated lysines 9 on histone 3. MPP8 level is elevated in several human primary tumor tissues, while knockdown of MPP8 in metastatic tumor cells leads to a regain of epithelial characteristics accompanied by a significant reduction of cell motility and invasiveness, suggesting that MPP8 contributes to EMT and tumor malignant progression. Mechanistic characterization revealed that MPP8 represses transcription of E-cadherin by directly binding to methyl-H3K9 marks on the promoter of this key EMT regulator.

Based on the importance of methyl-H3K9 binding by MPP8 in E-cadherin gene silencing and EMT as well as the potential druggability of its “cavity insertion” binding mode, we hypothesized that specifically inhibiting MPP8-H3K9me interaction could have therapeutic value in cancer treatment. To explore this possibility, we developed several chemical probes, among which two compounds displayed potential to antagonize methyl-H3K9 binding by MPP8 in our initial characterization.

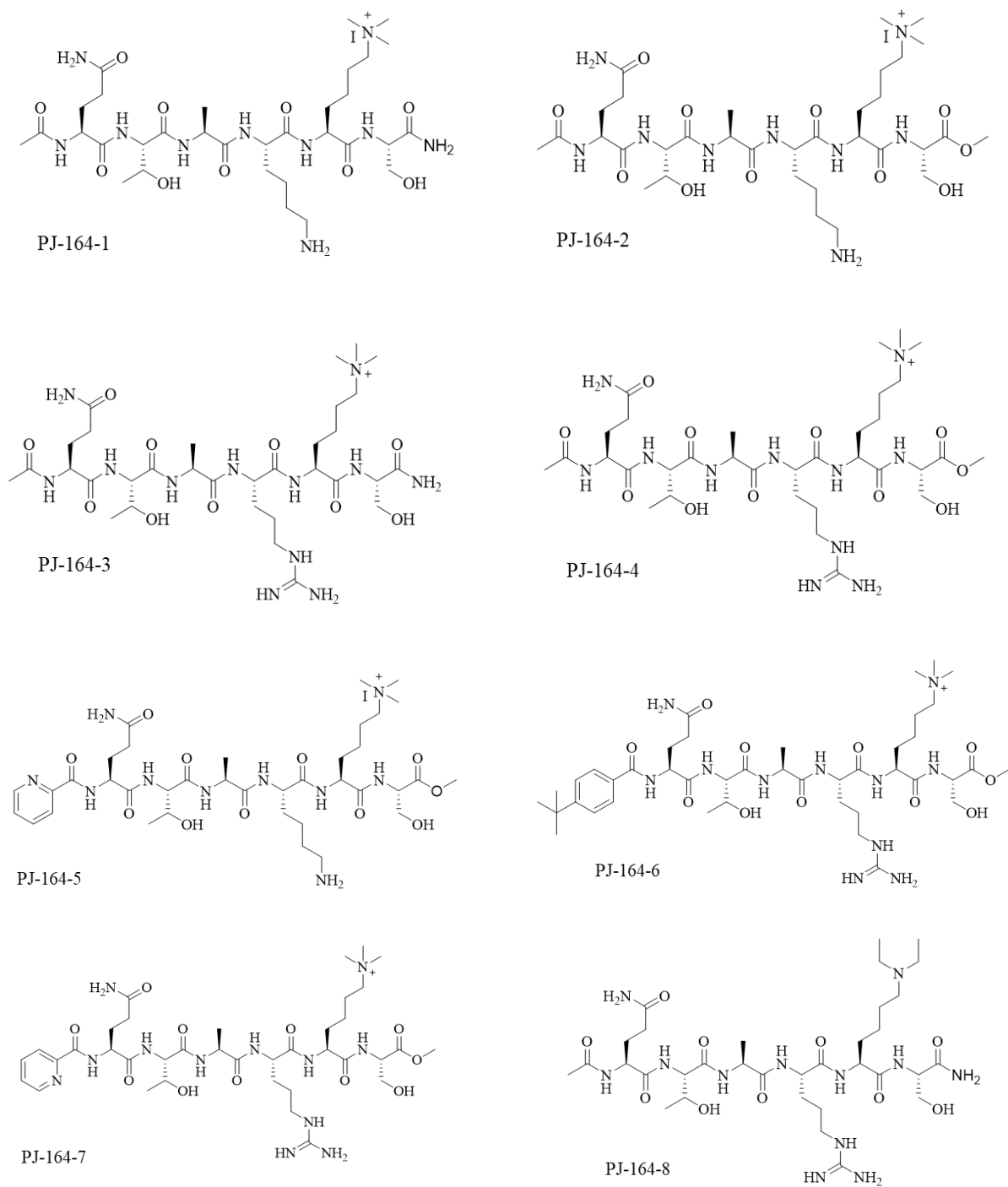


Figure 5.1 Peptides designed to disrupt H3K9me3-MPP8 interaction (PJ-164-1 – PJ-164-8)

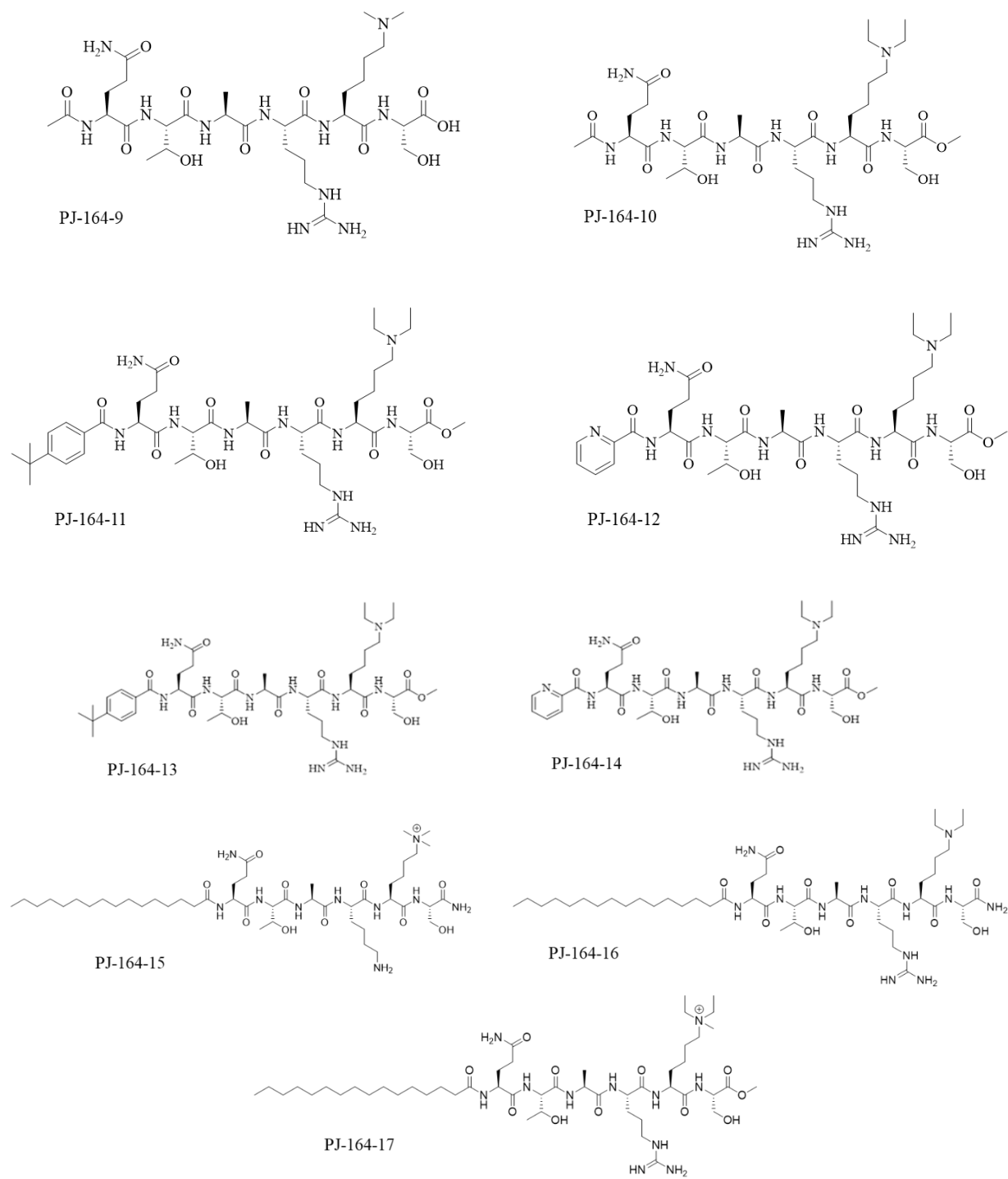
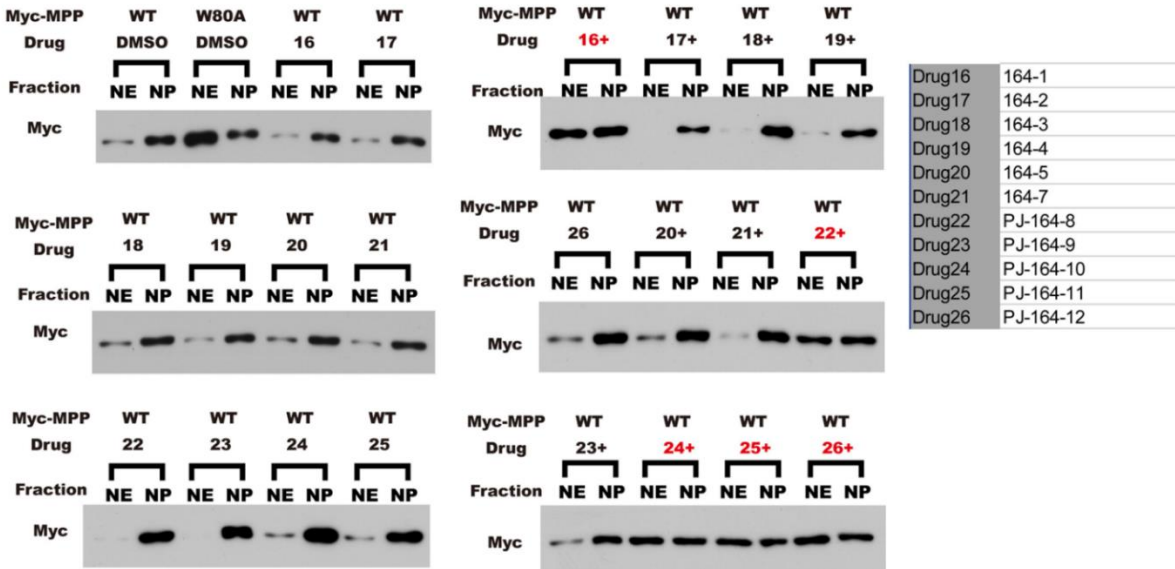
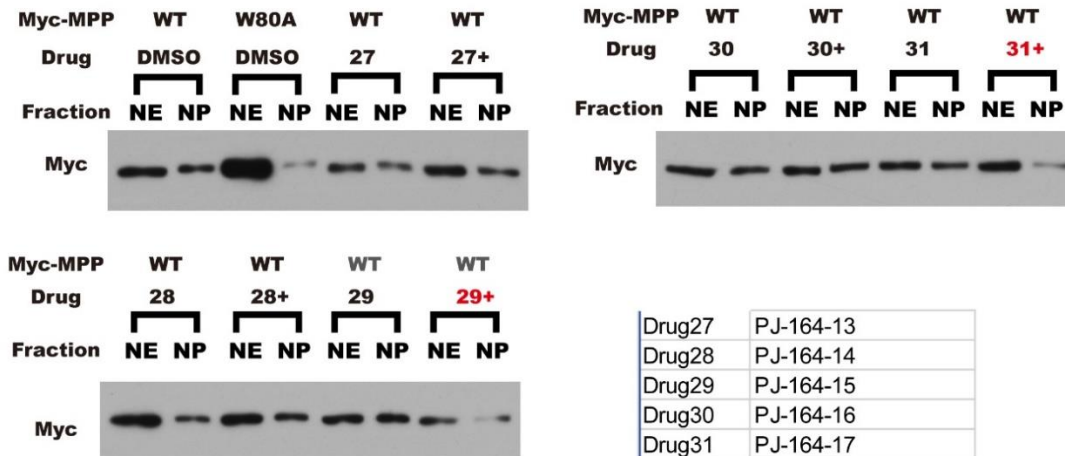


Figure 5.2 Peptides designed to disrupt H3K9me3-MPP8 interaction (PJ-164-9 – PJ-164-17)

drugs were dissolved in DMSO at 10mM, final concentration in medium and buffers is 20µM
16+: drug included in lysis buffer
16: drug not included in lysis buffer

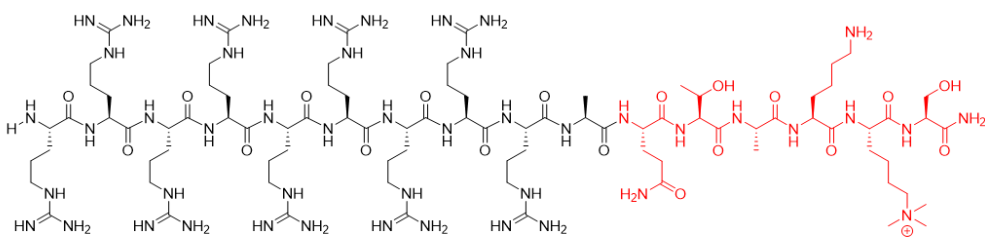


transfection---24hr---Add drug---24hr---fraction(With drug in NE buffer)
 drugs were dissolved in DMSO at 10mM, final concentration in medium and buffers is 20µMS

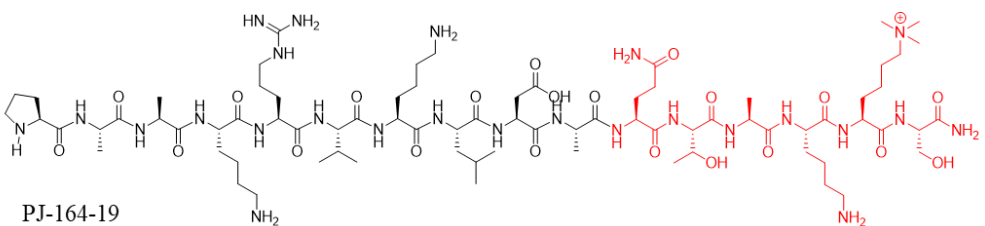


27: means drug only in cell culture
 27+: means drug also in lysis buffer

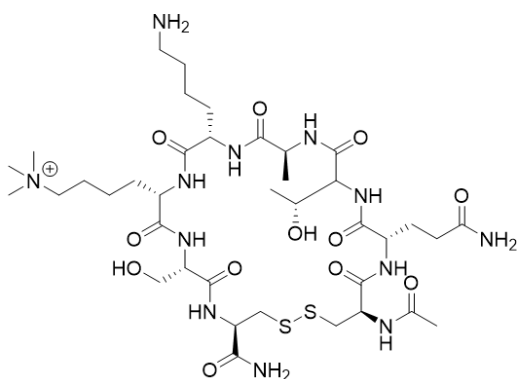
Figure 5.3 Western blot from cell fractionation studies (PJ-164-13 – PJ-164-17).



PJ-164-18



PJ-164-19



PJ-164-20

Figure 5.4 Structure of designed cell-penetrating and cyclic peptides.

5.2 Results and Discussion

Because EMT is very important in converting early stage tumors into invasive malignancies,²³ and a major obstacle to successful anti-cancer therapy, previous works suggest that blocking MPP8-H3K9me interactions could have potential therapeutic value. The crystal structure of MPP8/H3K9me3 complex showed that the major interaction points are on K9me3 in the aromatic cage of MPP8 chromodomain,^{22, 24} including side chain N-CH₃ groups projected toward the three rings, dimethyl group toward Asp87, and trimethyl group to the open side of the cage. There are some other residues from H3, which have direct interactions with MPP8, including Gln5, Thr6, Ala7 and Arg8.^{22, 24} Based on these reported structural data and the predicted relatively

high druggability of chromodomain among different methylated lysine binding motifs,²⁵ we designed and synthesized 24 compounds (Figure 5.1, Figure 5.2, Figure 5.4, and Figure 5.5) which are expected to reproduce the hydrophobic and charged interactions described and thus bind to the aromatic cage of MPP8 chromodomain.

The design of these compounds was based on the core binding region of histone 3(H3), ⁵QTARKS¹⁰.

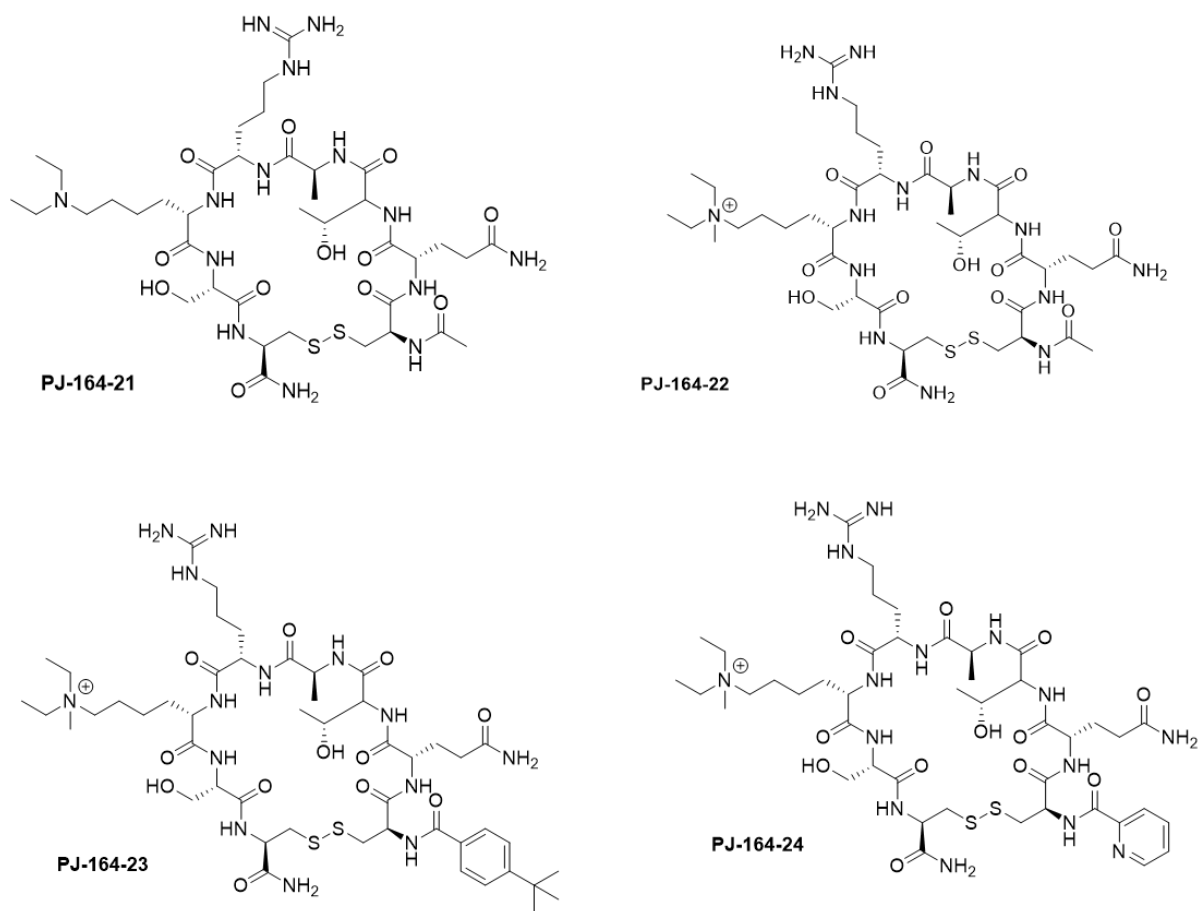


Figure 5.5 Structure of designed cyclic peptides.

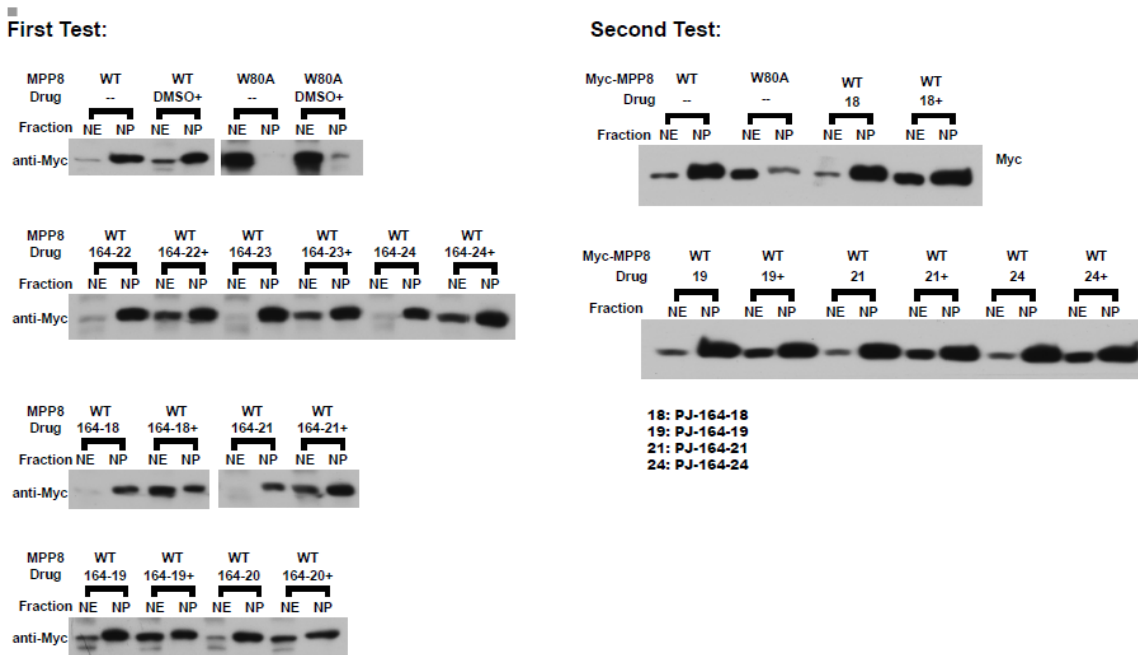


Figure 5.6 Western blot of cell fractionation assay for peptides PJ 164-18 – PJ 164-24.

This site contains Lysine 9 (K9), which is one of the preferential methylation sites for histone 3. We introduced various modifications on Lysine 9 including methylation (di- and tri-methylation), acetylation (di- and tri-acetylation), or a combination of both.

At first, we assessed the antagonistic effects of our designed alkylated lysine variants on H3K9me-MPP8 interaction, using cell fractionation assay followed by western blot analysis.

Myc-MPP8-wt or W80A was first expressed in 293T cells. Cell fractionation was then performed on the transfected cells and cytoplasmic (cyto), nuclear extract (NE) and Nuclear pellet (NP) fractions were collected by a previously described protocol.²⁶ Because the localization of MPP8 in the cell is in the Chromatin-bound Nuclear Pellet fraction (NP), the potency of the compounds is strongly correlated to their ability to dissociate MPP8 from the NP into the NE.²¹

The western blot of the cell fractionation assay for our first set of designed compounds revealed that compounds **PJ-164-1**, **PJ-164-8**, **PJ-164-11**, and **PJ-164-12** were able to dislodge

MPP8 from the nuclear pellet into the nuclear extract (Figure 5.3 and Figure 5.6). This implies that these compounds could compete for MPP8 binding with the wild type H3K9me.

Encouraged by our initial attempt, we further modified our design to include the cyclic variants of active compounds and we added some arginine residues to the N-terminus to enhance cell penetration. Interestingly, compounds **PJ-164-18**, **PJ-164-19**, **PJ-164-21** and **PJ-164-24** were also able to increase the band intensity due to its interaction with MPP8 (Figure 5.6).

5.3 Conclusion

Modulation of H3K9me3 signalling with small molecules has been a subject of intense research. Inhibitors that could antagonize the methyl reading function of MPP8 may be next generation anti-cancer agents.

5.4 General information

Peptide Synthesis

All peptides used in this study were synthesized by the standard Fmoc-based solid phase peptide synthesis protocol using the Burrell Wrist-Action shaker. All Fmoc protected α -L-amino acids, and Rink amide resin (0.7mmol/g, 200-400 mesh) and 2-Chlorotrityl chloride resin (0.98 mmol/g, 100-200 mesh) were purchased from Chem-Impex International, Inc. All other Solvents and reagents were purchased from either Sigma Aldrich or Fisher Scientific and used without further purification.

For each amino acid coupling, 2 equivalents of Fmoc-amino acid, 4equivalents each of DIC and HOBt were used and the coupling cycle was repeated, followed by capping with 1 equivalent of acetic anhydride and 2 equivalents of pyridine. Fmoc-deprotection was done with 20%piperidine in DMF. The final peptide was cleaved from the resin using a cleavage cocktail:95%TFA,2.5%TIS,2.5% Water for 3h.TFA was removed by evaporation and the crude

peptide was dissolved in acetonitrile and water. The peptides were analyzed and purified on a Waters Breeze 2 HPLC System, and then lyophilized on a Labconco Lyophilizer

For cyclic peptides, Fmoc-Cys (Trt)-OH was added to the N- and C- termini during synthesis. Cyclization of the fully deprotected lyophilized peptide was achieved in solution-H₂O/Acetonitrile (1:1) with 2 equivalents of N-Chlorosuccinimide (NCS).²⁷ The reaction was allowed to stir for 15mins and then lyophilized.

For peptides synthesized on 2-chlorotrityl chloride resin, 2 equivalents of the second Fmoc-amino acid residue (synthesis starts at the C-terminus), and 6 equivalents each of DIPEA were reacted in DCM for 2 hours, followed by Fmoc-deprotection. The next amino acid was then added and the cycle described above was repeated to achieve the synthesis of the desired sequence. After capping, the cleavage cocktail -Acetic acid/Trifluoroethanol/DCM in 1:1:8 ratio was added and the peptidyl- resin was allowed to shake for 2h after which the peptide solution was concentrated by vacuum and Acetic acid was removed by co-evaporation with hexane. By using this strategy, the protection group on the side chains are preserved for further coupling reactions in solution.

To obtain the desired complete sequence for peptides synthesized on Chlorotrityl chloride resin, we converted the C-terminus to a methyl ester of Serine. The protected peptide obtained after evaporation (1 eq.) and H-Ser-(OtBu)-OMe. HCl (1.2 eq.) were dissolved in 10ml DMF. DIPEA (2.2 eq.) and TBTU (1.3 eq.) were added to the stirring solution .²⁸The reaction was allowed to stir for 2h at room temperature. The reaction was then diluted with brine and extracted with EtOAc. The organic layer was further washed with brine two more times and the then dried over Sodium Sulfate. The solvent was removed by vacuum evaporation and the residue was redissolved in a 95:2.5:2.5 mixture of TFA /TIS/H₂O to deprotect all side chain groups. Deprotection reaction was allowed to run for 2h and volatiles were removed under reduced

pressure and the crude peptide was dissolved in acetonitrile and water. The peptides were analyzed and purified on a Waters Breeze 2 HPLC System by gradient elution (0.1% TFA in H₂O, 0.1% TFA in Acetonitrile) and then lyophilized on a Labconco Lyophilizer

Synthesis of Building Blocks

Synthesis of N^α-Fmoc-N^ε-diethyl-Lysine (5b)

Compound 5a (2.5g, 5.34 mmol) was dissolved in TFA (20mL) at 0°C and was stirred for 3h at room temperature. TFA was then evaporated and the residue was dissolved in MeOH (50 mL) and stirred on ice bath. Acetaldehyde (3.051mL, 54.32 mmol) was added. After 15 mins, NaCNBH₃ (1.28g, 20.37 mmol) was added and allowed to stir for another 15 mins. After 15 mins, Acetaldehyde and NaCNBH₃ were added again and the reaction mixture was stirred for 2h. TLC was done in MeOH/H₂O (95:5) and a R_f ~ 0.3 confirmed the completion of the reaction. The reaction was acidified with 1M HCl to adjust the pH to about 3 and was then purified with silica gel column using Chloroform/MeOH (19/1, v/v) as eluent. The pure product (5b, 2.2g) was obtained after removal of solvent by vacuum evaporation.

Synthesis of N^α-Fmoc-N, N-diethyl-N-methyl Lysine (5c)

Compound 5b (1.0g, 2.4 mmol) was dissolved in ethanol (10mL) and was stirred at room temperature. NaHCO₃ (0.63g, 7.2 mmol) and CH₃I (733μL, 12.0 mmol) were added and the reaction mixture was sealed and stirred for 2days. Reaction was monitored by TLC (MeOH/DCM 1:7; R_f ~ 0.1). Purification was done with silica gel column using Chloroform/MeOH (19/1, v/v) as eluent. The pure product (5c, 0.3g) was obtained after removal of solvent by vacuum evaporation.

Synthesis of N^{α} -Fmoc- N^{ϵ} -Dimethyl-Lysine (5d)^{29, 30}

Compound 5a (2.5g, 5.34 mmol) was dissolved in TFA (20mL) at 0°C and was stirred for 3h at room temperature. TFA was then evaporated and the residue was dissolved in MeOH (50 mL) and stirred on ice bath. 37% aqueous Formaldehyde (1.167mL, 14.95 mmol) was added. After 15 mins, NaCNBH₃ (1.28g, 20.37 mmol) was added. And allowed to stir for another 15 mins. After 15 mins, Formaldehyde and NaCNBH₃ were added again and the reaction mixture was stirred for 2h. TLC was done in MeOH/H₂O (95:5) and a R_f ~ 0.4 confirmed the completion of the reaction. The reaction was acidified with 1M HCl to adjust the pH to about 3 and was then purified with silica gel column using Chloroform/MeOH (19/1, v/v) as eluent. The pure product (5d, 2.0g) was obtained after removal of solvent by vacuum evaporation.

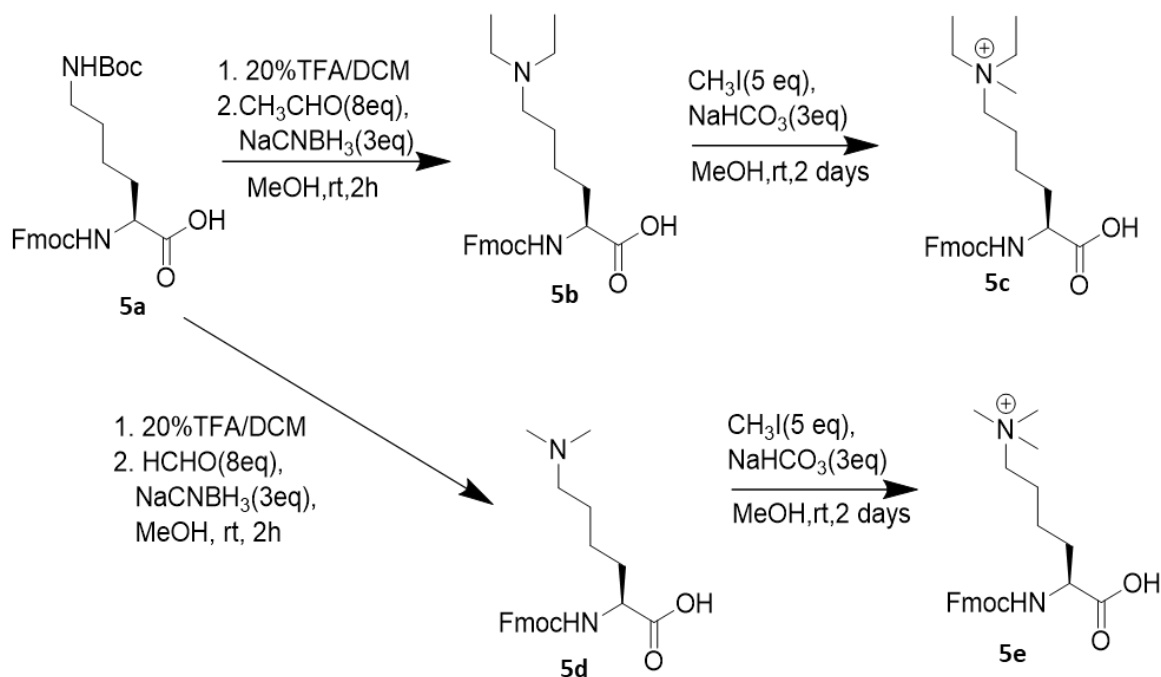


Figure 5.7 Synthetic scheme for the reductive alkylation of Lysine.

Synthesis of *N^α*-Fmoc-*N^ε*-Trimethyl-Lysine (5e)^{29, 30}

Compound 5d (1.0g, 2.5 mmol) was dissolved in ethanol (10mL) and was stirred at room temperature. NaHCO₃ (0.63g, 7.5 mmol) and CH₃I (780μL, 12.5 mmol) were added and the reaction mixture was sealed and stirred for 2 days. Reaction was monitored by TLC (MeOH/DCM 1:7; R_f ~ 0.2). Purification was done with silica gel column using Chloroform/MeOH (19/1, v/v) as eluent. The pure product (5e, 0.6g) was obtained after removal of solvent by vacuum evaporation.

Cell fractionation assay

Myc-MPP8-wt or W80A was expressed in 293T cells and the transfected cells were fractionated into cytoplasmic extract (cyto), nuclear extract (NE) and nuclear pellet (NP) with a Dounce homogenizer as was previously described.^{21, 26} The different compounds were dissolved in DMSO at a concentration of 10mM and were included during the procedure to a final test concentration of 20μM. The presence of MPP8 in different fractions was then analyzed by western blot. Lysis buffer was used as a control.

5.5 References

1. M. Arkin, *Current Opinion in Chemical Biology*, 2005, **9**, 317-324.
2. M. Esteller, *Carcinogenesis*, 2006, **27**, 1121-1125.
3. T. Kouzarides, *Cell*, 2007, **128**, 693-705.
4. S. B. Hake, A. Xiao and C. D. Allis, *British Journal of Cancer*, 2004, **90**, 761-769.
5. B. D. Strahl and C. D. Allis, *Nature*, 2000, **403**, 41.
6. M. A. Adams-Cioaba and J. Min, *Biochemistry and Cell Biology*, 2009, **87**, 93-105.
7. Y. Liu, K. Liu, S. Qin, C. Xu and J. Min, *Pharmacology & Therapeutics*, 2014, **143**, 275-294.
8. K. Liu, Y. Liu, J. L. Lau and J. Min, *Pharmacology & Therapeutics*, 2015, **151**, 121-140.
9. C. Xu, C. Bian, W. Yang, M. Galka, H. Ouyang, C. Chen, W. Qiu, H. Liu, A. E. Jones, F. MacKenzie, P. Pan, S. S.-C. Li, H. Wang and J. Min, *Proceedings of the National Academy of Sciences*, 2010, **107**, 19266-19271.
10. C. Xu and J. Min, *Protein & Cell*, 2011, **2**, 202-214.
11. J. Eryilmaz, P. Pan, M. F. Amaya, A. Allali-Hassani, A. Dong, M. A. Adams-Cioaba, F. MacKenzie, M. Vedadi and J. Min, *PLoS one*, 2009, **4**, e7274.

12. Y. Guo, N. Nady, C. Qi, A. Allali-Hassani, H. Zhu, P. Pan, M. A. Adams-Cioaba, M. F. Amaya, A. Dong, M. Vedadi, M. Schapira, R. J. Read, C. H. Arrowsmith and J. Min, *Nucleic Acids Research*, 2009, **37**, 2204-2210.
13. S. D. Taverna, H. Li, A. J. Ruthenburg, C. D. Allis and D. J. Patel, *Nature Structural & Molecular Biology*, 2007, **14**, 1025.
14. Y. Huang, J. Fang, M. T. Bedford, Y. Zhang and R.-M. Xu, *Science (New York, N.Y.)*, 2006, **312**, 748-751.
15. R. Margueron, N. Justin, K. Ohno, M. L. Sharpe, J. Son, W. J. Drury Iii, P. Voigt, S. R. Martin, W. R. Taylor, V. De Marco, V. Pirrotta, D. Reinberg and S. J. Gambin, *Nature*, 2009, **461**, 762.
16. R. E. Collins, J. P. Northrop, J. R. Horton, D. Y. Lee, X. Zhang, M. R. Stallcup and X. Cheng, *Nature Structural & Molecular Biology*, 2008, **15**, 245.
17. H. Li, S. Ilin, W. Wang, E. M. Duncan, J. Wysocka, C. D. Allis and D. J. Patel, *Nature*, 2006, **442**, 91.
18. P. R. Nielsen, D. Nietlispach, H. R. Mott, J. Callaghan, A. Bannister, T. Kouzarides, A. G. Murzin, N. V. Murzina and E. D. Laue, *Nature*, 2002, **416**, 103.
19. S. A. Jacobs and S. Khorasanizadeh, *Science (New York, N.Y.)*, 2002, **295**, 2080-2083.
20. J. Min, Y. Zhang and R.-M. Xu, *Genes & Development*, 2003, **17**, 1823-1828.
21. K. Kokura, L. Sun, M. T. Bedford and J. Fang, *The EMBO Journal*, 2010, **29**, 3673-3687.
22. J. Li, Z. Li, J. Ruan, C. Xu, Y. Tong, P. W. Pan, W. Tempel, L. Crombet, J. Min and J. Zang, *PloS one*, 2011, **6**, e25104.
23. H. Peinado, D. Olmeda and A. Cano, *Nat Rev Cancer*, 2007, **7**, 415-428.
24. Y. Chang, J. R. Horton, M. T. Bedford, X. Zhang and X. Cheng, *Journal of molecular biology*, 2011, DOI: S0022-2836(11)00283-X [pii]10.1016/j.jmb.2011.03.018.
25. C. Santiago, K. Nguyen and M. Schapira, *J Comput Aided Mol Des*, 2011, **25**, 1171-1178.
26. J. Fang, H. Wang and Y. Zhang, in *Methods in Enzymology*, Academic Press, 2003, vol. 377, pp. 213-226.
27. T. M. Postma and F. Albericio, *RSC Advances*, 2013, **3**, 14277-14280.
28. J. I. Stuckey, B. M. Dickson, N. Cheng, Y. Liu, J. L. Norris, S. H. Cholensky, W. Tempel, S. Qin, K. G. Huber, C. Sagum, K. Black, F. Li, X.-P. Huang, B. L. Roth, B. M. Baughman, G. Senisterra, S. G. Pattenden, M. Vedadi, P. J. Brown, M. T. Bedford, J. Min, C. H. Arrowsmith, L. I. James and S. V. Frye, *Nature Chemical Biology*, 2016, **12**, 180.
29. H. Chi, M. S. Islam, T. K. Nsiama, T. Kato and N. Nishino, *Amino acids*, 2014, **46**, 1305-1311.
30. Z.-P. Huang, J.-T. Du, Y.-F. Zhao and Y.-M. Li, *International Journal of Peptide Research and Therapeutics*, 2006, **12**, 187-193.

CHAPTER 6 : CONCLUSION AND FUTURE OUTLOOK

In this chapter, we will be providing a summary of all the projects and their possible future outlook. We also suggest a way forward for the design of inhibitors of protein-protein interactions in pathological conditions.

An interesting inference from all our studies is a confirmation of the notion of hotspot residues. We have demonstrated that a peptide can be completely changed or modified (except for the position of contact residues), and still retain its minimal function. We have also shown that peptide mimics bearing groups that mimic the functionality of the natural peptide or protein exhibited equal or better activity than the template peptide. For instance, our designed peptidomimetic for HIV-1 fusion inhibition showed better or equal antiviral activity, despite the modifications introduced. However, there is the need to evaluate the effects of varying the modification point along the length of the template peptide. This will help us to evaluate how substitution at those points could modulate the activity of the resulting peptide. This will also provide better structural insights to the design of potent inhibitors and could provide a template for the design of antiviral agents. Also, this strategy could be adapted for other viral systems with similar mode of entry and infection mechanisms.

Talking about the amyloid system, many reported and ongoing research have demonstrated the adoption of same or similar proven strategies across various amyloid systems. For instance, many inhibitors of amyloid fibril formation have been derived from the amyloid forming units, peptide segments, and full length peptide of amyloidogenic proteins, while many others are from

rational design. Although, some dual inhibitors have been discovered through fortuitous means, not many compounds have been developed for dual-action against multiple amyloid systems. Despite the lack of sequence homology in the amyloid forming units of different amyloidogenic proteins, there are great similarities in the morphological features of their amyloid fibers. This implies that intramolecular interactions which promote cross- β -sheet assembly are a major driving force of aggregation. As such, functionalities that could provide such interactions could be considered in the design of such multiple/dual-acting amyloid inhibitor.

Together, these works reveal design patterns and provide deeper insights for the advancement of drug discovery.

APENDIX A: PUBLISHING RIGHTS

7/3/2018

Rightslink® by Copyright Clearance Center



RightsLink®

Home

Account Info

Help



Title: Structure and Function of AApeptides
Author: Olapeju Bolarinwa, Alekhya Nimmagadda, Ma Su, et al
Publication: Biochemistry
Publisher: American Chemical Society
Date: Jan 1, 2017
Copyright © 2017, American Chemical Society

Logged in as:
Olapeju Bolarinwa
Account #:
3000953247

LOGOUT

PERMISSION/LICENSE IS GRANTED FOR YOUR ORDER AT NO CHARGE

This type of permission/license, instead of the standard Terms & Conditions, is sent to you because no fee is being charged for your order. Please note the following:

- Permission is granted for your request in both print and electronic formats, and translations.
- If figures and/or tables were requested, they may be adapted or used in part.
- Please print this page for your records and send a copy of it to your publisher/graduate school.
- Appropriate credit for the requested material should be given as follows: "Reprinted (adapted) with permission from (COMPLETE REFERENCE CITATION). Copyright (YEAR) American Chemical Society." Insert appropriate information in place of the capitalized words.
- One-time permission is granted only for the use specified in your request. No additional uses are granted (such as derivative works or other editions). For any other uses, please submit a new request.

If credit is given to another source for the material you requested, permission must be obtained from that source.

BACK

CLOSE WINDOW

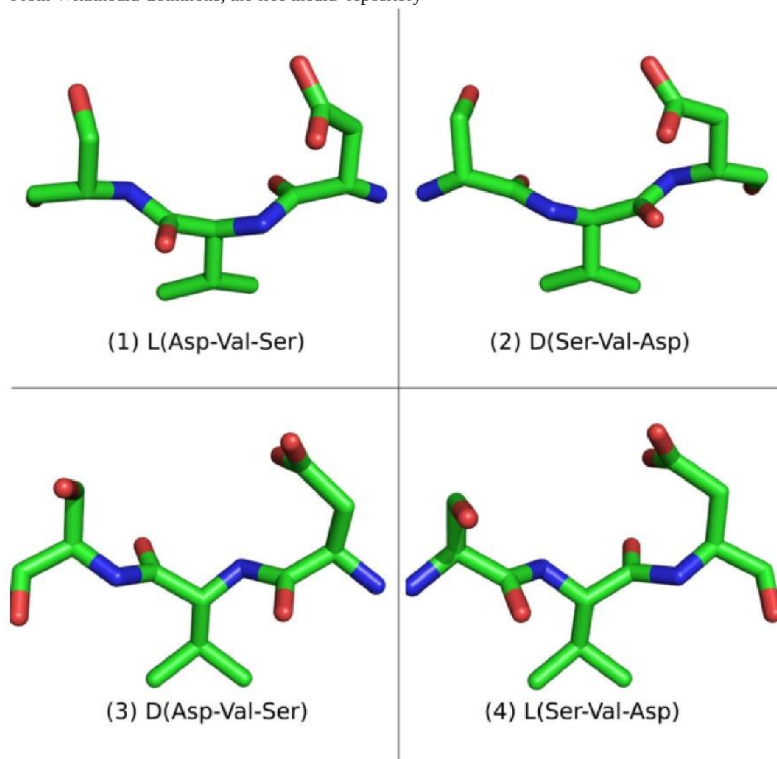
Copyright © 2018 Copyright Clearance Center, Inc. All Rights Reserved. [Privacy statement](#). [Terms and Conditions](#). Comments? We would like to hear from you. E-mail us at customer care@copyright.com

<https://s100.copyright.com/AppDispatchServlet>

1/1

File:L-peptideD-peptideAnalogues.png

From Wikimedia Commons, the free media repository



Size of this preview: 611 × 599 pixels

Original file (2,055 × 2,015 pixels, file size: 875 KB, MIME type: image/png)

Summary

Description	English: Image used in Peptidomimetics wikipedia page. Figure 2. An L-peptide and its analogues. An L-peptide (1) sequence has three analogues: the D-enantiomer (3) with the same sequence, the retro L-peptide (4) with the inverted sequence, and the retro-inverso D-peptide(2), with all D-amino acids and the inverted sequence. In this image (1) and (3) are shown from C-terminus on the left to N-terminus on the right, while (2) and (4) are shown from N-terminus to C-terminus. Note that (1) and (2) have similar side chain positions; one is the retro-inverso sequence of the other. The same applies to (3) and (4).
Date	26 May 2010
Source	Own work

Author Pablo.gainza

Licensing



I, the copyright holder of this work, release this work into the **public domain**. This applies worldwide.

In some countries this may not be legally possible; if so:

*I grant anyone the right to use this work **for any purpose**, without any conditions, unless such conditions are required by law.*

File history

Click on a date/time to view the file as it appeared at that time.

	Date/Time	Thumbnail	Dimensions	User	Comment
current	06:55, 26 May 2010		2,055 × 2,015 (875 KB)	Pablo.gainza (talk contribs)	{{Information Description={{en} 1=Image used in Peptidomimetics wikipedia page. Figure 2. An L-peptide and its analogues. An L-peptide (1) sequence has three analogues: the D-enantiomer (3) with the same sequence, the retro L-peptide (4) with the invert

- You cannot overwrite this file.

File usage on Commons

There are no pages that link to this file.

File usage on other wikis

The following other wikis use this file:

- Usage on en.wikipedia.org
 - Peptidomimetic
- Usage on hu.wikipedia.org
 - Bioinformatika

Retrieved from <https://commons.wikimedia.org/w/index.php?title=File:L-peptideD-peptideAnalogues.png&oldid=275879844>

This page was last edited on 1 January 2018, at 14:34.